FREQUENCY OFFSET ESTIMATION FOR ORTHOGONAL FREQUENCY DIVISION MULTIPLEXING

NG KIM PIAU
(*B. ENG (HONS), NUS*)

A THESIS SUBMITTED

FOR THE DEGREE OF MASTER OF ENGINEERING

DEPARTMENT OF

ELECTRICAL AND COMPUTER ENGINEERING

NATIONAL UNIVERSITY OF SINGAPORE

2003

Acknowledgements

I would first like to thank my supervisor, Professor Tjhung, for being willing to accept me as his project student even though I did not do a communications related project for my B.Eng degree. His support, enthusiasm, persistent encouragement and guidance made the course of work a rewarding and pleasant one.

I would also like to extend my thanks to my parents, for giving the moral and financial support to take up the course. And to my brother, Hsiao Piau, my good friends, Khai Sheng, Yu Qiang and Choon Kiat for their help and encouragement in the course of my work.

Table of Contents

Acknowledgement i

Table of Contents ii

List of Tables v

List of Figures vi

List of Symbols ix

Summary xi

1 Introduction 1

1.1 Background 1

1.2 Orthogonal Frequency Division Multiplexing 2

1.2.1 Introduction of Orthogonal Frequency Division Multiplexing 2

1.2.2 Applications of OFDM 4

1.2.3 Advantages and Disadvantages of OFDM 5

1.3 Estimation of Carrier Frequency Offset in OFDM 7

1.4 Thesis Organisation 9

1.5 Contribution of Thesis 10

2 Signal Model and effect of a carrier frequency offset 12

2.1 Signal Model 12

2.2 Effect of frequency offset 18

2.3 Theoretical Bound for Signal Interference Ratio 26

3 Estimation of carrier frequency offset 30

3.1 Deterministic maximum likelihood estimation of carrier frequency offset 30

3.2 Cost function ambiguity due to channel nulls 44

3.2.1 Derivation of criterions to avoid cost function ambiguity 44

3.2.2 Physical interpretation of the cost function ambiguity criterion 50

4 Performance of frequency offset estimator 58

4.1 Mean Squared error of estimator 58

4.2 Performance of estimator in a AWGN channel 67

4.2.1 *MSE* against SNR 67

4.2.2 *MSE* against N_{Act} 68

4.2.3 *MSE* of modified cost function against P 69

4.2.4 *MSE* against N_X 70

4.3 Performance of estimator in a Rayleigh Channel 72

4.3.1 *MSE* against N_X 72

4.3.2 Random placement of sub-carriers coupled with deterministic hopping over blocks 76

5 Search schemes for finding global cost function minimum 80

5.1 Direct search of global minimum using cost function 82

5.1.1 Initial bracketing of local minima using cost function 82

5.1.2 Finding a local minimum from a bracketing interval 85

5.1.2.1 Golden search 85

5.1.2.2 Parabolic Interpolation 86

5.2 Transforming problem of minima search to root search 88

5.2.1 Bracketing of local minima using derivative 89

5.2.2 Locating roots of cost function derivative 90

5.2.2.1 bisection 90

5.2.2.2 Newton Raphson Method 91

5.3 Further reduction of computational load 92

5.4 Simulation results 93

6 Conclusions and future topics 96

6.1 Conclusions 96

6.2 Suggestions for further works 99

References 100

Appendix A - List of Publications 102

List of Tables

5.1 Average number of iterations required to estimate local minimum 93

List of Figures

1.1	Typical OFDM (a) and FDM (b) sub-carrier spectrums	3
1.2	Basic Cyclic Prefix Based OFDM system	3
2.1	OFDM System Block Diagram	13
2.2	Diagram depicting channel effects	16
2.3	Plot of $f(p)$	21
2.4	Placement of activated sub-carriers to minimise ICI	23
2.5	Placement of sub-carriers for system with alternate clusters of activated and null sub-carriers	24
2.6	Plot of $ICI_{Avg,m}$ against N_X.	25
2.7	Variance of normalised $E[\|I_m[k]\|]^2$ over $\Omega_{A,m}$ against N_X	25
2.8	Plot of SIR against v_o	28
2.9	Plot of SIR against v_o (for various N_X)	28
3.1	Plot of cost functions based on total activated sub-carrier energy and total null-sub-carrier energy	37
3.2	Plot of cost function based on null-sub-carrier energy from v_e= -4 to 4	37
3.3	Plot of cost function based on null-sub-carrier energy for a regular sub-carrier placement	38
3.4	Plot of cost function based on null-sub-carrier energy for a irregular sub-carrier placement	39
3.5	Plot of $E_{N,Z}(k,v)$ against null sub-carrier index, k for different v_e	40

3.6	Example of null sub-carriers used in computation of modified cost function	41
3.7	Null sub-carriers used in computation of $J_{N \bmod,Z}(v_e)$ in the case where the activated sub-carriers are placed consecutively from 0 to $N_A - 1$	41
3.8	Plot of $J_{N \bmod,Z}(v_e)$ for frequency offset within sub-carrier spacing	42
3.9	Plot of $J_{N \bmod,Z}(v_e)$ for frequency offsets over entire range of -N/2 to N/2	43
3.10	Diagram illustrating the occurrence of cost function ambiguity due to periodicity in sub-carrier placement	51
3.11	Plot of cost function showing the presence of multiple global minima due to periodicity in sub-carrier placement	51
3.12	Diagram illustrating the occurrence of cost function ambiguity due to channel nulls	52
3.13	Plot of cost function showing presence of multiple global minima due to channel null	53
3.14	Plot of Channel Amplitude Response, $\}C[k]\|$, cost function showing presence of multiple minima due to channel null	53
3.15	Diagram illustrating why cost function ambiguity will not occur due to channel nulls when hopping is used	56
4.1	Plot of the *MSE* of v_e against SNR (dB) for a AWGN channel	67
4.2	Plot of the *MSE* of v_e against N_A for a AWGN channel	68
4.3	Plot of the *MSE* of v_e against P using modified cost function for a AWGN channel	70
4.4	Plot of the *MSE* of v_c against SNR with various N_X for a AWGN channel	71
4.5	Plot of *MSE* of estimator in Rayleigh Channel with N_X=4, 8,16,32	72
4.6	Simulation example showing the problem of 'channel nulls'	73
4.7	Plot showing the probability of occurrence of absolute normalised estimate error exceeds 1, against SNR (dB)	74

4.8	Plot of mean amplitude response for occurrences where the absolute estimate error exceeds 1	75
4.9	Plot of *MSE* against SNR for N_A=10	78
4.10	Plot of *MSE* against SNR for N_A=32	78
4.11	Plot of *MSE* against SNR for N_A=60	79
4.12	Plot of *MSE* against SNR for N_A=63	79
5.1	Incorrect search interval when $J_{N,Z}(v_c)$ is sampled at integer intervals and fine search is conducted over integer interval that yielded the lowest cost	81
5.2	The bracketing intervals containing the local minima extracted from $J_{N,Z}(v_c)$	84
5.3	An iteration of Golden Search	85
5.4	Iteration of Parabolic Interpolation	87
5.5	Derivative of $J_{N,Z}(v_c)$	88
5.6	One iteration of Bisection	91
5.7	Plot of error rate against β	94
5.8	Plot of mean number of bracketing intervals evaluated against β	95

List of Symbols

N	Number of sub-carriers in an OFDM system
N_b	Number of OFDM symbols used in the estimation of carrier frequency offset
N_A	Number of activated sub-carriers in each OFDM symbol
N_N	Number of null sub-carriers in each OFDM symbol
$\Omega_{A,m}$	Set of activated sub-carriers for the m^{th} OFDM symbol used in estimation
$\Omega_{N,m}$	Set of null sub-carriers for the m^{th} OFDM symbol used in estimation
T	OFDM symbol period
L	Length of the cyclic prefix
$c[n]$	The discrete channel impulse response
$C[k]$	The N-point DFT of the discrete channel impulse response
Δf	Actual carrier frequency offset
v_o	Relative carrier frequency offset
v_c	Relative carrier frequency offset correction
v_e	Relative carrier frequency offset error
$S_m[k]$	The data symbol modulated on the k^{th} sub-carrier of the m^{th} OFDM symbol used for estimation
$x_m[n]$	The n^{th} transmitted baseband sample of the m^{th} OFDM symbol used for estimation
$y_m[n]$	The n^{th} received baseband sample of the m^{th} OFDM symbol used for estimation, in the absence of AWGN
$r_m[n]$	The n^{th} received baseband sample of the m^{th} OFDM symbol used for estimation, in the presence of AWGN
$z_m[n]$	The result of applying frequency correction to $r_m[n]$
$w_m[n]$	The AWGN component corresponding to the n^{th} received time domain sample of the m^{th} OFDM symbol used for estimation

σ_w^2	Variance of complex AWGN
σ_S^2	Variance of complex AWGN
$X_m[k]$	N-point DFT of $x_m[n]$
$Z_m[k]$	N-point DFT of $z_m[n]$
$W_m[k]$	N-point DFT of $w_m[n]$, after frequency offset correction
$J_{A,Z}(v_e)$	Cost function based on the total energy of the activated sub-carriers
$J_{N,Z}(v_e)$	Cost function based on the total energy of the null sub-carriers
$J_{N \bmod,Z}(v_e)$	Modified cost function based on the total energy of the null sub-carriers

Summary

Orthogonal Frequency Division Multiplexing (OFDM) is a multi-carrier modulation technique relying on the use of multiple orthogonal sub-carriers for high data-rate transmissions over frequency selective channels at low complexity. The presence of a carrier frequency offset between the transmitter and receiver destroys this orthogonality among the sub-carriers, resulting in inter-carrier interference (ICI), causing severe degradation in the bit error rate performance. Hence, effective elimination of the carrier frequency offset is of paramount importance in OFDM and is the focus of this thesis. A flexible OFDM framework is considered where the placement of the activated sub-carriers is arbitrary and may vary from one OFDM symbol to another. The effects of ICI in relation to sub-carrier placement were examined and the maximum likelihood estimate (MLE) of the carrier frequency offset was formulated based on a block of received OFDM symbols. The MLE is found by searching for the offset that minimises the total energy of the null sub-carriers and may become ambiguous in the presence of channel nulls. Using our framework, the criterion to avoid this ambiguity through the judicious placement of the null sub-carriers was derived. The criterion is more generalized as compared to previous work. In addition to this, the mean squared error of the estimator was also derived using small perturbation analysis. Simulations carried out verified the theoretical results obtained. Furthermore, we proposed a random sub-carrier placement strategy coupled with deterministic hopping to cope with the ambiguity problem and examined its performance. Lastly, we explored the various search schemes for finding the MLE. In particular we found that transforming the problem of minima search to root search can reduce the number of search iterations.

Chapter 1

Introduction

1.1 Background

The increasing demand for wireless multimedia and future-generation mobile communication systems has led to intense interest on modulation techniques that can provide broadband transmission over wireless channels. Bandwidth efficiency is one of the most important criteria in the design of a communication system. The designer must decide how to efficiently utilise the available channel bandwidth in order to transmit the information reliably within the transmission power and receiver complexity constraints.

For high-speed data transmission over mobile radio channels, multipath propagation is predominant and it causes Inter-Symbol Interference (ISI). This is a major obstacle to overcome as it causes bit errors at the receiver and results in the degradation in performance of a communication system. The degree of degradation is dependent on the frequency response characteristics of the channel.

For communication in a mobile radio channel, one approach is to employ a single carrier system in which the information sequence is transmitted serially at some specified rate. In such a channel, the time dispersion is generally much greater than the symbol rate, resulting in ISI. In this case, an equaliser, at the cost of increased receiver complexity, is necessary to compensate for the channel distortion,

An alternate approach is multicarrier modulation, which is based on the concept of channel partitioning. Channel partitioning methods divide a wideband, frequency selective channel into a number of parallel narrowband sub channels. The bandwidth of each sub channel is set sufficiently small so that the channel frequency response is almost constant within the sub channel. Instead of having a single carrier being modulated by a single data stream, multiple carriers, each simultaneously modulated by a data stream, are employed in a multicarrier system. Equalisation is no longer necessary to remove the ISI, as it is negligible. Theoretically speaking, multicarrier techniques can yield transmission rates close to the channel capacity [1].

1.2 Orthogonal Frequency Division Multiplexing

1.2.1 Introduction

Orthogonal Frequency Division Multiplexing (OFDM) is a multicarrier modulation technique whose fundamental principle originates from Chang [2] and over the years a number of researchers have investigated this technique [3, 4, 5, 6].

In contrast with the conventional Frequency Division Multiplexing (FDM), the spectrums of the individual carriers in an OFDM symbols are allowed to mutually overlap, therefore giving optimum spectrum efficiency. The individual sub-carriers Figure 1.1 shows typical spectrums of a OFDM and a FDM signal.

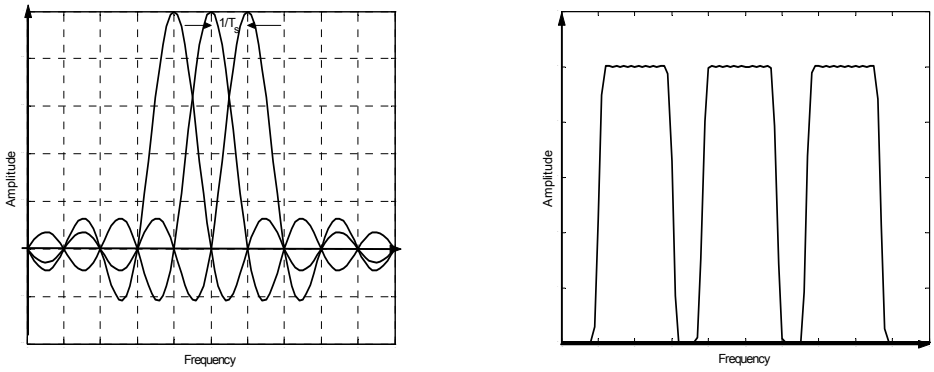

a) b)

Figure 1.1 Typical OFDM (a) and FDM (b) sub-carrier spectrums

In order to maintain orthogonality of the carriers on a symbol interval, the carriers must be synthesised in a manner such that they are spaced in frequency at exactly the reciprocal of the symbol interval, i.e. $1/T_s$. Such synthesis can be accomplished perfectly in principle by using the discrete fourier transform (DFT). In such a scheme, the serial data stream is first spilt into N streams via a serial to parallel converter. An N-point IDFT is then performed to generate the baseband samples to be transmitted. A basic cyclic prefix, DFT based OFDM system setup is shown in Figure 1.2.

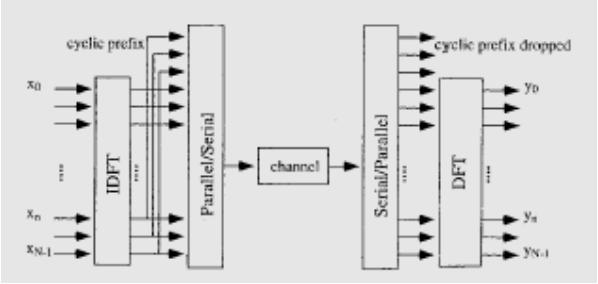

Figure 1.2 - Basic Cyclic Prefix Based OFDM system

1.2.2 Applications of OFDM

The recent evolution of integrated circuit digital signal processing chips has made it practical to implement OFDM for high-speed data transfer applications. The recent successful applications in OFDM include:

i. Digital Audio Broadcasting (DAB)

Standardized by European Technical Standards Institute (ETSI) in 1995, Digital Audio Broadcasting (DAB) was the first standard to use OFDM. DAB makes a single frequency network and the efficient handling of multipath delay spread resulting in improved CD quality sound, new data services, and higher spectrum efficiency.

ii. Terrestrial Digital Video Broadcasting

A personal area network (pan) broadcasting industry group created Digital Video Broadcasting (DVB) in 1993. DVB produced a set of specifications for the delivery of digital television over cable, DSL and satellite. In 1997 the terrestrial network, Digital Terrestrial Television Broadcasting (DTTB), was standardized. DTTB utilizes OFDM in the 2,000 and 8,000 sub-carrier modes.

iii. Magic WAND

The Magic Wireless ATM Network Demonstrator (WAND) was a result of the European Advanced Communications Technology and Server (ACTS) program. A prototype of a wireless OFDM-based ATM network was implemented by Magic WAND. This prototype largely impacted standards activities in the 5GHz band as a result of employing OFDM-based modems and gaining acceptance for OFDM in high-rate wireless communications and forming the basis for HiperLAN2.

iv. IEEE 802.11a/HiperLAN2 and MMAC Wireless LAN

OFDM in the new 5GHz band is comprised of 802.11a, HiperLAN2, and WLAN standards. In July 1998, IEEE selected OFDM as the basis for the new 802.11a 5GHz standard in the U.S. targeting a range of data rates up to 54 Mbps. In Europe, ETSI project Broadband Radio Access Networks (BRAN) is now working on three extensions for OFDM in the HiperLAN standard: (i) HiperLAN2, a wireless indoor LAN with a QoS provision; (ii) HiperLink, a wireless indoor backbone; and (iii) HiperAccess, an outdoor, fixed wireless network providing access to a wired infrastructure. In Japan, consumer electronics companies and service providers are cooperating in the MMAC project to define new wireless standards similar to those of IEEE and ETSI BRAN.

1.2.3 Advantages and disadvantages of OFDM

i. Advantages

In an OFDM system, orthogonality between the sub-carriers results in high spectral efficiency. With its parallel transmission scheme, a wide-band high data rate stream is converted into multiple narrow-band, lower bit rate streams. In high data rate serial transmission, a deep fade in a mobile channel causes burst errors. In contrast, each OFDM symbol generally has a duration that is much longer than the coherence time of the channel. As a result, there is only slight distortion to the many data symbols which are time interleaved in an OFDM symbol. Hence, the data symbols may still be correctly demodulated. The multi-carrier nature of OFDM also allows transmission of the same information-bearing signal in many different carriers, permitting frequency diversity [7,8].

In addition to this, the availability of inexpensive DSP and VLSI technologies has made implementation of OFDM systems practical and flexible.

ii. Disadvantages

Before demodulation of sub-carriers can take place, an OFDM receiver has to perform at least 2 synchronization tasks. Firstly, the symbol timing boundaries have to be determined to minimise the effects of ISI. Secondly, it has to estimate and correct for the carrier frequency offset of the received signal with respect to the receiver because such an offset will destroy the orthogonality between the sub-carriers and introduces inter carrier interference (ICI). A related problem is phase noise, since a practical oscillator produces a carrier that is phase modulated by random phase jitter. As a result, the frequency, which is the time derivative of the phase, is never perfectly constant, thereby causing ICI in an OFDM receiver. For single carrier systems, phase noise and frequency offsets only give degradation in the received signal-to-noise ratio (SNR), rather than introducing interference. This is the reason that the sensitivity to phase noise and frequency offset are often mentioned as disadvantages of OFDM relative to single carrier systems. An OFDM signal consists of a number of independently modulated sub-carriers that can result in a large peak-to average power ratio (PAPR) when added up coherently. When N_s signals are added with the same phase, they produce a peak power that is N_s times the average power. High PAPR is also a major problem in OFDM as a large PAPR increases the complexity of the analogue-to-digital and digital-to-analogue converters and reduces the efficiency of the RF power amplifier employed in the system.

1.3 Estimation of Carrier Frequency Offset in OFDM

In OFDM, the presence of a carrier frequency offset causes a loss of orthogonality among the sub-carriers and introduces inter-carrier interference [9], causing a reduction in SIR and degradation in system performance [10]. Hence estimation and removal of the carrier frequency offset is of paramount importance in an OFDM system and this has received considerable attention in recent years.

The extensive literature on carrier frequency offset estimation for OFDM can be categorised as data-aided [11,12] schemes or non-data-aided (blind) [9, 13-15, 17, 18, 19, 20] schemes that only rely on the received OFDM symbols. In [11], a training method based on the transmission of an OFDM symbol with identical halves was proposed and its acquisition range was extended in [12] by using one training symbol with more than 2 identical parts. On the other hand, a blind technique was proposed in [9] and is based on the maximum likelihood estimate of 2 consecutive and identical received blocks. For this technique, the estimation range is restricted to less than half the sub-carrier spacing. In addition to this, carrier frequency offset estimators that exploit the cyclic prefix are also presented in [21], which include a minimum variance unbiased carrier frequency offset estimator.

Although the ease in handling frequency selective channels constitutes OFDM's primary success factor, most blind carrier frequency offset estimators deal with frequency non-selective channels [14, 15, 21]. The generalisation of cyclic carrier frequency offset estimators to frequency selective channels is given in [17].

Subspace based approaches relying on the insertion of null sub-carriers at the transmitter are derived in [15, 18,19] but did not address the performance of the estimators in a frequency selective channel. The consistency of these estimators, as well as those proposed in [16, 22], are not assured in the presence of channel nulls, which can occur in a frequency selective channel.

The approach in [13] also relies on the insertion of null sub-carriers and the offset estimate is found by finding the frequency offset that minimises the total energy of the null sub-carriers. To overcome the inherent problem of channel nulls in a frequency selective channel, the sub-carriers are deterministically hopped over the block of OFDM symbols used for estimation. The estimation range is restricted to the sub-carrier spacing. In [23], the maximum likelihood estimate based on the received time domain samples of the received OFDM symbol is formulated and is found to coincide with the estimate in [13]. The criteria that determine if a particular sub-carrier placement will cause the inconsistency of the estimator when applied in a frequency selective estimate are also derived.

In this thesis, the maximal likelihood approach in [13, 23] was adopted as it is semi-blind where only the placement of the activated sub-carriers of the transmitted OFDM symbol needs to be known to the receiver.

1.4 Thesis organisation

The organisation of this thesis is as follows:

Chapter 1 - The concept of OFDM is introduced together with the critical problem of carrier frequency offset estimation. A review of the available techniques follows and an account of the thesis outline and contribution is given.

Chapter 2- The signal model for a general and flexible OFDM system used in this thesis is formulated and the effect of a carrier frequency offset is discussed with respect to the placement of the activated sub-carriers.

Chapter 3 - The maximum likelihood estimator of the carrier frequency offset, the criterion to avoid the ambiguity of this estimator in the presence of channel nulls as applied to our general OFDM system, is derived. This is followed by a physical interpretation of the criterion

Chapter 4 – The theoretical derivation for the mean squared error of the estimator is derived using small perturbation analysis. Simulation studies for an AWGN channel and Rayleigh channel are presented and compared to the theoretical results. A random placement of sub-carrier coupled with deterministic hopping is proposed and its performance is analysed.

Chapter 5- The techniques to search the frequency offset estimate efficiently are explored and a comparison of their performances made.

Chapter 6- Concludes the findings in this thesis

1.5 Contribution of Thesis

We have adopted a flexible OFDM system where the sub-carrier placement is arbitrary and is allowed to vary from one OFDM symbol to another. The signal model formulated and the derivations are based on this general model and are more generalised when compared to those in [13] where the carrier placement follows a regulated pattern and [23] where the carrier placement is the same for all OFDM symbols used in estimation of the carrier frequency offset. We also noted that the sub-carrier placements that minimise the average intercarrier interference coincide with those that minimise the estimator's mean squared error.

In [23], a criterion was derived to determine if a particular carrier placement can avoid estimator ambiguity in the presence of channel nulls. However, this criterion was derived for a system where the sub-carrier placement was fixed for all OFDM symbol used for estimation. We derived a more general criterion for our system that can be used to explain explicitly how deterministic hopping in [13] can also help to cope with the ambiguity of the estimate due to the channel nulls. Furthermore, despite addressing the problem of channel nulls, there has been little experimental evidence to suggest that such channel nulls would indeed pose a significant problem when the estimator is applied to a Rayleigh channel. We show via simulations, the probability of such occurrences, and that the occurrence of large estimate errors coincides with the channel null occurrence predicted by the derived criterion. Moreover though [13] suggests the use of deterministic hopping to combat the channel null problem, the periodic placement of the activated sub-carriers meant that the estimation range is restricted unless all carriers are placed consecutively and then deterministically

hopped. We propose an alternate placement strategy, where the placement of the sub-carriers is made pseudo-randomly and then the allocation pattern is deterministically hopped from symbol to symbol. We compare the performance of the proposed strategy to that in [13].

Finding the frequency offset estimate involves searching for the global minimum of a cost function that contains multiple minima. The number of local minima is typically the number of sub-carriers in the system. Little has been mentioned on how this global minimum can be searched efficiently. The gradient descent method proposed in [13] is only suitable for frequency estimation within a sub-carrier spacing and its rate of convergence is very sensitive to the descent step. In our work, we explore the search techniques that are more efficient than uniform exhaustive search and do not require the setting a weight parameter that affects the convergence rate. In particular, we suggest transforming the problem of minima search to that of root search by taking the 1^{st} and 2^{nd} derivative of the cost function. This is practically feasible because these derivatives can be implemented in a FFT like manner. We found that the number of iterations required to reach convergence is the best among the schemes considered.

Chapter 2

Signal model and the effect of a carrier frequency offset

In this chapter, we first describe the details of the OFDM system that will be considered for the estimation of the carrier frequency offset. We introduce the notation used and discuss the generation of the OFDM signal samples for transmission, the impairments to this signal due to channel effects like multipath propagation, additive noise and frequency offset, and how the correction of the frequency offset at the receiver is performed. Then we examine the effects of a carrier frequency offset on the system performance.

2.1 Signal Model

The system considered in this thesis is general as we consider a partially loaded system, with some sub-carriers being modulated by data symbols while other sub-carriers are unmodulated, termed as activated and null sub-carriers respectively. The placement of the activated and null carriers are considered to be arbitrary and can vary from one OFDM symbol to another.

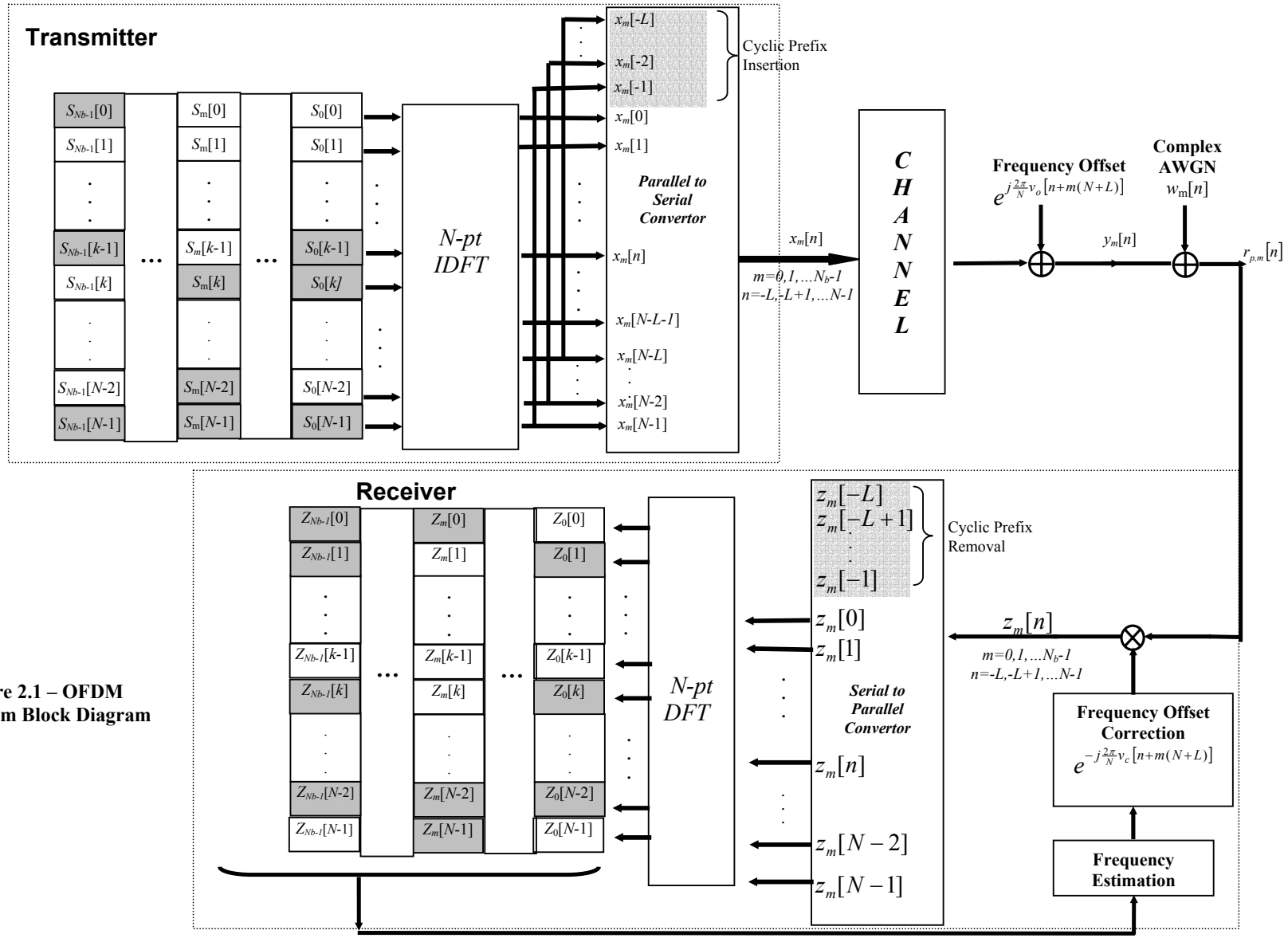

Figure 2.1 – OFDM System Block Diagram

Figure 2.1 shows the basic system structure of an OFDM system with a total of N sub-carriers. Carrier frequency offset estimation is performed using N_b OFDM symbols observed at the receiver.

The set of N_A activated and N_N null sub-carriers for the m^{th} OFDM symbol will be denoted by $\Omega_{A,m}$ and $\Omega_{N,m}$ respectively, where $m \in \{0,1,...,N_b - 1\}$, $N_A + N_N = N$. The data symbol used to modulate the k^{th} sub-carrier, $k \in \Omega_{A,m}$, is denoted by $S_m[k]$. We use the equivalence that $S_m[k] = 0$ for $k \notin \Omega_{A,m}$ for the null carriers. Modulation is assumed to be of the PSK type.

Denoting OFDM symbol period (excluding cyclic prefix) to be T, the sampling interval is given by $\frac{T}{N}$. The t^{th} transmitted baseband signal sample, corresponds to the n^{th} sample of the m^{th} OFDM symbol in the p^{th} estimation block. It is obtained by performing a N-pt IDFT operation on the data symbols, and then appending a cyclic prefix of length L at the start of the IDFT output samples, yielding

$$x_{p,m}[n] = \frac{1}{N} \sum_{k \in \Omega_{A,m}} S_{p,m}[k] e^{j\frac{2\pi}{N}kn} \tag{2.1}$$

for $n = -L+1,...,0,...,N-1$, $m \in \{0,1...N_b - 1\}$, $p \in \{-\infty,...\infty\}$

After passing through the channel and experiencing a carrier frequency offset, the received baseband samples, in the absence of AWGN can be expressed as

$$y_{p,m}[n] = \sum_{\tau=-\infty}^{\infty} x_{p,m}[\tau] c[t-\tau] e^{j\frac{2\pi}{N}v_o t} \tag{2.2}$$

for $n = -L+1,...,0,...,N-1$, $m \in \{0, \quad 1, \quad ..., \quad N_b - 1\}$, $p \in \{-\infty,...\infty\}$

where

$t = (pN_b + m)(N + L) + n$,

$\tau = (p'N_b + m')(N + L) + n'$, $p' \in \{-\infty, ...\infty\}$, $m' \in \{0, ...N_b - 1\}$, $n' \in \{-L, ...N - 1\}$

$c[t] = g_T[t] * h[t] * g_R[t]$, is the baseband channel impulse response between the receiver and transmitter;

Δf is the actual carrier frequency offset

$v_o = \Delta f T$, is defined as the relative frequency offset, v_o lies in the full acquisition range of $-N/2$ to $N/2$.

Substituting (2.1) into (2.2), we obtain, for n=-L, …, N-1,

$$\begin{aligned} y_{p,m}[n] &= \sum_{\tau=-\infty}^{\infty} \frac{1}{N} \sum_{k \in \Omega_{A,m'}} S_{p',m'}[k] e^{j\frac{2\pi}{N}kn'} c[t-\tau] e^{j\frac{2\pi}{N}v_o t} \\ &= \frac{1}{N} \sum_{p'=-\infty}^{\infty} \sum_{m'=0}^{N_b-1} \sum_{n'=-L}^{N-1} \sum_{k \in \Omega_{A,m'}} S_{p',m'}[k] e^{j\frac{2\pi}{N}kn'} \\ &\quad .c[((p-p')N_b + (m-m'))(N+L) + (n-n')] e^{j\frac{2\pi}{N}v_o t} \end{aligned} \tag{2.3}$$

In this thesis, we assume the channel to have a finite duration impulse response of order L, i.e. $c[n] = 0$ for $n < 0, n > L$. As depicted in Figure 2.2, ISI occurs only to received samples for n=-L to -1.

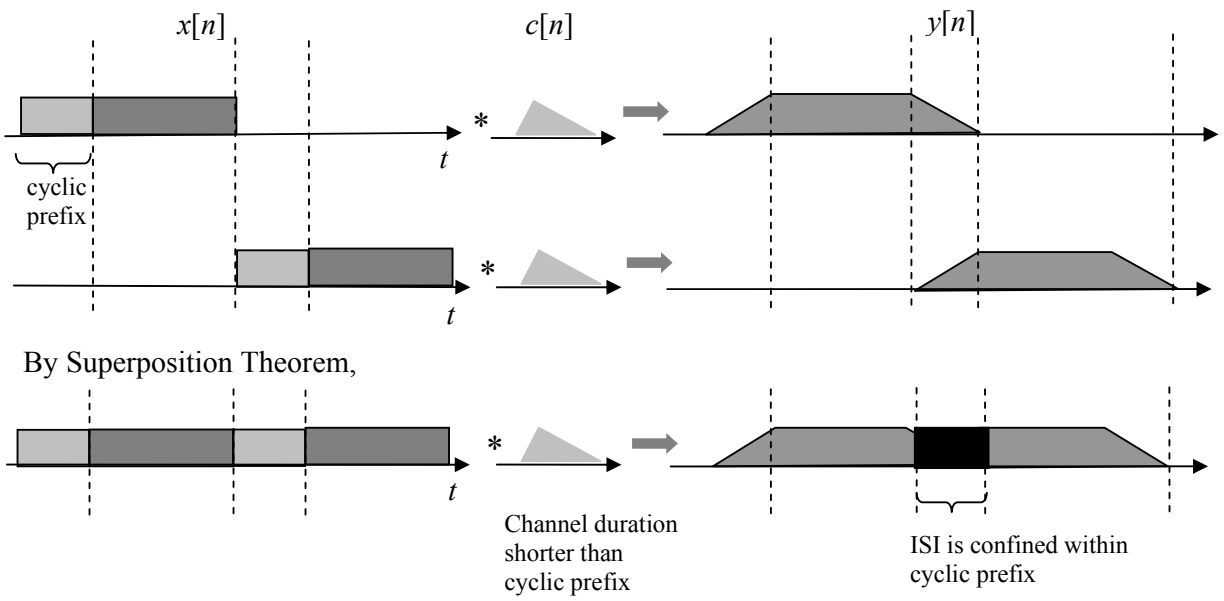

Figure 2.2 – Diagram depicting channel effects

At the receiver end, the cyclic prefix is removed. Hence, for n = 0, 1…N-1, the received samples, $y_{p,m}[n]$, are independent of all transmitted OFDM symbols, other than the corresponding m^{th} OFDM symbol in the p^{th} estimation block transmitted. Hence, (2.3) can be further simplified to yield

$$y_{p,m}[n] = \frac{1}{N} \sum_{k \in \Omega_{A,m'}} S_{p,m}[k] \mathrm{e}^{\mathrm{j}\frac{2\pi}{N}\nu_o t} \sum_{n'=-L}^{N-1} c[n-n'] e^{j\frac{2\pi}{N}kn'} \tag{2.4}$$

Replacing $r = n - n'$, and using the properties that $c[r]e^{-j\frac{2\pi}{N}kr}$ is periodic with N and $c[n] = 0$ for $n < 0, n > L$

$$\begin{aligned} \sum_{n'=-L}^{N-1} c[n-n'] e^{j\frac{2\pi}{N}kn'} &= \sum_{r=n+L}^{n-(N-1)} c[r] e^{j\frac{2\pi}{N}k(n-r)} \\ &= e^{j\frac{2\pi}{N}kn} \sum_{r=0}^{L} c[r] e^{-j\frac{2\pi}{N}kr} \\ &= e^{j\frac{2\pi}{N}kn} C[k] \end{aligned} \tag{2.5}$$

where $C[k]$ is the *N*-point DFT of the channel impulse response, $c[n]$. This results in the simple expression given by.

$$y_{p,m}[n] = \frac{1}{N} \sum_{k \in \Omega_{A,m'}} S_{p,m}[k] C[k] e^{j\frac{2\pi}{N} v_o t} \tag{2.6}$$

Hence, by appending a cyclic prefix of length greater than the channel impulse response at the start of the transmitted OFDM symbol and removing the cyclic prefix at the receiver end, ISI is effectively removed.

We assume the signal is received in the presence of AWGN, $w_{p,m}[n]$, which is complex noise with its real and complex components being uncorrelated (hence independent) and have equal variance of $\frac{1}{2}\sigma_W^2$. Hence the received signal samples are given by

$$r_{p,m}[n] = y_{p,m}[n] + w_{p,m}[n] \tag{2.6a}$$

The effects of a carrier frequency offset is corrected by multiplying the received time domain OFDM symbol with a frequency offset correction term thus we have,

$$z_{p,m}[n] = r_{p,m}[n] e^{-j\frac{2\pi}{N} v_c t} \tag{2.7}$$

For demodulation of the OFDM symbol, a *N*-pt DFT is applied to (2.7) and this gives

$$Z_{p,m}[k] = Y_{p,m}[k] + W_{p,m}[k] \tag{2.8a}$$

where

$$Y_{p,m}[k] = \sum_{n=0}^{N-1} y_{p,m}[n] e^{-j\frac{2\pi}{N} v_c [n+(pNb+m)(N+L)]} e^{-j\frac{2\pi}{N} kn} \tag{2.8b}$$

$$W_{p,m}[k] = \sum_{n=0}^{N-1} w_{p,m}[n] e^{-j\frac{2\pi}{N} v_c [n+(pNb+m)(N+L)]} e^{-j\frac{2\pi}{N} kn} \tag{2.8c}$$

Due to the circular symmetry of the complex AWGN, the statistics of $W_{p,m}[k]$ is unaffected by the frequency offset correction ν_c with $E\left[W_{p,m}[k]\right]=0$ and $E\left[\left|W_{p,m}[k]\right|^2\right]=N\sigma_w^2$.

From (2.5) and (2.8b), we can see that in the absence of a frequency offset, and consequently the frequency offset correction, the demodulated symbols are given by

$$Z_{p,m}[k]=C[k]S_{p,m}[k]+W_{p,m}[k] \tag{2.9}$$

Hence, provided that the channel impulse response is shorter than the cyclic prefix, the demodulated data symbol is simply the data symbol multiplied by the channel frequency response coefficient (evaluated at the sub-carrier frequency) corrupted by additive noise.

2.2 Effect of Frequency Offset

In this sub section, we examine the effect of a frequency offset to an OFDM system. We consider only a single block of N_b OFDM symbols by setting p=0 and omitting it in subsequent notation. In the scenario where no frequency offset correction is performed (ν_c = 0), after DFT demodulation of (2.6), we obtain the signal component as,

$$\begin{aligned} Y_m[k] &= \frac{1}{N}\sum_{n=0}^{N-1}\left(e^{j\frac{2\pi}{N}\nu_o[n+(N+L)m]}\sum_{k'\in\Omega_{A,m}}C[k']S_m[k']e^{j\frac{2\pi}{N}nk'}\right)e^{-j\frac{2\pi}{N}nk} \\ &= \frac{1}{N}e^{j\frac{2\pi}{N}\nu_o m(N+L)}\sum_{k'\in\Omega_{A,m}}C[k']S_m[k']dirc\left(\nu_o+k'-k\right). \end{aligned} \tag{2.10a}$$

where

$$dirc(x) = \sum_{n=0}^{N-1} e^{j\frac{2\pi}{N}xn} = \left(\frac{\sin \pi x}{\sin(\pi x / N)} \right) e^{j\frac{\pi}{N}(N-1)x} \tag{2.10b}$$

Eq (2.10b) is obtained using the property of Geometric progression.

The demodulated signal component (2.10a) can be expressed as a sum of the signal component, $X_m[k]$, and an intercarrier interference (ICI) component, $I_m[k]$,

where

$$X_m[k] = C[k]S_m[k]\left(\frac{1}{N} dirc(v_0) e^{j\frac{2\pi}{N}v_o m(N+L)} \right) \tag{2.11a}$$

$$I_m[k] = \frac{1}{N}\left(\sum_{\substack{k' \in \Omega_{A,m} \\ k' \neq k}} C[k']S_m[k'] dirc(v_o + k' - k) \right) e^{j\frac{2\pi}{N}v_o m(N+L)} \tag{2.11b}$$

The demodulated signal in the presence of AWGN, (2.8a), can be therefore be written as the sum of the useful signal, ICI and AWGN components.

$$Z_m[k] = X_m[k] + I_m[k] + W_m[k] \tag{2.12}$$

From (2.11a), we see that the presence of a frequency offset reduces the useful signal amplitude and this reduction is independent of the position of the activated carriers. In addition, the loss of orthogonality between the OFDM carriers causes leakage from other activated sub-carriers to sub-carrier with index *k*, introducing ICI as given by (2.11b).

Evaluating the statistical properties of $X_m[k]$ and $I_m[k]$,

$$E\left[\left|X_m[k]\right|^2\right] = E\left[\left|C[k]S_m[k]\right|^2\right]\left(\frac{1}{N^2}\left|dirc(v_0)\right|^2\right) \tag{2.13}$$

$$E\left[\left|I_m[k]\right|^2\right] = \frac{1}{N^2}\sum_{\substack{k_1\in\Omega_{A,m}\\ k_1\neq k}}\sum_{\substack{k_2\in\Omega_{A,m}\\ k_2\neq k}} E\left[C[k_1]S_m[k_1]C^*[k_2]S_m^*[k_2]\right] .dirc\left(v_o+(k_1-k)\right).dirc^*\left(v_o+(k_2-k)\right) \tag{2.14}$$

Assuming the data symbols are uncorrelated and have zero mean and variance σ_S^2, i.e.

$$E\left[C[k_1]S_m[k_1]\right] = 0 \tag{2.15a}$$

$$E\left[C[k_1]S_m[k_1]C^*[k_2]S_m^*[k_2]\right] = C^2\sigma_S^2\delta[k_1-k_2] \tag{2.15b}$$

where

$$C^2 = E\left[\left|C[k]\right|^2\right] \tag{2.15c}$$

Eq (2.14) can be simplified as

$$E\left[\left|I_m[k]\right|^2\right] = \mathrm{C}^2\sigma_S^2\left(\sum_{\substack{k'\in\Omega_{A,m}\\ k'\neq k}}\frac{1}{N^2}\left|\mathrm{dirc}\left(v_o+(k'-k)\right)\right|^2\right) \tag{2.16a}$$

or equivalently

$$E\left[\left|I_m[k]\right|^2\right] = \mathrm{C}^2\sigma_S^2\sin^2(\pi v_o)\left(\frac{1}{N^2}\sum_{\substack{k'\in\Omega_{A,m}\\ k'\neq k}}\frac{1}{\sin^2\left(\pi\left(v_o+k'-k\right)/N\right)}\right) \tag{2.16b}$$

using (2.10b) and $\sin^2\left[\pi\left(v_o+k'-k\right)\right] = \sin^2(\pi v_o)$

If the placement of the sub-carriers is arbitrary, then to minimise the average normalised ICI, the following needs to be minimised:

Define

$$ICI_{avg,m} = \frac{1}{N_{A,m}} \sum_{k \in \Omega_{A,m}} \left(\sum_{\substack{k' \in \Omega_{A,m} \\ k' \neq k}} \frac{1}{N^2} \left| dirc\left(\nu_o + (k' - k)\right) \right|^2 \right) \tag{2.17}$$

We examine the term in the summation in (2.17). Define

$$f(p) = \frac{1}{N^2} \left| dirc\left(\nu_o + p\right) \right|^2 \qquad p \in Z \tag{2.18}$$

This represents the ICI contribution by one activated sub-carrier on another, with p being the distance between them. Figure 2.3 shows the plots of the $f(p)$ for N=16, with $\nu_o = \pm 0.4$. The function is periodic with N and decreases sharply (superlinearly) as p increases towards $N/2$ before increasing sharply as p increases towards N.

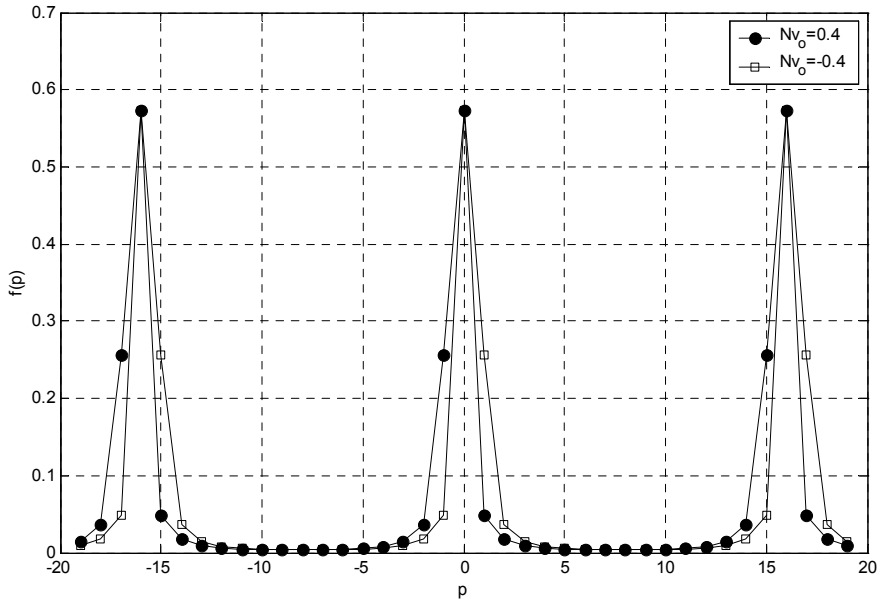

Figure 2.3 - Plot of $f(p)$

Consider a system with N sub-carriers and 2 activated sub-carriers, labelled A and B, which are placed at carrier index k_1 and k_2 respectively. We assume that the carrier frequency offset is within half a sub-carrier spacing but is equally probable to be positive or negative.

It is easy to see that the ICI power on A by B, $|I_m[k_1]|^2$, is equal to the ICI power on B by A, $|I_m[k_2]|^2$. The magnitude depends on the circular distance between the A and B, as given $\min[|k_1 - k_2| , N-|k_1-k_2|]$. $ICI_{Avg,m}$ is minimised when A and B are placed maximally apart at a distance of $N/2$ as shown in Figure 2.4a.

Next, we consider the case where there are 3 activated carriers, A, B, C placed at equidistance d apart as shown in Figure 2.4b. Since $f(d)- f(d+|\delta|) < f(d-|\delta|)- f(d)$, for $|\delta|< d$ and $d+|\delta|< N/2$, the penalty incurred in moving the sub-carrier A towards B by $|\delta|$ is higher than the reduction in penalty as sub-carrier A is being shifted away from the C by the same distance $|\delta|$. Using this argument, and fixing the placement of C, shifting either A or B or both would result in the increment in the $ICI_{avg,m}$.

For example, shifting A and B towards C would increase the ICI power on C by A and B (and vice versa). This increment is larger than the decrement in the ICI power on A and B (and vice versa) as they are shifted away from each other. Hence, $ICI_{avg,m}$ is minimum when A, B and C are placed at equidistance apart as in the case of 2 sub-carriers.

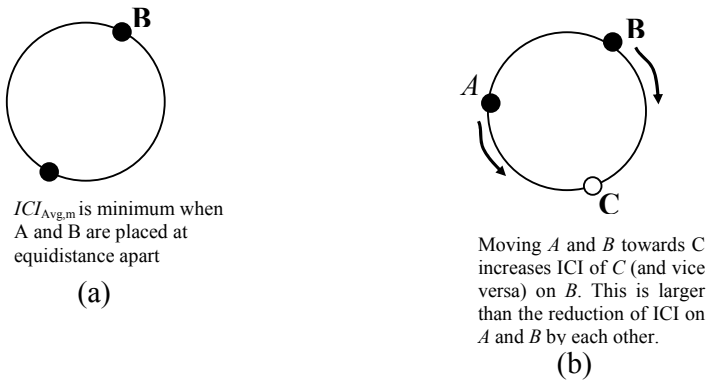

Figure 2.4 – Placement of activated sub-carriers to minimise ICI

As Figure 2.2 shows that the ICI contributed by a consecutive activated sub-carrier is much higher than that at other positions, this suggests that $ICI_{avg,m}$ is maximum when all the activated sub-carriers are consecutively placed and is minimum when the activated sub-carriers are equally spaced, if possible. However, since the sub-carriers can only be placed at discrete positions, the following approach to minimise $ICI_{avg,m}$ is proposed.

1) When the number of null sub-carriers exceeds the number of activated sub-carriers, the activated sub-carriers should be distributed at equidistance apart
2) When the number of activated sub-carriers exceeds the number of null sub-carriers, the null sub-carriers should be distributed at equidistance apart. This will minimise the number of consecutive activated subcarriers.

To test the validity of the approach, systems with N= 8 and 16, 17, 32 sub-carriers were considered. By varying the number of activated sub-carriers, $N_{A,m,}$ from 1 to N and testing all possible combinations of activated sub-carriers placement using (2.16), the suggested approach was found to be valid and minimises $ICI_{avg,m}$ among all possible sub-carrier placement.

In another simulation, a system with N=256, N_A = 128 and N_N =128 was considered. A group of N_X consecutive activated sub-carriers is placed next to a group of N_X consecutive null sub-carriers as shown in Figure 2.5. The values of N_X= 1, 2, 4, 8, 16, 32, 64 and 128 were tested.

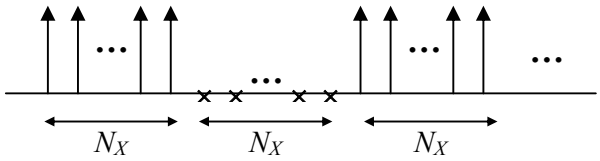

Figure 2.5 – Placement of sub-carriers for system with alternate clusters of activated and null sub-carriers

Figure 2.6 shows the plot of $ICI_{Avg,m}$ averaged over $\Omega_{A,m}$, against N_X for various frequency offsets, v_o =0.1, 0.2, 0.3, 0.4 and 0.5. The solid line represents the theoretical values while the markers denote the simulated results. It can be seen that $ICI_{Avg,m}$ is minimised when N_X=1, that is, when the activated and the null carriers are alternately placed. As more and more activated sub-carriers are clustered together, $ICI_{Avg,m}$ increases.

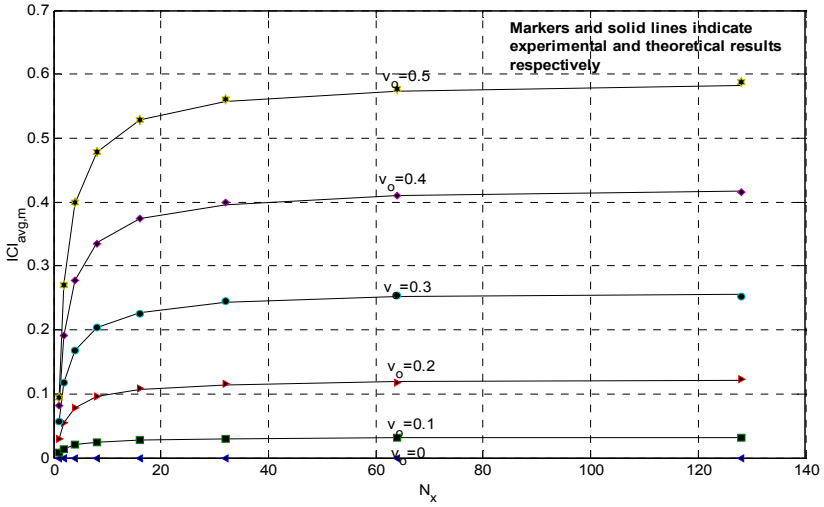

Figure 2.6 – Plot of $ICI_{Avg,m}$ against N_x.

Figure 2.7 shows the plot of variance of normalised $E[|I_m[k]|^2]$ among the activated sub-carriers, for various frequency offsets, $v_{o.}$ = 0.2, 0.3, 0.4 and 0.5. The variance is minimum for N_X =1 as there are no immediate neighbouring activated sub-carriers contributing significant *ICI*. For small values of *Nx*, the number of activated sub-carriers contributing significant *ICI* is small, causing the *ICI* to vary much among the activated sub-carriers. As N_X increases, the number of activated sub-carriers causing significant *ICI* increases and the averaging effect meant that this variation decreases

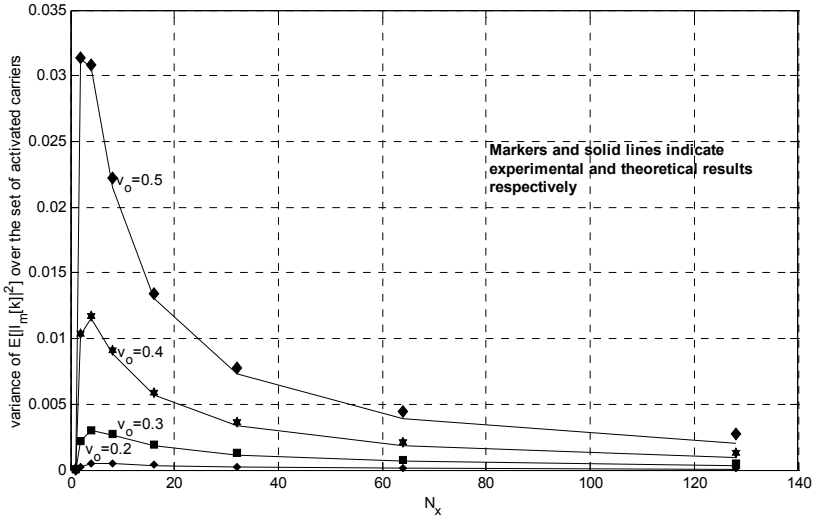

Figure 2.7 - Variance of normalised $E[|I_m[k]|]^2$ over $\Omega_{A,m}$ against N_X

2.3 Theoretical Bound for Signal-to-Interference Ratio

In [9], a numerical upper bound for $E\left[\left|I_m[k]\right|^2\right]$ was determined for case where the activated carriers are consecutively placed, i.e. $\Omega_{A,m} = \{0, 1, \ldots N_{A,m} - 1\}$ by considering that the summation in (2.16b) is bounded as follows

$$\sum_{\substack{k'=0 \\ k' \neq k}}^{N_{A,m}-1} \frac{1}{\sin^2\left(\pi\left(\nu_o + k' - k\right)/N\right)} \leq \sum_{\substack{k'=0 \\ k' \neq k}}^{N-1} \frac{1}{\sin^2\left(\pi\left(\nu_o + k' - k\right)/N\right)} \tag{2.19}$$

For the general system considered in this thesis, we note that we can still apply the similar inequality that

$$\sum_{\substack{k' \in \Omega_{A,m} \\ k' \neq k}} \frac{1}{\sin^2\left(\pi\left(\nu_o + k' - k\right)/N\right)} \leq \sum_{\substack{k'=0 \\ k' \neq k}}^{N-1} \frac{1}{\sin^2\left(\pi\left(\nu_o + k' - k\right)/N\right)} \tag{2.20}$$

Using the property that $\sin^2(\pi x/N)$ is periodic with period N, the summation is shown to be independent of k, as seen below.

$$\begin{aligned} \frac{1}{N^2} \sum_{\substack{k=0 \\ k \neq k}}^{N-1} \frac{1}{\sin^2\left(\pi\left(\nu_o + k' - k\right)/N\right)} &= \frac{1}{N^2} \sum_{\substack{p=k \\ p \neq 0}}^{N-1+k} \frac{1}{\sin^2\left(\pi\left(\nu_o + p\right)/N\right)} \\ &= \frac{1}{N^2} \sum_{\substack{p=1 \\ p \neq 0}}^{N-1} \frac{1}{\sin^2\left(\pi\left(\nu_o + p\right)/N\right)} \end{aligned} \tag{2.21}$$

For this analysis, we restrict the frequency offset ν_o to be within ±0.5 since exceeding this range, the correspondence between the demodulated sequence $Z_m[k]$ and the original sequence $X_m[k]$ for each k will not be distinguishable.

The summation (2.21) is an even function w.r.t v_o. and it has been numerically shown that the summation is monotonically increasing with $|v_o|$. In addition, its variation with N is negligible for $N \geq 256$ (usually less than 10^{-6}) [26]. By the numerical evaluation,

$$0.3333\Big|_{|v_o|=0} \leq \frac{1}{N^2}\sum_{p=1}^{N-1}\frac{1}{\sin^2\left(\pi\left(|v_o|+p\right)/N\right)} \leq 0.5947\Big|_{|v_o|=0.5} \tag{2.22}$$

Hence

$$E\left[\left(I_m[k]\right)^2\right] < \mathrm{C}^2\sigma_S^2\left(\frac{1}{N^2}\sum_{\substack{p\in\Omega_{A,m}\\ p\neq k}}\frac{1}{\sin^2\left(\pi\left(|v_o|+p\right)/N\right)}\right) \tag{2.23}$$

We define the average Signal to Interference Ratio as

$$SIR_{avg,m} = \frac{1}{N_{A,m}}\sum_{k\in\Omega_{A,m}}\left(\frac{E\left[\left|X_m[k]\right|^2\right]}{E\left[\left|I_m[k]+W_m[k]\right|^2\right]}\right) \tag{2.24}$$

Using the inequality (2.22),

$$\begin{aligned} SIR_{avg,m} &\geq \frac{1}{N^2}\frac{C^2\sigma_S^2\left|dirc\left(v_0\right)\right|^2}{0.5947\,C^2\sigma_S^2\sin^2\left(\pi v_0\right)+N^2\sigma_\eta^2} \\ &= \frac{1}{N^2}\frac{\left|dirc\left(v_0\right)\right|^2}{0.5947\sin^2\left(\pi v_0\right)+\dfrac{N^2\sigma_\eta^2}{C^2\sigma_S^2}} \\ &= \frac{1}{N^2}\left(\frac{\left|dirc\left(v_0\right)\right|^2}{0.5947\sin^2\left(\pi v_0\right)+\left(SNR\right)^{-1}}\right) \end{aligned} \tag{2.25}$$

where the signal to noise ratio is defined as $SNR = \dfrac{C^2 s^2}{N^2\sigma_\eta^2}$.

Figure 2.8 shows the simulated and the lower bound as given by (2.24) for a half loaded system with N=256, N_A = 128 and activated sub-carriers being consecutively placed. The results were averaged over 100 trials.

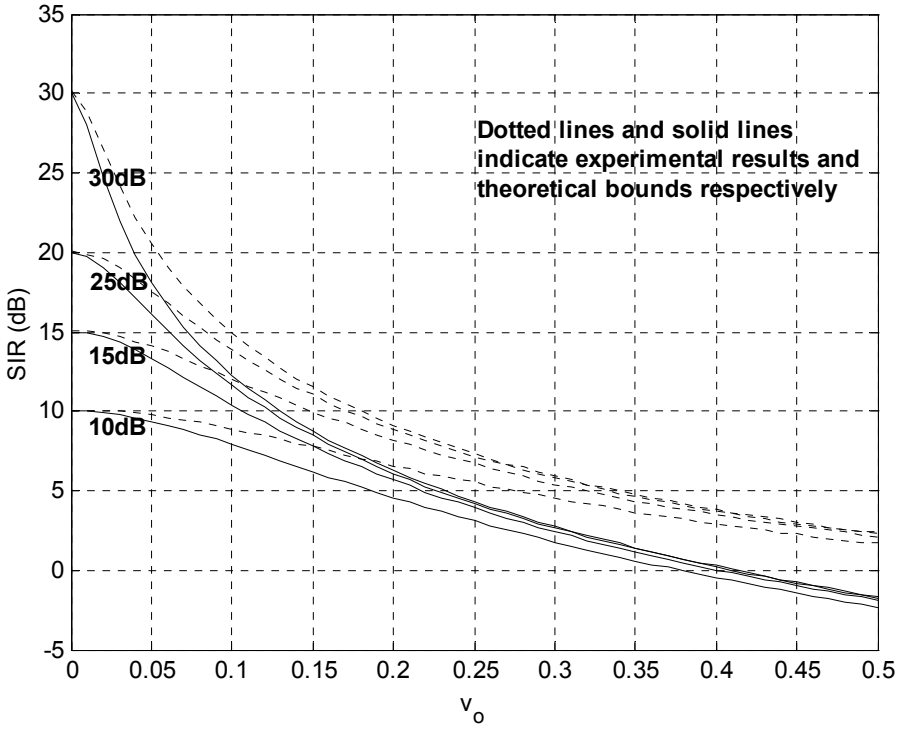

Figure 2.8 – Plot of SIR against v_o

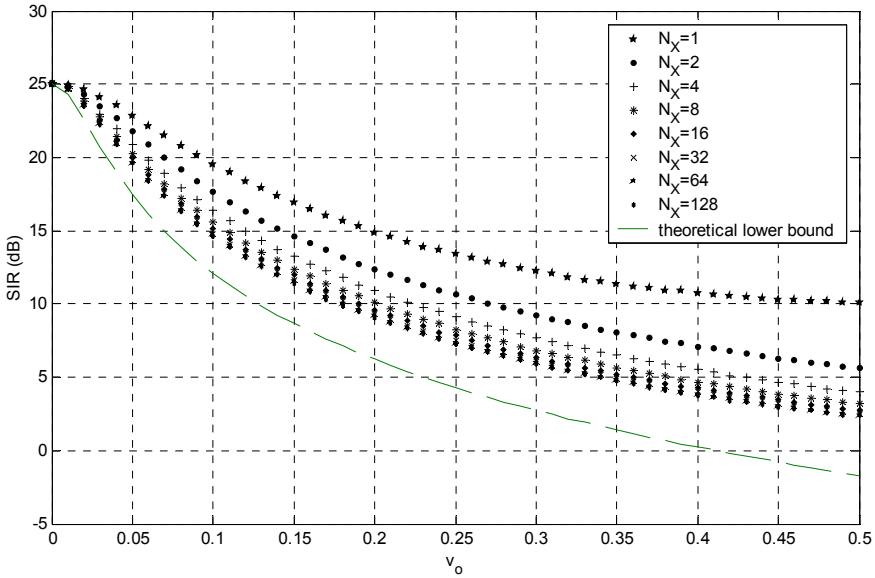

Figure 2.9 – Plot of SIR against v_o (for various N_X)

Figure 2.9 shows the simulated and the lower bound as given by (2.25) for a half loaded system with N=256, N_A = 128. The placement of the sub-carriers is as shown in Figure 2.4 where each cluster of N_X = 1, 2 , 4, 8, 16, 32, 64 and 128 activated sub-carriers alternates with the same number of null-sub-carriers. The results were averaged over 100 trials. As expected, the best *SIR* is achieved when the carriers are spaced equally apart. *SIR* decreases as the number of clustered activated sub-carriers, N_X increases. This reduction in *SIR* (with the increase in N_X) is less significant when N_X large.

Chapter 3

Estimation of carrier frequency offset

In this chapter, we formulate the deterministic maximum likelihood estimate (MLE) of the carrier frequency offset based on a received block of N_b OFDM symbols. As described in Chapter 2, the placement of the activated and null-carriers are arbitrary and are allowed to vary for each OFDM symbol. The criterions to avoid the ambiguity in the estimate are derived based on this setup and a physical interpretation of the criteria was given.

3.1 Deterministic maximum likelihood estimation of carrier frequency offset

The deterministic MLE approach was discussed in [23]. For our system where the activated and null sub-carriers are placed arbitrarily for each OFDM symbol, we follow the procedure in [24] to formulate the MLE of frequency offset, v_o.

We consider the channel, symbols and frequency offset, v_o, to be unknown but deterministic, and the *pdf* of received (observed) symbols is given by

$$p(\mathbf{r}|\mathbf{p},v_c)=\frac{1}{\left(\pi\sigma_W^2\right)^N}\exp\left(\frac{-1}{\sigma_W^2}\sum_{m=0}^{N_b-1}\sum_{n=0}^{N-1}\left|y_m[n]-\frac{1}{N}e^{j\frac{2\pi}{N}nv_c}\cdot\sum_{k'\in\Omega_{A,m}}p_{m,k'}\,e^{j\frac{2\pi}{N}nk'}\right|^2\right) \tag{3.1}$$

Or in matrix notation for easier manipulation

$$p(\mathbf{r}\mid\mathbf{p},v_c)=\frac{1}{\left(\pi\sigma_W^2\right)^N}\exp\left(\frac{-1}{\sigma_W^2}\sum_{m=0}^{N_b-1}\left\|\mathbf{r}_m-\frac{1}{N}diag(\boldsymbol{\theta})\mathbf{W}_m\mathbf{p}_\mathbf{m}\right\|^2\right) \tag{3.2}$$

where

$$\mathbf{r}=\begin{bmatrix}\mathbf{r_0} & \mathbf{r_1} & \mathbf{...} & \mathbf{r}_{N_b-1}\end{bmatrix}^{\mathrm{T}}$$

$$\mathbf{r}_m=\begin{bmatrix}r_m[0] & r_m[1] & ... & r_m[N-1]\end{bmatrix}^{\mathrm{T}}$$

$$\mathbf{p}=\begin{bmatrix}\mathbf{p}_0 & \mathbf{p}_1 & \mathbf{...} & \mathbf{p}_{N_b-1}\end{bmatrix}^{T}$$

$$\mathbf{p}_m=\begin{bmatrix}p_{m,0} & p_{m,1} & \cdots & p_{m,N_A-1}\end{bmatrix}^{\mathrm{T}}$$

$$p_{m,k'}=e^{j\frac{2\pi}{N}v_c(N+L)m}C[k']S_m[k']$$

$$\boldsymbol{\theta}=\begin{bmatrix}1 & e^{j\frac{2\pi}{N}v_c} & e^{j\frac{2\pi}{N}2v_c} & ... & e^{j\frac{2\pi}{N}(N-1)v_c}\end{bmatrix}^{T}$$

$$\mathbf{W_m}=\begin{bmatrix}w_{k',n}\end{bmatrix},$$

$$w_{k'n}=e^{j\frac{2\pi}{N}nk}$$

$n=0,1,...,N-1$; k'=0,1… N_A-1; $m=0,1,...,N_b-1$

k is the k'th element in $\Omega_{A,m}$

$\|.\|$ denotes the Frobenius Norm.

r contains the N_b observation vectors, each belonging to a OFDM symbol (time domain) with the cyclic prefix removed. We assume that the frequency offset, v_o remains constant over the N_b symbols. The MLE of ν_0 and $p_{m,k}$, denoted by $\hat{v}_0$ and $\hat{p}_{m,k}$ respectively, $k \in \Omega_{A,m}$, would therefore be given by the values of ν_c and $p_{m,k}$ that maximises (3.2).

This is equivalent to minimising the function

$$\sum_{m=0}^{N_b-1} \left\| \mathbf{r}_m - \left(\frac{1}{N} diag(\boldsymbol{\theta}) \mathbf{W}_\mathbf{m} \mathbf{p}_\mathbf{m} \right) \right\|^2 \tag{3.3}$$

Note that for a given value of ν_c, the function is quadratic w.r.t $p_{m,k}$. Hence, the minimum is obtained by finding the value of $p_{m,k}$ which causes the partial derivative to be zero.

$$\begin{aligned}
&\frac{\partial}{\partial \mathbf{R}_\mathbf{m}} \left(\left\| \mathbf{r}_m - \left(\frac{1}{N} diag(\boldsymbol{\theta}) \mathbf{W}_m \right) \mathbf{p}_\mathbf{m} \right\|^2 \right) \\
&= \frac{\partial}{\partial \mathbf{R}_\mathbf{m}} \left[\left(\mathbf{r}_m - \left(\frac{1}{N} diag(\boldsymbol{\theta}) \mathbf{W}_m \right) \mathbf{p}_\mathbf{m} \right)^H \left(\mathbf{r}_m - \left(\frac{1}{N} diag(\boldsymbol{\theta}) \mathbf{W}_m \right) \mathbf{p}_\mathbf{m} \right) \right] \\
&= -\frac{1}{N} \left[\left(\mathbf{r}_m - \left(\frac{1}{N} diag(\boldsymbol{\theta}) \mathbf{W}_m \right) \mathbf{p}_\mathbf{m} \right)^H \left(\frac{1}{N} diag(\boldsymbol{\theta}) \mathbf{W}_m \right) \right. \\
&\qquad \left. + \left(\frac{1}{N} diag(\boldsymbol{\theta}_m) \mathbf{W}_m \right)^H \left(\mathbf{r}_m - \left(\frac{1}{N} diag(\boldsymbol{\theta}_m) \mathbf{W}_m \right) \mathbf{p}_\mathbf{m} \right) \right] \\
&= -\frac{2}{N} \left(\frac{1}{N} diag(\boldsymbol{\theta}_m) \mathbf{W}_m \right)^H \left(\mathbf{r}_m - \left(\frac{1}{N} diag(\boldsymbol{\theta}_m) \mathbf{W}_m \right) \mathbf{p}_\mathbf{m} \right)
\end{aligned} \tag{3.4}$$

Equating (3.4) to zero and finding $\mathbf{p}_\mathbf{m}$.

$$\begin{aligned}\mathbf{p_m} &= \left(\left(\frac{1}{N}diag(\boldsymbol{\theta})\mathbf{W}_m\right)^H\left(\frac{1}{N}diag(\boldsymbol{\theta})\mathbf{W}_m\right)\right)^{-1}\left(\frac{1}{N}diag(\boldsymbol{\theta})\mathbf{W}_m\right)^H\mathbf{r}_m \\ &= N\left(\mathbf{W}_m^H diag(-\boldsymbol{\theta})diag(\boldsymbol{\theta})\mathbf{W}_m\right)^{-1}\left(diag(\boldsymbol{\theta})\mathbf{W}_m\right)^H\mathbf{r}_m \\ &= \left(diag(\boldsymbol{\theta})\mathbf{W}_m\right)^H\mathbf{r}_m\end{aligned} \tag{3.5}$$

where we use the property that $\left(\mathbf{W}_m^H diag(-\boldsymbol{\theta})diag(\boldsymbol{\theta})\mathbf{W}_m\right)^{-1} = \left(\mathbf{W}_m^H\mathbf{W}_m\right)^{-1} = \frac{1}{N}\mathbf{I}$

Finally, substituting (3.5) into (3.3), we obtain the MLE of the frequency offset, v_0, as the value of ν_c that minimises

$$\begin{aligned}&\sum_{m=0}^{N_b-1}\left\|\mathbf{r}_m - \left(\frac{1}{N}\left(diag(\boldsymbol{\theta})\mathbf{W}_m\right)\right)\left(diag(\boldsymbol{\theta})\mathbf{W}_m\right)^H\mathbf{r}_m\right\|^2 \\ &= \sum_{m=0}^{N_b-1}\left(\boldsymbol{\Gamma}^H\boldsymbol{\Gamma}\right) \\ &= \sum_{m=0}^{N_b-1}\left(\mathbf{r}_m^H\boldsymbol{\Lambda}^H\boldsymbol{\Lambda}\mathbf{r}_m\right) \\ &= \sum_{m=0}^{N_b-1}\mathbf{r}_m^H\left(I - \frac{1}{N}\left(diag(\boldsymbol{\theta})\mathbf{W}_m\mathbf{W}_m^H diag(-\boldsymbol{\theta})\right)^H\right)^2\mathbf{r}_m\end{aligned} \tag{3.6}$$

where

$$\boldsymbol{\Gamma} = \left(I - \left(\frac{1}{N}\left(diag(\boldsymbol{\theta})\mathbf{W}_m\right)\right)\left(diag(\boldsymbol{\theta})\mathbf{W}_m\right)^H\right)\mathbf{r}_m$$

$$\boldsymbol{\Lambda} = I - \frac{1}{N}\left(diag(\boldsymbol{\theta})\mathbf{W}_m\mathbf{W}_m^H diag(-\boldsymbol{\theta})\right)$$

Noting that $\boldsymbol{\Lambda}^H = \boldsymbol{\Lambda}$, and using the fact that the matrix is idem-potent, i.e. $\boldsymbol{\Lambda}^2 = \boldsymbol{\Lambda}$ we obtain the MLE of ν_0 as the value which minimises

$$\begin{aligned}&\sum_{m=0}^{N_b-1}\mathbf{r}_m^H\mathbf{r}_m - \mathbf{r}_m^H\left(\frac{1}{N}\left(diag(\boldsymbol{\theta})\mathbf{W}_m\mathbf{W}_m^H diag(-\boldsymbol{\theta})\right)^H\right)\mathbf{r}_m \\ &= \sum_{m=0}^{N_b-1}\left\|\mathbf{r}_m\right\|^2 - \frac{1}{N}\left\|\mathbf{W}_m^H diag(-\boldsymbol{\theta})\mathbf{r}_m\right\|^2\end{aligned} \tag{3.7}$$

or equivalently,

$$\arg\min_{v_c}\left(N\sum_{m=0}^{N_b-1}\sum_{n=0}^{N-1}\left|r_m[n]\right|^2 - \sum_{m=0}^{N_b-1}\sum_{k'\in\Omega_{A,m}}\left|\sum_{n=0}^{N-1}e^{-j\frac{2\pi}{N}nk'}\left(r_m[n]e^{-j\frac{2\pi}{N}v_c[(N+L)m+n]}\right)\right|^2\right) \tag{3.8}$$

Note that $z_m[n] = r_m[n]e^{-j\frac{2\pi}{N}v_c[(N+L)m+n]}$ as defined in (2.7).

Let the first and second term in (3.8) be *A* and *B* respectively, i.e.

$$A = N\sum_{m=0}^{N_b-1}\left(\sum_{n=0}^{N-1}\left|r_m[n]\right|^2\right) \tag{3.9a}$$

$$\begin{aligned} B &= N\sum_{m=0}^{N_b-1}\sum_{k'\in\Omega_{A,m}}\left|\sum_{n=0}^{N-1}z_m[n]e^{-j\frac{2\pi}{N}nk'}\right|^2 \\ &= \sum_{m=0}^{N_b-1}\sum_{k'\in\Omega_{A,m}}\left|Z[k']\right|^2 \end{aligned} \tag{3.9b}$$

.

A is independent of v_c and *B* is always greater or equal to zero. The MLE of v_0 can therefore be further simplified as

$$\hat{v}_0 = \arg\max_{v_c}\left(\sum_{m=0}^{N_b-1}\left|\sum_{k'\in\Omega_{A,m}}Z_m[k']\right|^2\right) \tag{3.10}$$

Rewriting (3.9a) and using the Parseval's Relation,

$$\begin{aligned} A &= N\sum_{m=0}^{N_b-1}\left(\sum_{n=0}^{N-1}\left|r_m[n]e^{-j2\pi v_c[(N+L)m+n]}\right|^2\right) \\ &= N\sum_{m=0}^{N_b-1}\left(\sum_{n=0}^{N-1}\left|z_m[n]\right|^2\right) \\ &= \sum_{m=0}^{N_b-1}\left(\sum_{k'=0}^{N-1}\left|Z_m[k']\right|^2\right) \\ &= B + D \end{aligned} \tag{3.11}$$

where

$$D = \sum_{k'\in\Omega_{N,m}}\left|Z_m[k']\right|^2 \tag{3.12}$$

Substituting (3.11) into (3.8), *B* will be eliminated and the MLE is equivalent to

$$\hat{v}_0 = \arg\min_{v_c}\left(\sum_{m=0}^{N_b-1}\sum_{k'\in\Omega_{N,m}} Z_m[k']^2\right) \tag{3.13}$$

Summary of Procedure for finding the MLE of v_o

1. First multiply the received samples, $r_m[n]$ with $e^{-j\frac{2\pi}{N}\nu_c[(N+L)m+n]}$, where ν_c is an estimate of the frequency offset, v_o , to yield the sequence $z_m[n]$
2. Perform a *N*-pt DFT on the corrected received sequence to yield $Z_m[k]$.
3. Conducting a search over v_c, the MLE of v_o is the value v_c that
   a) maximises the sum of the energy of the activated sub-carriers as given by $J_{A,z}(v_c)$ or equivalently
   b) minimises the sum of the energy of the null sub-carriers as given by $J_{N,z}(v_c)$.

   where

$$J_{A,z}(v_c) = \frac{1}{N_b}\sum_{m=0}^{N_b-1}\sum_{k'\in\Omega_{A,m}} \left|Z_m[k']\right|^2 \tag{3.15a}$$

$$J_{N,z}(v_c) = \frac{1}{N_b}\sum_{m=0}^{N_b-1}\sum_{k'\in\Omega_{N,m}} \left|Z_m[k']\right|^2 \tag{3.15b}$$

   The factor of $1/N_b$ is introduced to both (3.15a) and (3.15b) to normalise the cost function against the number of blocks used for estimation.

The equivalence in both MLE criterions is due to the fact that altering the frequency offset correct term simply introduces an evolving phase shift to the received samples. The energy of the received samples is unaltered by this evolving phase shift. The total energy of the received samples (in time domain) is the sum of the energy of the activated sub-carriers and the energy of the null sub-carriers (in frequency domain), scaled by a factor of N. Therefore, finding the value of v_c which maximises the energy of the activated sub-carriers is equivalent to finding the value of v_c which minimises the energy of the null sub-carriers.

We note that the cost functions given by (3.15a) and (3.15b) can also be viewed as functions of v_e defined as frequency offset estimate error, i.e. $v_e = v_c - v_o$. Figure 3.1 shows the normalised (by σ_S^2) cost functions as given by (3.15a) and (3.15b). The number of sub-carriers is N=64, the number of activated sub-carriers is N_A=32. The activated sub-carriers are placed consecutively from index 0 to 31. The channel is ideal and there is no additive noise.

It is obvious from the figures that the total null and activated sub-carrier energies add up to a constant (32) for all frequency offsets.

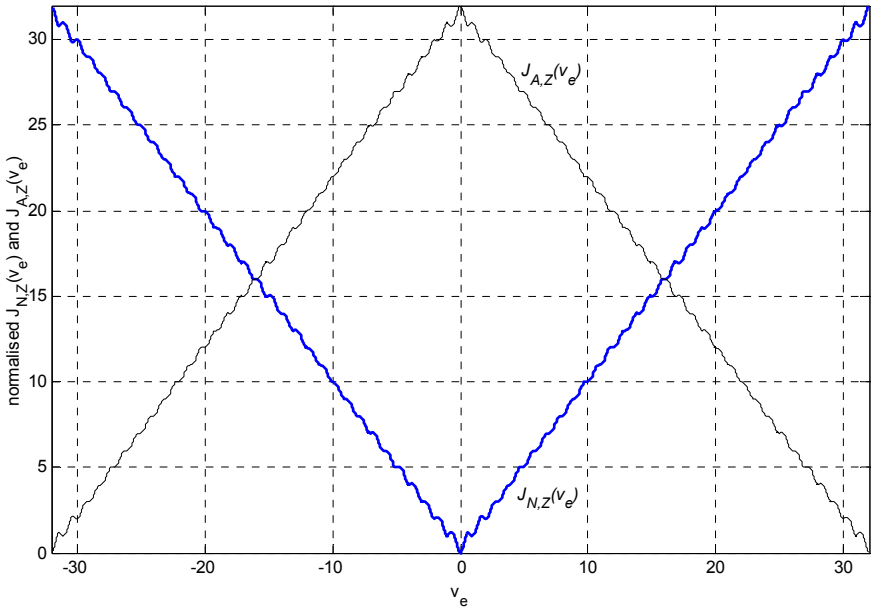

Figure 3.1 – Plot of cost functions based on total activated sub-carrier energy and total null-sub-carrier energy

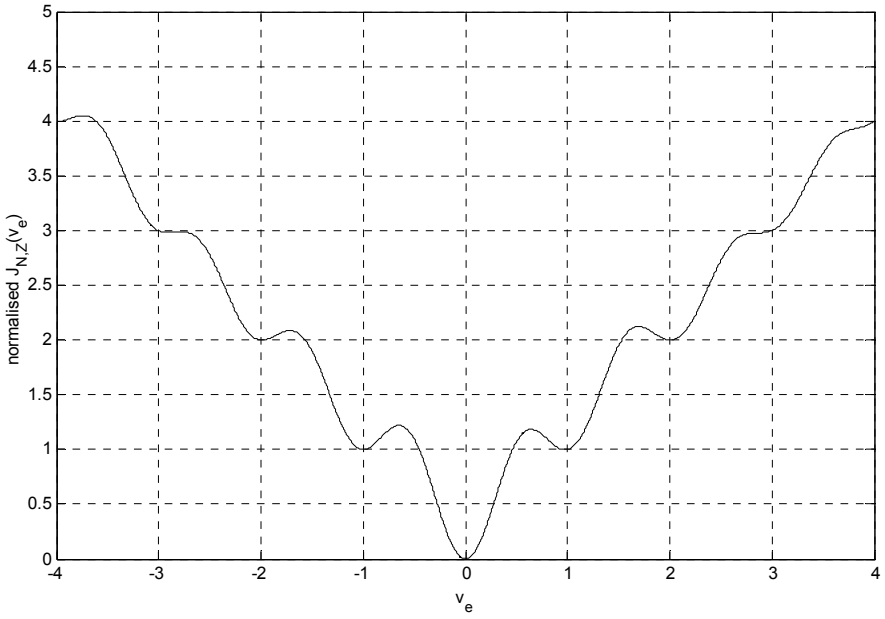

Figure 3.2 – Plot of cost function based on null-sub-carrier energy from v_e= -4 to 4

Figure 3.2 shows a close-up of the cost function for the frequency offset from -4 to +4. It can be seen that when the frequency offset v_e exceeds ±0.5, the cost function has multiple local minima, which poses a problem during the search for the global minima.

Since we allow the placement of the sub-carriers to be arbitrary, the general shape of the cost function would also vary depending on the placement of the null-sub-carriers. Figures 3.3 and 3.4 show 2 examples of the cost function for the same system with N=64, N_A=32 and the activated sub-carriers placed in the manner as marked by the solid bars at the bottom of each figure. Note that the shapes of the cost function are drastically different.

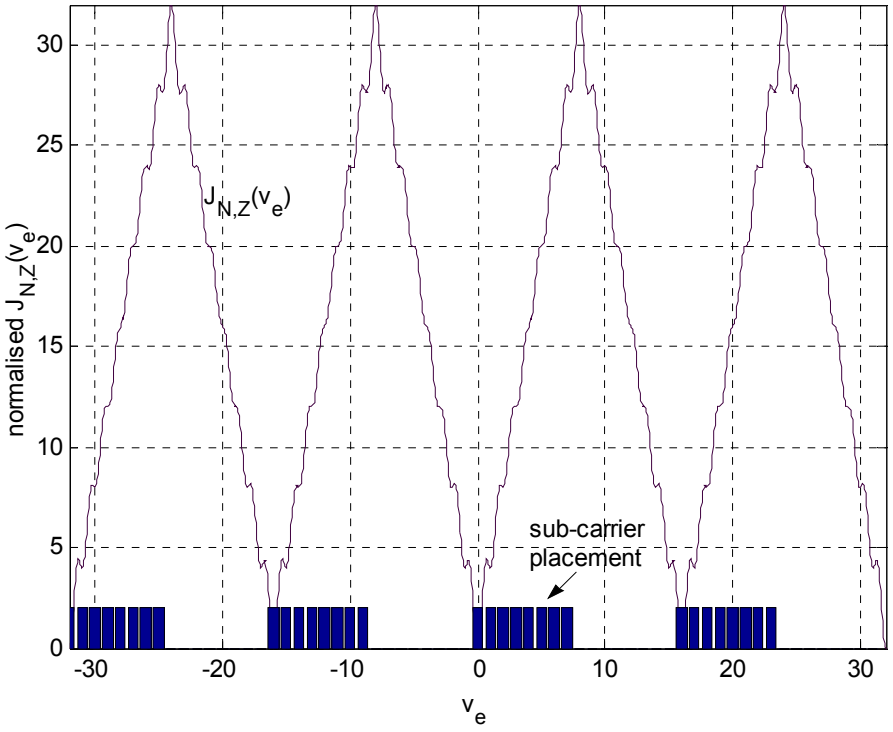

Figure 3.3 – Plot of cost function based on null-sub-carrier energy for a regular sub-carrier placement

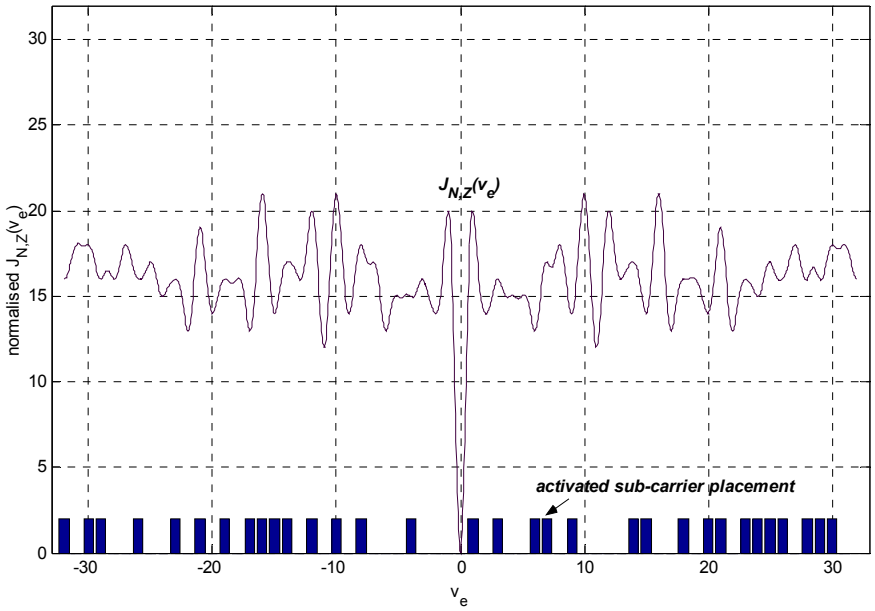

Figure 3.4 – Plot of cost function based on null-sub-carrier energy for a irregular sub-carrier placement

Since the cost function is the sum of all the energy that spills into the null sub-carriers, averaged over the N_b OFDM symbols, we examine the contribution of each null sub-carrier to the cost function. Denote the energy of the null sub-carrier placed at the l^{th} position, averaged over N_b blocks as

$$E_{N,z}(k,v_e)=\frac{1}{N_b}\sum_{m=0}^{N_b-1}\left|Z_m[k]\right|^2 \quad k\in\Omega_{N,m} \tag{3.16a}$$

Expanding (3.16a) using (2.8a), (2.8b) and (2.6), we obtain

$$\begin{aligned}
&E_{N,z}(k,v_e)\\
&=\frac{1}{N_b}\sum_{m=0}^{N_b-1}\left|\sum_{n=0}^{N-1}\left(\frac{1}{N}\sum_{k'\in\Omega_{A,m}}C[k']S_m[k']e^{j\frac{2\pi}{N}k'n}e^{-j\frac{2\pi}{N}v_e[(N+L)m+n]}\right)e^{-j\frac{2\pi}{N}nk}+W_m[k]\right|^2\\
&=\frac{1}{N_b}\sum_{m=0}^{N_b-1}\left|\frac{1}{N}\sum_{k'\in\Omega_{A,m}}C[k]S_m[k]\;dirc(k'-k-v_e)+W_m[k]\right|^2
\end{aligned} \tag{3.16b}$$

Based on the discussion in Chapter 2, it is expected that most of energy leakage would be in null sub-carriers that are positioned near the activated sub-carriers. Figure 3.5 shows the distribution of $E_{N,z}(k,v_e)$ w.r.t to k at a frequency offset of v_e = 0.4, for a system with N=256 sub-carriers, half loaded i.e. N_A = 128, and the activated carriers are positioned at sub-carrier indices {0,1,…127} for all OFDM symbols.

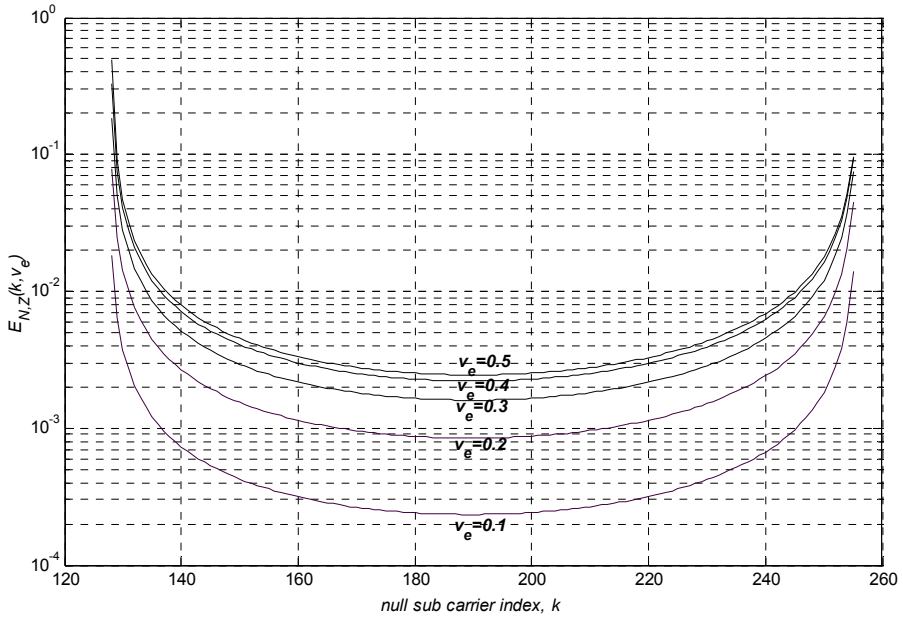

Figure 3.5 – Plot of $E_{N,z}(k,v_e)$ against null sub-carrier index, *k* for different *v*

For frequency offsets that are within a sub-carrier spacing, the contribution to the cost function decreases as the null sub-carriers become farther away from the activated sub-carriers, a simpler cost function can be adopted by only considering null sub-carriers that are placed within distance p to the nearest activated carrier. This cost function is therefore no longer a MLE based on the observed OFDM symbol (time domain). Figure 3.6 illustrates the null sub-carriers that will be used in the computation of the modified cost function.

Note that when the distance between 2 activated sub-carriers is less than p, all null sub-carriers (if they exist) in between the 2 activated sub-carriers would be used for the computation of the cost function.

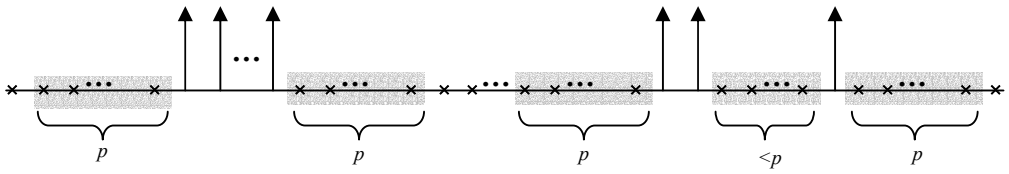

Figure 3.6 – Example of null sub-carriers used in computation of modified cost function

Denote this modified cost function as.

$$J_{N_{\mathrm{mod}},z}(v_e) := \frac{1}{N_b}\sum_{m=0}^{N_b-1}\left(\sum_{k\in\Omega_{N_{\mathrm{mod}},m}}|Z_m[k]^2\right) \tag{3.17}$$

where $\Omega_{N_{\mathrm{mod}},m}$ is a subset of $\Omega_{N,m}$. An element, k, in $\Omega_{N,m}$ is also an element in $\Omega_{N_{\mathrm{mod}},m}$ if $min[\,|k-l|, N-|k-l|\,] \le p$ for at least one element l in $\Omega_{A,m}$.

In the case of where the activated sub-carriers are placed from 0 to N_A-1, the null sub-carriers to be considered for the cost function would be N_A, $N_A + 1 \ldots N_A + p$ and $N_A + p$, $N_A + p + 1$, …, $N_A - 1$ and the cost function would be given by

$$J_{N_{\mathrm{mod}},z}(v_e) = \frac{1}{N_b}\sum_{m=0}^{N_b-1}\left[\sum_{k=N_A}^{N_A+p-1}|Z_m[k]^2 + \sum_{k=N-p}^{N-1}|Z_m[k]^2\right] \tag{3.18}$$

Figure 3.7 shows the sub-carriers that are being utilised for the cost function

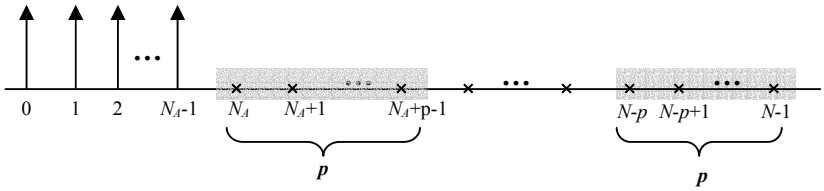

Figure 3.7 – null sub-carriers used in computation of $J_{N_{\mathrm{mod}},z}(v_e)$ in the case where the activated sub-carriers are placed consecutively from 0 to N_A–1

Figure 3.8 shows the plot of the modified cost function, $J_{N_{\mathrm{mod}},z}(v_e)$ against frequency offset (within a sub-carrier spacing) for different values of p. The placement of the activated sub-carriers is consecutive in this case. Note that in this case, as p increases, the increment to the cost function becomes less significant.

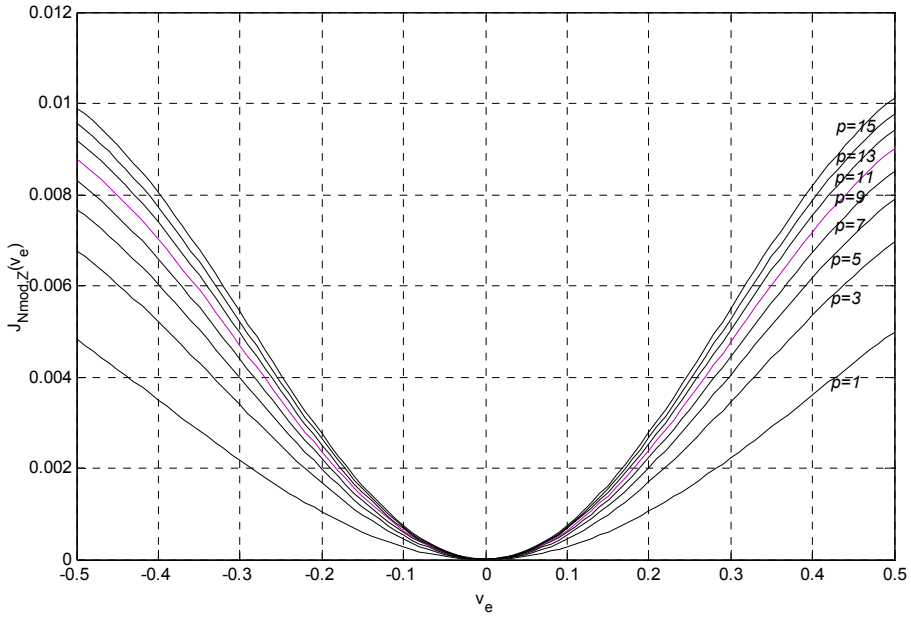

Figure 3.8 - Plot of $J_{N_{\mathrm{mod}},z}(v_e)$ for frequency offset within sub-carrier spacing

Figure 3.9 shows the plot of $J_{N_{\mathrm{mod}},z}(v_e)$ when the frequency offset is over the entire range for different values of p. Note that the modified cost function is different from that in Figure 3.1. The region where the modified cost function remains relatively constant corresponds to the frequency offsets where the activated sub-carriers are rotated into the bins of null sub-carriers that are not considered in the computation of the cost function. The modified cost function can still be used for offset estimation over the maximum range of $\pm N/2$ in this case, since there is only one global minimum point corresponding to v_e=0.

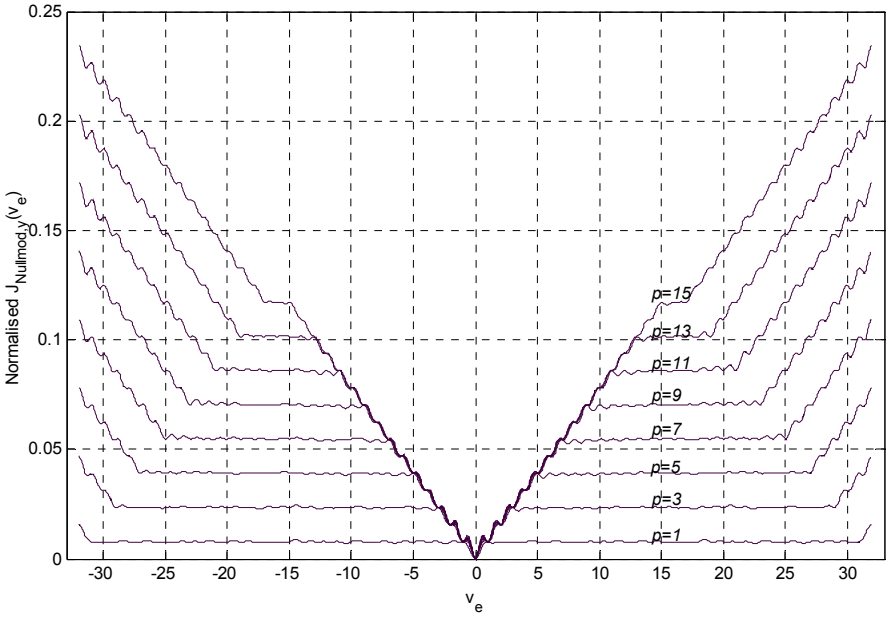

Figure 3.9 - Plot of $J_{N_{\mathrm{mod}},z}(v_e)$ for frequency offsets over entire range of -*N*/2 to *N*/2

.

3.2 Cost Function Ambiguity Due to Channel Nulls

In section 3.1, we formulated the MLE of v_o as the frequency offset correction, v_c, that maximises the energy of the activated sub-carriers or minimises the energy of the null sub-carriers. In this section, we discuss the ambiguity that may arise through the use of such energy cost functions. We adopt the same approach as in [23] for our general OFDM system, but use the null-carrier cost function instead of the activated carrier cost function that was used in [23]. The criteria we derived to avoid the cost function ambiguity are more generic and allows a greater degree of freedom in the placement of the activated sub-carriers within an OFDM symbol.

3.2.1 Derivation of criterions to avoid Cost Function Ambiguity

We consider the minimization of the cost function based on the null sub-carrier energy and examine the properties of $J_{N,z}(v_e)$ in the absence of noise. Note that

$$J_{N,Z}(v_e) = \sum_{k \in \Omega_{N,m}} E_{N,Z}(k, v_e).$$

Hence using (3.16c) where in the absence of additive noise,

$$J_{N,Z}(v_e) = \frac{1}{N_b} \sum_{m=0}^{N_b-1} \sum_{k \in \Omega_{N,m}} \left| \frac{1}{N} \sum_{k' \in \Omega_{A,m}} C[k'] S_m[k'] dirc(k' - k - v_e) \right|^2 \tag{3.19}$$

Denoting the set of all integers as **Z**, we note that

1) $dirc(x) = dirc(x \bmod N)$

2) $dirc(xN) = N;$ $\quad x \in \mathbf{Z}$

4) $dirc(x) = 0;$ $\quad x \in \mathbf{Z}$ and $x \bmod N \neq 0$

5) $0 < |dirc(x)| < N;$ $\quad x \notin \mathbf{Z}$

The cost function is always greater or equal to zero. It is minimum (at zero) when the frequency offset estimate error is zero, i.e. the frequency offset estimate coincides with the actual frequency offset. When the error is non-integer in value, the cost function is greater than zero.

However, in the case where the error is an integer, i.e. $v_e \in \mathbf{Z}$, it is possible that $J_{N,z}(v_e) = J_{N,z}(0) = 0$. This results in ambiguity in the cost function, since there are now multiple global minima. It is no longer possible to differentiate between the correct global minimum at v_e=0 and the other erroneous global minima.

To further investigate the occurrence of this problem, we use the property,

$$dirc(k'-k-v_e) = N\delta\left[(k'-k-v_e) \bmod \mathrm{N}\right], \qquad v_e \in \mathbf{Z} \tag{3.20}$$

And expanding (3.19) using (3.20)

$$\begin{aligned}
J_{N,z}(v_e) &= \frac{1}{N_b}\frac{1}{N^2}\sum_{m=0}^{N_b-1}\sum_{k'\in\Omega_{N,m}}\sum_{\substack{k_1\in\Omega_{A,m}\\ k_2\in\Omega_{A,m}}}\Psi_m[k_1]\Psi_m^*[k_2] \\
&\quad .dirc(k_1-k'-v_e)dirc^*(k_2-k'-v_e) \\
&= \frac{1}{N_b}\sum_{m=0}^{N_b-1}\sum_{k'\in\Omega_{N,m}}\sum_{\substack{k_1\in\Omega_{A,m}\\ k_2\in\Omega_{A,m}}}\delta\left[(k_1-k'-v_e) \bmod N\right]\delta\left[(k_2-k'-v_e) \bmod N\right] \\
&\quad .\Psi_m[k_1]\Psi_m^*[k_2]e^{j\frac{\pi}{N}(k_1-k_2)(N-1)} \\
&= \frac{1}{N_b}\sum_{m=0}^{N_b-1}\sum_{k'\in\Omega_{N,m}}\sum_{\substack{k_1\in\Omega_{A,m}\\ k_2\in\Omega_{A,m}}}\delta\left[(k_1-k'-v_e) \bmod N\right]\delta\left[(k_1-k_2) \bmod N\right] \\
&\quad .\Psi_m[k_1]\Psi_m^*[k_2]e^{j\frac{\pi}{N}(k_1-k_2)(N-1)} \\
&= \frac{1}{N_b}\sum_{m=0}^{N_b-1}\sum_{k'\in\Omega_{N,m}}\sum_{k\in\Omega_{A,m}}\delta\left[(k-k'-v_e) \bmod N\right]\left|\Psi_m[k]\right|^2
\end{aligned} \tag{3.21a}$$

where

$$\Psi_m[k] = C[k]S_m[k] \tag{3.21b}$$

At v=0, the cost function is zero because $\delta[(k-k')\bmod \mathrm{N}] = 0$ as $k \in \Omega_{A,m}$, $k' \in \Omega_{N,m}$ are elements from disjoint sets, i.e. $k - k' \neq 0$.

Ambiguity in the cost function arises when the cost function is zero for some non-zero integer value(s) of ν_e. Examining (3.21a) which involves a summation of terms, the ambiguity occurs when the product

$$|\Psi_m[k]|^2 \sum_{k' \in \Omega_{N,m}} \delta[(k-k'-v_e)\bmod \mathrm{N}] = 0 \tag{3.22}$$

$$\forall k \in \Omega_{A,m}$$

$$m = 0,1,...N_b - 1$$

This ambiguity is avoided if for at least one integer $k \in \Omega_{A,m}$, $m = 0,1\ldots N_b\text{-}1$,

$$\Psi_m[k] \neq 0; \qquad \text{AND} \tag{3.23a}$$

$$\sum_{k' \in \Omega_{N,m}} \delta[(k-k'-v_e)\bmod \mathrm{N}] \neq 0; \qquad \forall v_e \in \mathbf{Z} \tag{3.23b}$$

(3.23a) is solely dependent on the location of the channel zeros, since

$$\Psi_m[k] = C[k]S_m[k]; \qquad \text{AND}$$

$$S_m[k] \neq 0; \qquad \forall\ k \in \Omega_{A,m},\ m = 0,1\ldots N_b\text{-}1$$

For a FIR channel of order L, the discrete channel impulse response is given by

$$c[l] = \sum_{n=0}^{L} c_n \delta[l-n] \tag{3.24a}$$

$$C(z) = \sum_{n=0}^{L} c_n z^{-n} \tag{3.24b}$$

$$C[k] = C(z)\big|_{z=e^{j\frac{2\pi}{N}k}} \tag{3.24c}$$

$C(z)$ is a polynomial of order L and contains at most L zeros. Correspondingly the DFT of the channel impulse response, $C[k]$ can contain at most L zeros coinciding with the centre of the DFT frequency bins.

We assume that the channel to be unvarying over the N_b OFDM symbols. A FIR channel of order L would result in $\Psi_m[k]$ being zero for at most L **distinct** values of k, m =0, 1,… , N_b-1. Hence, to satisfy condition (3.23a), there must be at least L+1 **distinct** sub-carriers activated over the N_b OFDM symbols.

Condition (3.23b) is solely dependent on the allocation of the null and activated sub-carriers $k' \in \Omega_{N,m}$ and $k \in \Omega_{A,m}$ respectively for m = 0, 1…N_b-1. It is obvious that without even taking the allocation of the null sub-carriers into consideration, the maximum possible acquisition range is $v_e \in \left(-\frac{N}{2}, \frac{N}{2}\right]$ because of the modulus operation. This is consistent with the periodicity of the DFT operation.

When there are no channel zeros, i.e. (3.23a) is satisfied, ambiguity in the cost function would still arise, when for some integer value ν within the desired acquisition range,

$$(k' + v_e) \bmod N \in \Omega_{N,m} \; ; \qquad k' \in \Omega_{N,m} \; , \; m = 0, 1, ..., N_b - 1 \tag{3.25}$$

Note that there is no ambiguity in the cost function if condition (3.23a) and (3.23b) are both satisfied for at least one integer value of k. As shown earlier, it is possible to have a maximum of L channel zeros. In the scenario where the positions of the L channel zeros are unknown, ambiguity in the cost function can still be avoided by

(i) ensuring that the number of distinct activated sub-carriers over the N_b OFDM symbols is greater than L (satisfying (3.23a)); and

(ii) For all v_e within the desired acquisition range, $v_e \in (-M, M]$, $\sum_{k\in\Omega_{A,m}} \sum_{k'\in\Omega_{N,m}} \delta[(k-k'-v_e) \bmod \mathrm{N}] \neq 0$ for at least L+1 distinct integer values of k, m=0, 1,… ,N_b-1

Note that condition (i) would hold true if condition (ii) is satisfied. By further inspecting condition ii, the overall condition to avoid cost function ambiguity can be viewed and summarised in the following manner:

We denote the set of OFDM symbol indices where the k^{th} carrier is activated as Λ_k. For example, if the 8th sub-carrier is activated only in the 0th, 3rd, 5th and 27th OFDM symbols within the block of N_b symbols, $\Lambda_8 = \{0,3,5,27\}$.

For a FIR channel of order L, cost function ambiguity can be avoided if

there are more than L values of k, $k \in \bigcup_{m=0}^{N_b-1} \Omega_{A,m}$ *, such that, for each k, one or more integer values of k',* $k' \in \bigcup_{m\in\Lambda_{k'}} \Omega_{N,m}$ *, is found to satisfy the equality* $(k-k'-v_e) \bmod \mathrm{N} = 0$, $v_e \in (-M, M]$.

For the special case where the set of the activated sub-carriers is the same for each OFDM symbol as in [23], and denoting it by Ω_N, we can further simplify the criterion to:

$$\forall\ v_e \in (-M, M],\ \textit{the desired acquisition range,}\ (k - k' - v_e) \bmod \mathrm{N} = 0$$

$$\textit{for at least L+1 integer values of } k \notin \Omega_N \textit{ for } \forall\ k' \in \Omega_N$$

This criterion is equivalent to the criterion as developed in [23], which is based on maximising the energy of the activated sub-carriers. In a practical scenario, we would expect the system to have more activated sub-carriers than null sub-carriers. From a computational point of view, the criterion developed based on the cost function of null sub-carriers is less computational intensive than the criterion based on the cost function of activated sub-carriers.

3.2.2 Physical interpretation of the cost function ambiguity criterion

(i) Cost function ambiguity due to sub-carrier placement

In this section, we attempt to explain with illustrations, the physical interpretation of the criterion. We consider the case where the carrier placement is fixed for all N_b symbols used for estimation.

First we consider cost function ambiguity due to sub-carrier placement alone, i.e. the channel frequency response is constant. Ambiguity occurs when the placement of the activated and null sub-carriers is periodic with q, where q is an integer greater than one. For such placements, a rotation introduced due to an integer frequency offset causes both the original and rotated sub-carrier allocation pattern to be "identical" w.r.t the DFT bins.

An example is shown in Figure 3.10. Each black circle with a number indicates an activated sub-carrier and its corresponding index. Each white circle with a number indicates a null sub-carrier. The numbers within the big circle marks the DFT bins. The DFT bins that are shaded in grey mark the bins that will be used for the computation of the cost function.

As shown in the figure, an integer shirt of ±4 and ±8 will result in ambiguity in the cost function. This is further illustrated in Figure 3.11 where it can be seen that there are 4 global minima in the cost function.

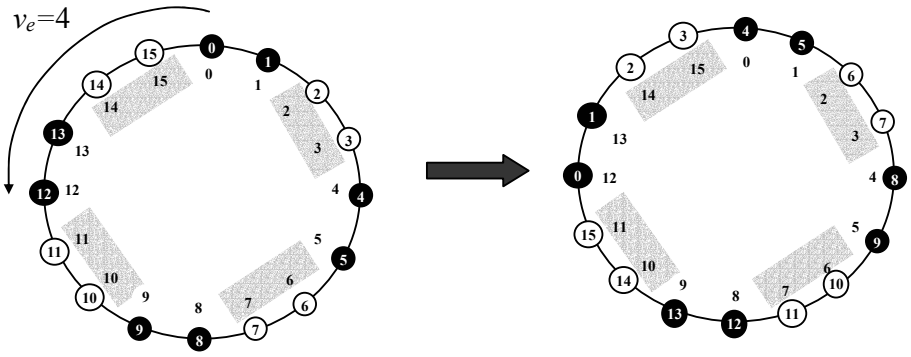

Figure 3.10 – Diagram illustrating the occurrence of cost function ambiguity due to periodicity in sub-carrier placement.

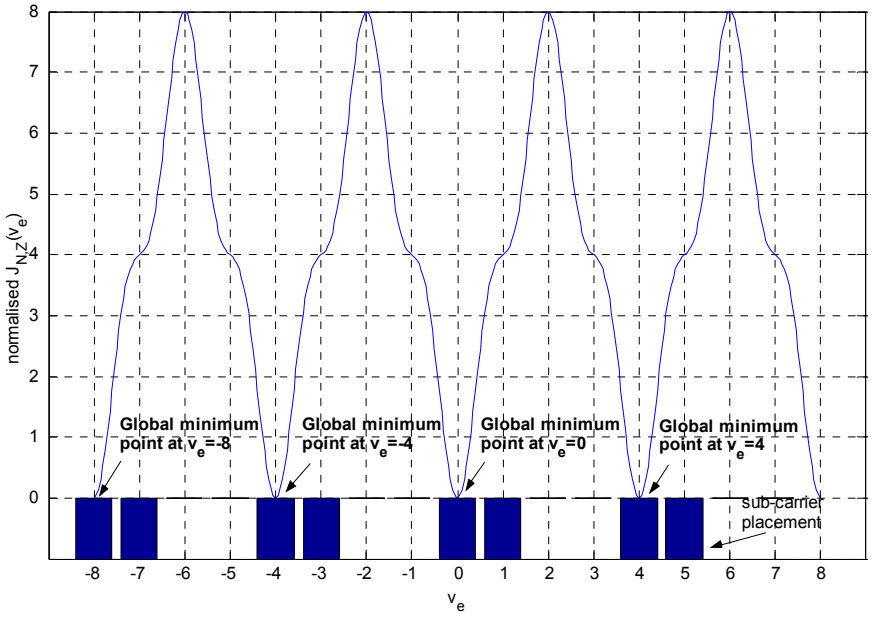

Figure 3.11 – Plot of cost function showing the presence of multiple global minima due to periodicity in sub-carrier placement

(ii) Cost function ambiguity due to channel nulls

Next we consider the cost function ambiguity due to the channel nulls. As an example, in a half loaded system with 8 sub-carriers where the null sub-carriers are placed consecutively, no ambiguity in cost function can possibly occur since carrier placement is not periodic. However, cost function ambiguity would occur when a channel null is present at activated sub-carrier index 0 for a frequency offset error of v_e=1, as shown in Figure 3.12.

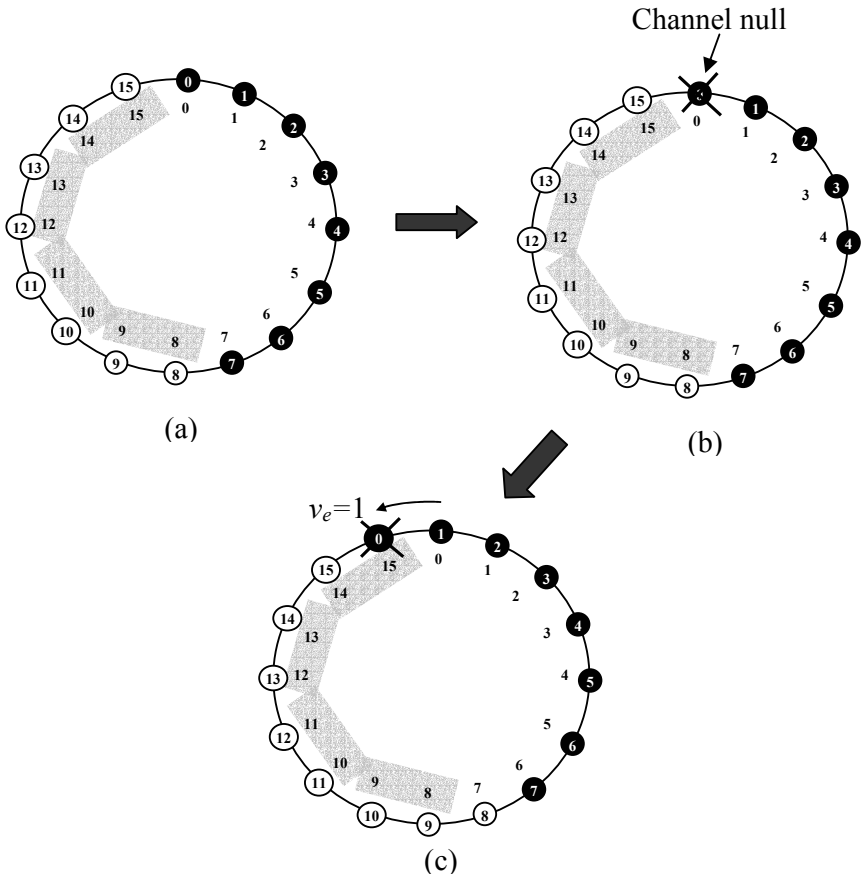

Figure 3.12 – Diagram illustrating the occurrence of cost function ambiguity due to channel nulls

Note: In the absence of noise, cost function ambiguity will still occur when activated sub-carrier index 0 is hit by a channel null. As illustrated in c, the computed cost function will be zero despite a frequency offset

Figure 3.13 shows the cost function in a frequency selective channel with zero AWGN. The channel amplitude response is shown in Figure 3.14. As illustrated, the channel null at sub-carrier index 0 causes the cost function to have multiple global minima at v_e=0 and 1 respectively, causing cost function ambiguity.

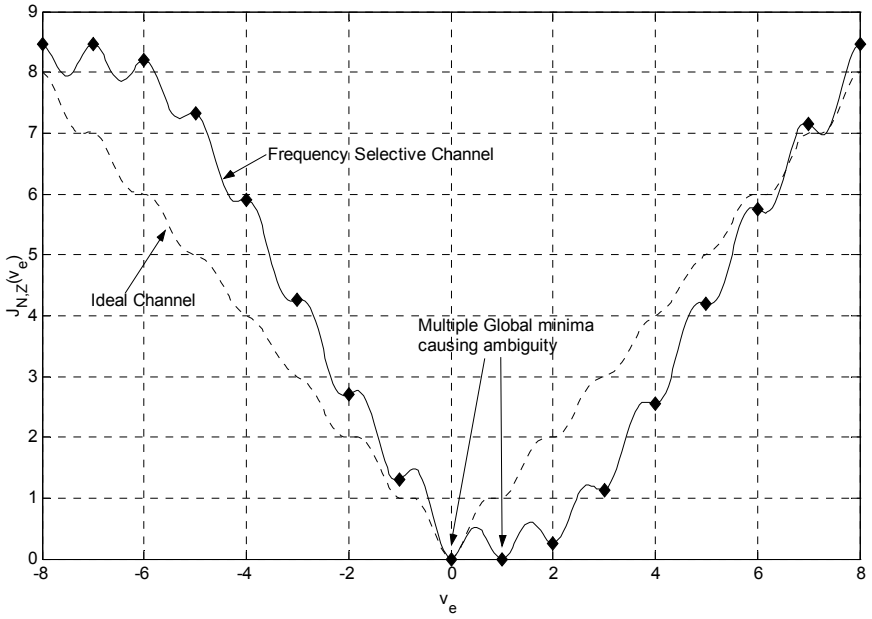

Figure 3.13 – Plot of cost function showing presence of multiple global minima due to channel null

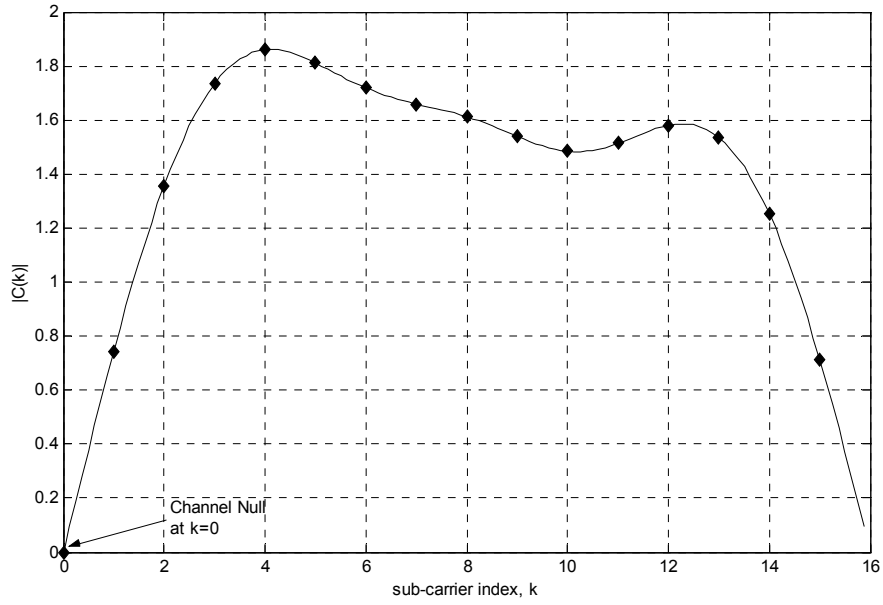

Figure 3.14 – Plot of Channel Amplitude Response, $|C[k]|$, cost function showing presence of multiple minima due to channel null

From Figure 3.12, the following can be concluded for a system with more than L activated sub-carriers placed consecutively from index i to $i + N_A$ -1. Cost function ambiguity will occur for a FIR channel of order L, if and only if there is a channel null at index i, or $i + N_A$ -1, or both.

Proof:

The set of activated sub-carriers is given by

$\Omega_A = \{i \bmod N, (i+1) \bmod N \ldots (i+N_A-1) \bmod N\}$ and

whereas the set of null-sub-carriers is given by

$\Omega_N = \{(i+N_A) \bmod N, (i+N_A+1) \bmod N \ldots (i+N-1) \bmod N\}$

In this specific case, the cost function in (3.21) is re-expressed as:

$$J_{N,Z}(v_e) = \frac{1}{N_b} \sum_{m=0}^{N_b-1} \sum_{k \in \Omega_A} |\Psi_m[k]|^2 \left(\sum_{k' \in \Omega_{N,m}} \delta[(k - k' - v_e) \bmod \mathrm{N}] \right) \tag{3.26}$$

Note that

$$\Psi_m[k] = 0 \text{ if } C[k] = 0 \qquad m = \{0, 1, 2, ..., N_b - 1\} \tag{3.27}$$

Denote the subset of elements in Ω_A that become elements in Ω_N, after a rotation of integer v_e (due to the frequency offset error) as $\widetilde{\Omega}_A$.

For v_e =0,

$$\widetilde{\Omega}_A = \{\phi\} \tag{3.28a}$$

For v =1,2… N/2-1,

$$\widetilde{\Omega}_A = \{i \bmod N, (i+1) \bmod N, \ldots, (i+v_e-1) \bmod N\} \tag{3.28b}$$

For v =-1-,2… N/2,

$$\widetilde{\Omega}_A = \{(i+N_A-1) \bmod N, (i+N_A) \bmod N, \ldots (i+N_A-v_e-1) \bmod N\} \tag{3.28c}$$

Hence the cost function (3.25) can be further simplified as

$$J_{N,Z}(v_e) = \frac{1}{N_b}\sum_{m=0}^{N_b-1}\sum_{k\in\widetilde{\Omega}_A}\left|S_m[k]\right|^2\left|C[k]\right|^2 \qquad (3.29)$$

If $C[k = i \bmod N] \neq 0$ and $C[k = (i + N_A - 1) \bmod N] \neq 0$, then cost function ambiguity is avoided because $k = i \bmod N$ or $k = (i + N_{Act} - 1) \bmod N$ are elements of $\widetilde{\Omega}_A$. Conversely, if cost function ambiguity is avoided, then there must be at least one element in $k \in \widetilde{\Omega}_A$ such that $C[k] \neq 0$. Note that for v_e=1 and -1, the only element in $\widetilde{\Omega}_A$ are i mod N and $(i+N_A-1)$ mod N respectively. As the magnitude of v_e increases, more elements are added into the set. Hence if cost function ambiguity is avoided, $C[k = i \bmod N] \neq 0$ and $C[k = (i + N_A - 1) \bmod N] \neq 0$.

Now we consider the more general case where the sub-carrier placement is allowed to vary over the N_b symbols. As an example, we consider the carrier placement in [13], where all activated sub-carriers are deterministically hopped by the same factor from one OFDM symbol to another.

We use the following example, depicted in Figure 3.15 to explain explicitly how hopping can cope with the cost function ambiguity problem. Consider the simple case where N_b=2 and the placement of the sub-carriers are from index 0 to 7 for the first OFDM symbol and 1 to 8 for the second symbol. Theoretically, the occurrence of a channel null at index 0 does not cause ambiguity to the cost function at a frequency offset error, v_e=1. This is because the activated sub-carrier with index 1 for the 2nd symbol will coincide with the DFT bin 0 used for the computation of the cost function.

Hence the cost function is non-zero in this case. To create cost function ambiguity, consecutive channel nulls have to occur at index 0 and 1 or at 7 and 8.

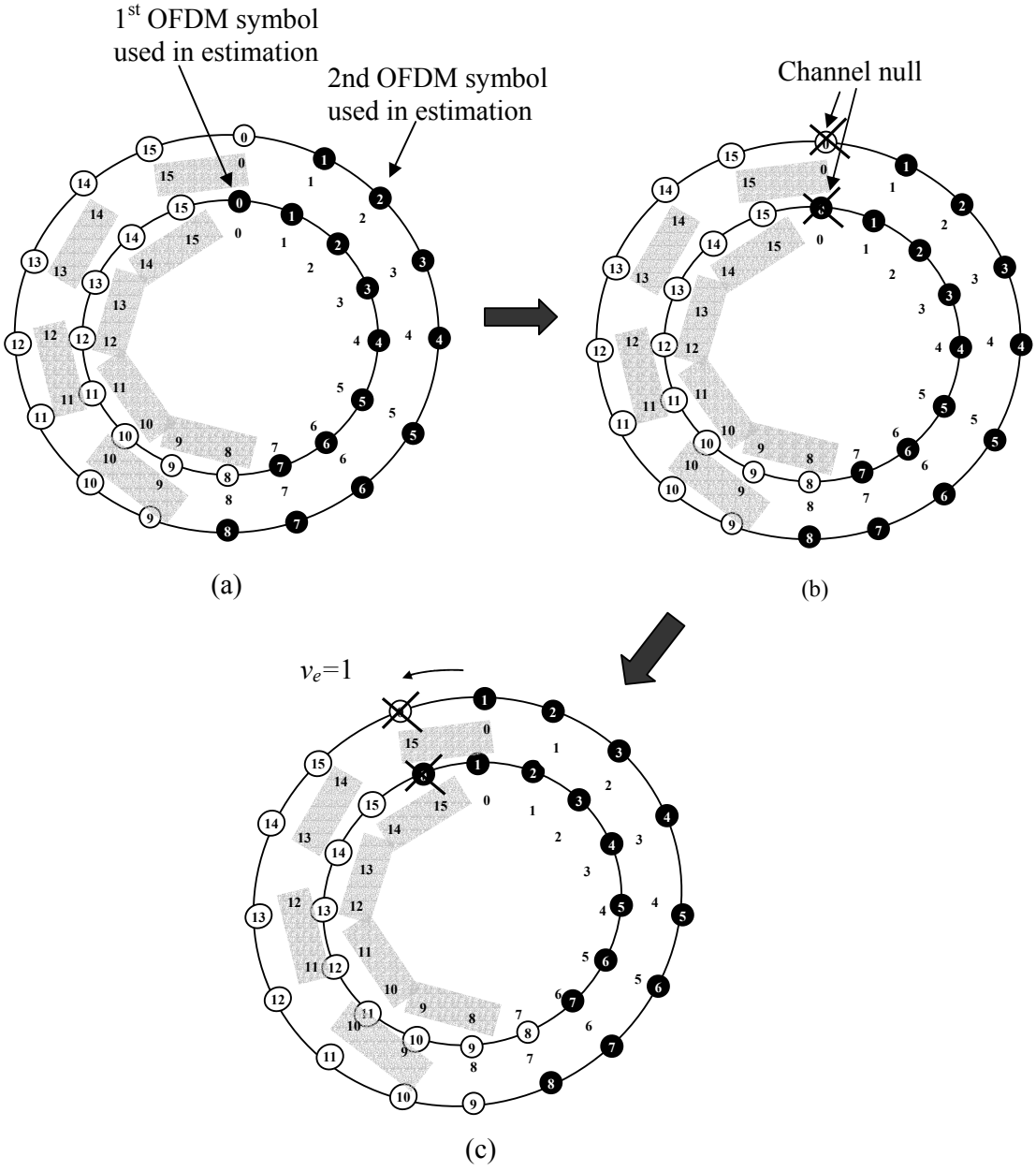

Figure 3.15 – Diagram illustrating why cost function ambiguity will not occur due to channel nulls when hopping is used

Note: In the absence of noise, cost function ambiguity will not occur in this case though activated sub-carrier index 0 of the 1st OFDM symbol is hit by a channel null. As illustrated in (c), the computed cost function will be zero because of the activated sub-carrier index 1 of the 2nd OFDM symbol coincides with the DFT bin 0 which is used for computation of the cost function

Using the above example, it can be seen that deterministically hopping the sub-carriers over the N_b OFDM symbols will provide additional robustness against the effects of channel nulls and prevent the cost function ambiguity as discussed.

Chapter 4

Performance of frequency offset estimator

In this chapter, the theoretical mean squared error of the maximum likelihood estimate of the frequency offset, v_o, is derived. The performance of the estimator is then tested under a AWGN and Rayleigh channel with an exponential power profile respectively and the results obtained are discussed.

4.1 Mean squared error of estimator

As shown in Chapter 3, the maximisation of the energy of the activated sub-carriers or the minimisation of the null sub-carriers proved to be equivalent using the Parseval's relation, would yield the same mean squared error (MSE). Hence, to determine the MSE of the estimator, we only need to examine the minimisation of the null sub-carrier energy, whose cost function is given by

$$J_{N,Z}(v_e) = \frac{1}{N_b}\sum_{m=0}^{N_b-1}\left(\sum_{k\in\Omega_{N,m}}\left|Z_m[k]\right|^2\right) \tag{4.1}$$

where v_e is the frequency offset error, $v_c - v_0$,

The derivation that follows is done using the small perturbation approach as in [13]. Here, we adopt a more general scenario where the arrangement of the activated and null sub-carriers is arbitrary. For the purpose of analysis, we denote the cost function in the absence of noise as

$$J_{N,Y}(v_e) = \frac{1}{N_b}\sum_{m=0}^{N_b-1}\left(\sum_{k\in\Omega_{N,m}}\left|Y_m[k]\right|^2\right) \tag{4.2}$$

and the perturbation in the cost function due to noise as

$$\Delta J_{N,Z}(v_e) = J_{N,Z}(v_e) - J_{N,Y}(v_e) \tag{4.3}$$

The true minimum point of the cost function in the absence of noise, $J_{N,Y}(v_e)$ is $v_e = 0$, or equivalently, when the frequency offset estimate is equal to the actual frequency offset v_0.

However, in the presence of noise, the cost function will be perturbed by $\Delta J_{N,Z}(v_e)$, which in turn perturbs the minimum point of the cost function. Denoting the mean squared error of the normalised frequency offset as $E\left[v_e^{\,2}\right]$ and considering the case where SNR is high, and the perturbation is small, and that we have localised the correct minima.

We rewrite the cost function in the presence of noise as the sum of the cost function in the absence of noise and the perturbation due to noise, i.e.

$$J_{N,Z}(v_e) = J_{N,Y}(v_e) + \Delta J_{N,Z}(v_e) \tag{4.4}$$

Using Taylor's expansion, we obtain

$$\left.\frac{dJ_{N,Z}(\Delta v_e)}{dv_e}\right|_{v_e=\Delta v_e} = \left.\frac{dJ_{N,Y}(v_e)}{dv_e}\right|_{v_e=0} + \left.\frac{d^2 J_{N,Y}(v_e)}{dv_e{}^2}\right|_{v_e=0} \Delta v_e + \ldots \left.\frac{d\Delta J_{N,Z}(v_e)}{dv_e}\right|_{v_e=0} + \left.\frac{d^2 \Delta J_{N,Z}(v_e)}{dv_e{}^2}\right|_{v_e=0} \Delta v_e + \ldots \tag{4.5}$$

Since the derivative of the cost function (1st term on R.H.S) and ignoring the 2nd order perturbation term, the 4th term on the R.H.S, we have

$$\Delta v \approx -\left(\left.\frac{d\Delta J_{N,Z}(v_e)}{dv_e}\right|_{v_e=0}\right) \Bigg/ \left(\left.\frac{d^2 \Delta J_{N,Y}(v_e)}{dv_e{}^2}\right|_{v_e=0}\right) \tag{4.6}$$

Since

$$J_{N,Z}(v_e) = \frac{1}{N_b}\sum_{m=0}^{N_b-1}\left(\sum_{k\in\Omega_{N,m}} |Y_m[k] + W_m[k]|^2\right) \tag{4.7a}$$

$$J_{N,Y}(v_e) = \frac{1}{N_b}\sum_{m=1}^{N_b}\left(\sum_{k\in\Omega_{N,m}} |Y_m[k]|^2\right) \tag{4.7b}$$

$$\Delta J_{N,Z}(v_e) = \frac{1}{N_b}\sum_{m=0}^{N_b-1}\left(\sum_{k\in\Omega_{N,m}} 2\,\mathrm{Re}\{\, Y_m[k]\; W_m{}^*[k]\} + |W_m[k]\,|^2\right) \tag{4.7c}$$

Expanding and ignoring 2nd order noise contributions, we obtain

$$\Delta J_{N,Z}(v_e) \approx \frac{1}{N_b}\sum_{m=0}^{N_b-1}\left(\sum_{k\in\Omega_{N,m}} 2\,\mathrm{Re}\{Y_m[k]\; W_m{}^*[k]\;\}\right) \tag{4.8}$$

Expanding (4.8) using (2.6),

$$\Delta J_{N,Z}(v_e) = \frac{2}{N_b}\sum_{m=0}^{N_b-1}\sum_{k\in\Omega_{N,m}} \mathrm{Re}\left(\sum_{n_1=0}^{N-1}\sum_{n_2=0}^{N-1}\rho_m[n_1]\gamma^*{}_m[n_2]e^{-j\frac{2\pi}{N}(v_e+k)(n_1-n_2)}\right)$$
$$= \frac{1}{N_b}\sum_{m=0}^{N_b-1}\sum_{k\in\Omega_{N,m}}\sum_{n_1=0}^{N-1}\sum_{n_2=0}^{N-1}\left(\rho_m[n_1]\gamma^*{}_m[n_2]+\rho^*{}_m[n_2]\gamma_m[n_1]\right)e^{-j\frac{2\pi}{N}(v_e+k)(n_1-n_2)}$$

(4.9a)

where

$$\rho_m[n] = y_m[n]e^{-j\frac{2\pi}{N}v_0 t} \tag{4.9b}$$

$$\gamma_m[n] = w_m[n]e^{-j\frac{2\pi}{N}v_0 t} \tag{4.9c}$$

Differentiating (4.9a)

$$\frac{\partial\Delta J_{N,Z}(v_e)}{\partial v_e}$$
$$= \frac{-j2\pi}{N_b}\sum_{m=0}^{N_b-1}\sum_{k\in\Omega_{N,m}}\sum_{n_1=0}^{N-1}\sum_{n_2=0}^{N-1}(n_1-n_2)\left(\rho_m[n_1]\gamma^*{}_m[n_2]+\rho^*{}_m[n_2]\gamma_m[n_1]\right)e^{-j\frac{2\pi}{N}(v_e+k)(n_1-n_2)}$$

(4.10a)

Evaluating at the true minimum pt, we obtain

$$\left.\frac{\partial\Delta J_{N,Z}(v_e)}{\partial v_e}\right|_{v_e=0}$$
$$= \frac{-j2\pi}{N_b}\sum_{m=0}^{N_b-1}\sum_{k\in\Omega_{A,m}}\sum_{n_1=0}^{N-1}\sum_{n_2=0}^{N-1}(n_1-n_2)\left(\rho_m[n_1]\gamma^*{}_m[n_2]+\rho^*{}_m[n_2]\gamma_m[n_1]\right)e^{-j\frac{2\pi}{N}k(n_1-n_2)}$$

(4.10b)

Taking the magnitude of (4.10b), squaring it and taking expectation, and after expansion, we obtain

$$E\left[\left|\left.\frac{\partial \Delta J_{N,Z}(v_e)}{\partial v_e}\right|_{v_e=0}\right|^2\right]$$
$$= \frac{4\pi^2}{N_b{}^2}\sum_{\substack{m_1=0\\ m_2=0}}^{N_b-1}\sum_{\substack{k_1\in\Omega_{N,m_1}\\ k_2\in\Omega_{N,m_2}}}\sum_{\substack{n_1=0\\ n_3=0}}^{N-1}\sum_{\substack{n_2=0\\ n_4=0}}^{N-1}(n_1-n_2)(n_3-n_4)e^{-j\frac{2\pi}{N}k_1(n_1-n_2)}e^{j\frac{2\pi}{N}k_2(n_3-n_4)}$$
$$.\left(E\left[\rho_{m_1}[n_1]\rho^*{}_{m_2}[n_3]\gamma^*{}_{m_1}[n_2]\gamma_{m_2}[n_4]\right]+E\left[\rho^*{}_{m_1}[n_2]\rho^*{}_{m_2}[n_3]\gamma_{m_1}[n_1]\gamma_{m_2}[n_4]\right]\right.$$
$$\left.+E\left[\rho_{m_1}[n_1]\rho_{m_2}[n_4]\gamma^*{}_{m_1}[n_2]\gamma^*{}_{m_2}[n_3]\right]+E\left[\rho^*{}_{m_1}[n_2]\rho_{m_2}[n_4]\gamma_{m_1}[n_1]\gamma^*{}_{m_2}[n_3]\right]\right) \quad (4.11)$$

Because of the circularity of the complex AWGN, the 2nd term and 3rd term in the expectation is equal to zero. i.e.

$$E\left[\gamma_{m_1}[n_1]\gamma_{m_2}[n_4]\right]=0 \quad (4.12a)$$

$$E\left[\gamma^*{}_{m_1}[n_2]\gamma^*{}_{m_2}[n_3]\right]=0 \quad (4.12b)$$

Hence,

$$E\left[\left|\left.\frac{\partial \Delta J_{N,Z}(v_e)}{\partial v_e}\right|_{v_e=0}\right|^2\right]$$
$$= \frac{4\pi^2}{N_b{}^2}\sum_{\substack{m_1=0\\ m_2=0}}^{N_b-1}\sum_{\substack{k_1\in\Omega_{N,m_1}\\ k_2\in\Omega_{N,m_2}}}\sum_{\substack{n_1=0\\ n_3=0}}^{N-1}\sum_{\substack{n_2=0\\ n_4=0}}^{N-1}(n_1-n_2)(n_3-n_4)e^{-j\frac{2\pi}{N}k_1(n_1-n_2)}e^{j\frac{2\pi}{N}k_2(n_3-n_4)}$$
$$.E\left[\rho_{m_1}[n_1]\rho^*{}_{m_2}[n_3]\gamma^*{}_{m_1}[n_2]\gamma_{m_2}[n_4]\right]+E\left[\rho^*{}_{m_1}[n_2]\rho_{m_2}[n_4]\gamma_{m_1}[n_1]\gamma^*{}_{m_2}[n_3]\right]$$
$$= \frac{4\pi^2}{N_b{}^2}\left\{\sum_{\substack{m_1=0\\ m_2=0}}^{N_b-1}\sum_{\substack{k_1\in\Omega_{N,m_1}\\ k_2\in\Omega_{N,m_2}}}\sum_{\substack{n_1=0\\ n_3=0}}^{N-1}\sum_{\substack{n_2=0\\ n_4=0}}^{N-1}(n_1-n_2)(n_3-n_4)e^{-j\frac{2\pi}{N}k_1(n_1-n_2)}e^{j\frac{2\pi}{N}k_2(n_3-n_4)}\right.$$
$$\left..E\left[\rho_{m_1}[n_1]\rho^*{}_{m_2}[n_3]\gamma^*{}_{m_1}[n_2]\gamma_{m_2}[n_4]\right]\right\}+$$
$$\frac{4\pi^2}{N_b{}^2}\left\{\sum_{\substack{m_1=0\\ m_2=0}}^{N_b-1}\sum_{\substack{k_1\in\Omega_{N,m_1}\\ k_2\in\Omega_{N,m_2}}}\sum_{\substack{n_1=0\\ n_3=0}}^{N-1}\sum_{\substack{n_2=0\\ n_4=0}}^{N-1}(n_1-n_2)(n_3-n_4)e^{-j\frac{2\pi}{N}k_1(n_1-n_2)}e^{j\frac{2\pi}{N}k_2(n_3-n_4)}\right. \quad (4.13)$$
$$\left..E\left[\rho^*{}_{m_1}[n_2]\rho_{m_2}[n_4]\gamma_{m_1}[n_1]\gamma^*{}_{m_2}[n_3]\right]\right\}$$

Interchanging m_1 & m_2, k_1 & k_2 and replacing n_3 with n_2, n_1 with n_4, the 1st term in the sum is observed to be equivalent to the 2nd term.

In addition, we assume the signal and noise components, $\rho_m[n]$ and $\gamma_m[n]$ are assumed to be uncorrelated. Therefore

$$E\left[\rho_{m_1}[n_1]\rho^*{}_{m_2}[n_3]\gamma^*{}_{m_1}[n_2]\gamma_{m_2}[n_4]\right] = E\left[\rho_{m_1}[n_1]\rho^*{}_{m_2}[n_3]\right]E\left[\gamma^*{}_{m_1}[n_2]\gamma_{m_2}[n_4]\right] \tag{4.14a}$$

Using (4.9b)

$$\begin{aligned}
&E\left[\rho_{m_1}[n_1]\rho^*{}_{m_2}[n_3]\right] \\
&= E\left[\rho_{m_1}[n_1]\rho^*{}_{m_2}[n_3]\right]\delta[m_1-m_2] \\
&= \frac{1}{N^2}E\left[\sum_{\substack{k_1\in\Omega_{A,m_1}\\ k_2\in\Omega_{A,m_1}}} \mathrm{C}[k_1]S_{m_1}[k_1]\, e^{-j\frac{2\pi}{N}n_1k_1}\mathrm{C}^*[k_2]S^*{}_{m_1}[k_2]\, e^{j\frac{2\pi}{N}n_3k_2}\right]\delta[m_1-m_2] \\
&= \frac{\sigma_S^2}{N^2}\sum_{\substack{k_1\in\Omega_{A,m_1}\\ k_2\in\Omega_{A,m_2}}} \mathrm{C}[k_1]\mathrm{C}^*[k_2]\,\delta[k_1-k_2]\delta[m_1-m_2]e^{-j\frac{2\pi}{N}n_1k_1}e^{j\frac{2\pi}{N}n_3k_2} \\
&= \frac{\sigma_S^2}{N^2}\sum_{k\in\Omega_{A,m_1}}\left|\mathrm{C}[k]\right|^2\delta[m_1-m_2]e^{-j\frac{2\pi}{N}(n_1-n_3)k}
\end{aligned} \tag{4.14b}$$

And

$$E\left[\gamma^*{}_{m_1}[n_2]\gamma_{m_2}[n_4]\right] = \delta[m_1-m_2]\delta[n_2-n_4]\sigma_w^2 \tag{4.14c}$$

Combining the results (4.14c) and (4.14b) and substituting into (4.13)

$$E\left[\left|\frac{\partial \Delta J_{N,Z}(v_e)}{\partial v_e}\Big|_{v_e=0}\right|^2\right] = \frac{8\pi^2}{N_b{}^2}\sum_{\substack{m_1=0\\m_2=0}}^{N_b-1}\sum_{\substack{k_1\in\Omega_{N,m_1}\\k_2\in\Omega_{N,m_2}}}\sum_{\substack{n_1=0\\n_3=0}}^{N-1}\sum_{\substack{n_2=0\\n_4=0}}^{N-1}(n_1-n_2)(n_3-n_4)e^{-j\frac{2\pi}{N}k_1(n_1-n_2)}e^{j\frac{2\pi}{N}k_2(n_3-n_4)}$$
$$.E\left[\rho_{m_1}[n_1]\rho^*{}_{m_2}[n_3]\right]E\left[\gamma^*{}_{m_1}[n_2]\gamma_{m_2}[n_4]\right]$$
$$= \frac{8\pi^2}{N_b{}^2}\sum_{\substack{m_1=0\\m_2=0}}^{N_b-1}\sum_{\substack{k_1\in\Omega_{N,m_1}\\k_2\in\Omega_{N,m_2}}}\sum_{\substack{n_1=0\\n_3=0}}^{N-1}\sum_{\substack{n_2=0\\n_4=0}}^{N-1}(n_1-n_2)(n_3-n_4)e^{-j\frac{2\pi}{N}k_1(n_1-n_2)}e^{j\frac{2\pi}{N}k_2(n_3-n_4)}$$
$$.\left(\frac{\sigma_S^2}{N^2}\sum_{k'\in\Omega_{A,m_1}}\left|\mathrm{C}[k']\right|^2 \mathrm{e}^{-j\frac{2\pi}{N}(n_1-n_3)l}\right)\sigma_w^2\delta[n_2-n_4]\delta[m_1-m_2]$$
$$= \frac{8\pi^2\sigma_S^2\sigma_w^2}{N^2N_b{}^2}\left\{\sum_{m=0}^{N_b-1}\sum_{\substack{k_1\in\Omega_{N,m}\\k_2\in\Omega_{N,m}}}\sum_{\substack{n_1=0\\n_3=0}}^{N-1}\left(\sum_{k'\in\Omega_{A,m}}\left|\mathrm{C}[k']\right|^2 \mathrm{e}^{-\mathrm{j}\frac{2\pi}{\mathrm{N}}(n_1-n_3)l}\right)\right.$$
$$\left.\left.\cdot\left(\sum_{n_2=0}^{N-1}(n_1-n_2)(n_3-n_2)e^{-j\frac{2\pi}{N}k_1(n_1-n_2)}e^{j\frac{2\pi}{N}k_2(n_3-n_2)}\right)\right\}\right.$$

(4.15)

After rearranging the terms,

$$E\left[\left|\frac{\partial \Delta J_{N,Z}(v_e)}{\partial v_e}\Big|_{v_e=0}\right|^2\right] = \frac{8\pi^2\sigma_w^2\sigma_S^2}{N_b^2N^2}\left\{\sum_{m=0}^{N_b-1}\sum_{k'\in\Omega_{A,m}}\left|\mathrm{C}[k']\right|^2\sum_{\substack{k_1\in\Omega_{N,m}\\k_2\in\Omega_{N,m}}}\right.$$
$$\left.\cdot\sum_{\substack{n_1=0\\n_2=0\\n_3=0}}^{N-1}(n_1-n_2)(n_3-n_2)e^{-j\frac{2\pi}{N}(n_1-n_3)k'}e^{-j\frac{2\pi}{N}k_1(n_1-n_2)}e^{j\frac{2\pi}{N}k_2(n_3-n_2)}\right\}$$

(4.16)

Proceeding in a similar approach, the cost function in the absence of noise is given by

$$J_{N,Y}(v_e) = \frac{1}{N_b}\sum_{m=0}^{N_b-1}\sum_{k\in\Omega_{N,m}}|Y_m[k]|^2$$
$$= \frac{1}{N^2 N_b}\sum_{m=0}^{N_b-1}\sum_{k\in\Omega_{N,m}}\sum_{\substack{n_1=0\\n_2=0}}^{N-1}\sum_{\substack{k_1'\in\Omega_{A,m}\\k_2'\in\Omega_{A,m}}} C[k_1']C^*[k_2']S_m[k_1']S_m^*[k_2']\, e^{-j\frac{2\pi}{N}\left[\left(n_1k_1'-n_2k_2'\right)+(v_e+k)(n_1-n_2)\right]}$$

(4.17)

And doing a double differentiation on (4.17), we obtain

$$\frac{\partial^2 J_{N,Y}(v_e)}{\partial v_e^{\,2}}$$
$$= \frac{-4\pi^2}{N_b N^2}\sum_{m=0}^{N_b-1}\sum_{k\in\Omega_{N,m}}\sum_{\substack{n_1=0\\n_2=0}}^{N-1}\sum_{\substack{k_1'\in\Omega_{A,m}\\k_2'\in\Omega_{A,m}}}(n_1-n_2)^2 C[k_1']C^*[k_2']S_m[k_1']S_m^*[k_2']e^{-j\frac{2\pi}{N}\left[\left(n_1k_1'-n_2k_2'\right)+(v_e+k)(n_1-n_2)\right]}$$

(4.18)

Evaluating (4.18) at v=0, taking magnitude, squaring it and finally taking expectation yields

$$E\left[\left|\frac{\partial^2 J_{N,Y}(v_e)}{\partial v_e^{\,2}}\right|^2\Bigg|_{v_e=0}\right] = \frac{16\pi^4}{N_b^{\,2}N^4}\sum_{\substack{m_1=0\\m_2=0}}^{N_b-1}\sum_{\substack{n_1=0\\n_2=0\\n_3=0\\n_4=0}}^{N-1}\left(\sum_{\substack{k_1\in\Omega_{N,m_1}\\k_2\in\Omega_{N,m_2}}} e^{-j\frac{2\pi}{N}k_1(n_1-n_2)}e^{j\frac{2\pi}{N}k_2(n_3-n_4)}\right)$$
$$\left(\sum_{\substack{k_1'\in\Omega_{A,m_1}\\k_2'\in\Omega_{A,m_1}}}\sum_{\substack{k_3'\in\Omega_{A,m_2}\\k_4'\in\Omega_{A,m_2}}}(n_1-n_2)^2(n_3-n_4)^2 e^{j\frac{2\pi}{N}n_1k_1'}e^{-j\frac{2\pi}{N}n_2k_2'}e^{-j\frac{2\pi}{N}n_3k_3'}e^{j\frac{2\pi}{N}n_4k_4'}\right.$$
$$\left.E\left[C[k_1']C^*[k_2']S_{m_1}[k_1']S_{m_1}^*[k_2']C^*[k_3']C[k_4']S_{m_2}^*[k_3']S_{m_2}[k_4']\right]\right)$$

(4.19)

And after much simplification,

$$E\left[\left|\frac{\partial^2 J_{null,y}(v)}{\partial v^2}\right|^2\Bigg|_{v=0}\right] = \frac{16\pi^4\sigma_S^4}{N_b{}^2N^4}\sum_{m=0}^{N_b-1}\sum_{k\in\Omega_{N,m_1}}\sum_{k'\in\Omega_{A,m}}|\mathrm{C}[k']|^2 \cdot\sum_{\substack{n_1=0\\n_2=0}}^{N-1}\left((n_1-n_2)^2 e^{-j\frac{2\pi}{N}(k-k')(n_1-n_2)}\right)^2 \tag{4.20}$$

Dividing (4.16) with (4.20), and some further simplification, we obtain,

$$E\left[(\Delta v)^2\right]\approx\left[\frac{4\pi^2\sigma_S^2}{N^3\sigma_N^2}\sum_{m=0}^{N_b-1}\sum_{k\in\Omega_{N,m}}\sum_{k'\in\Omega_{A,m}}\left|\mathrm{C}[k']\right|^2\left(\sum_{\substack{n_1=0\\n_2=0}}^{N-1}(n_1-n_2)^2\,\mathrm{e}^{-j\frac{2\pi}{N}(k-k')(n_1-n_2)}\right)\right]^{-1} \tag{4.21}$$

Using the relation

$$\sum_{\substack{n_1=0\\n_2=0}}^{N-1}(n_1-n_2)^2\,e^{-j\frac{2\pi}{N}(k-k')(n_1-n_2)} = \sum_{n=-N}^{N}\left(N-|n|\right)n^2\,e^{j\frac{2\pi}{N}(k-k')n} \tag{4.22}$$

We can express (4.21) as

$$E\left[(\Delta v_e)^2\right]\approx\left[\frac{4\pi^2\sigma_S^2}{N^3\sigma_N^2}\sum_{m=0}^{N_b-1}\sum_{k\in\Omega_{N,m}}\sum_{k'\in\Omega_{A,m}}\left|\mathrm{C}[k']\right|^2\sum_{n=-N}^{N}\left(N-|n|\right)n^2\,\mathrm{e}^{\mathrm{j}\frac{2\pi}{\mathrm{N}}(k-k')n}\right]^{-1}$$
$$=\left[\frac{8\pi^2\sigma_S^2}{N^3\sigma_N^2}\sum_{m_1=0}^{N_b-1}\sum_{k\in\Omega_{N,m}}\sum_{k'\in\Omega_{A,m}}\left|\mathrm{C}[k']\right|^2\sum_{n=1}^{N}\left(N-|n|\right)n^2\cos\left(\frac{2\pi}{N}(k-k')n\right)\right]^{-1} \tag{4.23}$$

We note that the *MSE* of the estimator is dependent on the number of blocks used for the estimator and for a fixed sub-carrier allocation, the *MSE* is inversely proportional to the number of OFDM symbols used in estimation. i.e.

$$E\left[(\Delta v_e)^2\right]=\left[\frac{8\pi^2\sigma_S^2}{N_bN^3\sigma_N^2}\sum_{k_1\in\Omega_N}\sum_{k'\in\Omega_A}|C[k']|^2\sum_{n=1}^{N}\left(N-|n|\right)n^2\cos\left(\frac{2\pi}{\mathrm{N}}(k-k')n\right)\right]^{-1} \tag{4.25}$$

where Ω_A and Ω_N are the set of activated and null sub-carriers respectively.

4.2 Performance of estimator in a AWGN Channel

Simulations were carried out to test the performance of estimator in an AWGN channel and the experimental and theoretical results obtained were compared. Trends observed are highlighted. In the experiments, the *SNR* is defined as $\frac{N_A^2 \sigma_S^{\ 2}}{\sigma_\eta^2}$.

4.2.1 *MSE* against SNR

In this simulation, a system with N=64, N_A=32, with different estimation block sizes, N_b=1, 4, 16 and 64 was tested for an AWGN channel. The activated sub-carriers are placed consecutively. Figure 4.1 shows the plot of the *MSE* of v_c against *SNR*. The solid lines show the experimental curves while the dashed lines show the theoretical curves for the experiment conducted over 1600 trials.

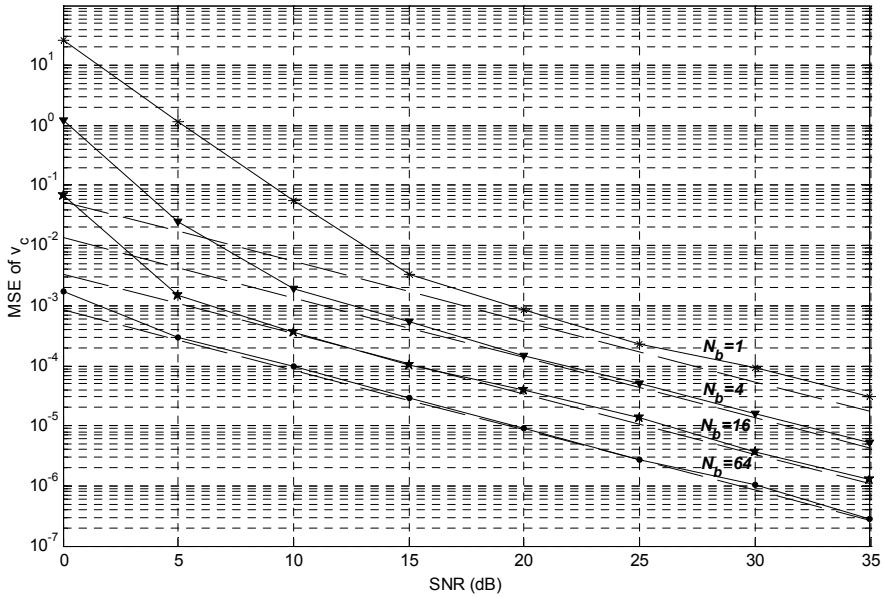

Figure 4.1 - Plot of the *MSE* of v_c against SNR (dB) for a AWGN channel

As shown in the figure, the theoretical curves fit the experimental curves well when the SNR is high. This is an assumption used in the theoretical derivation of the estimator. Note that as the number of blocks, N_b, used for estimation increases, the experimental result starts to fit the theoretical result at a lower *SNR*.

4.2.2 *MSE* against N_A

In the next simulation, a system with N=64, N_b=64 was tested for various number of activated sub-carriers, N_A=1, 8, 16, 32, 48, 56, 63 for a AWGN channel. The placement of the activated sub-carriers is consecutive. Figure 4.2 shows the plot of the *MSE* of v_c against N_A. The simulation was conducted at an SNR of 15dB over 1600 trials. Solid lines and dashed lines depict the experimental and theoretical results respectively.

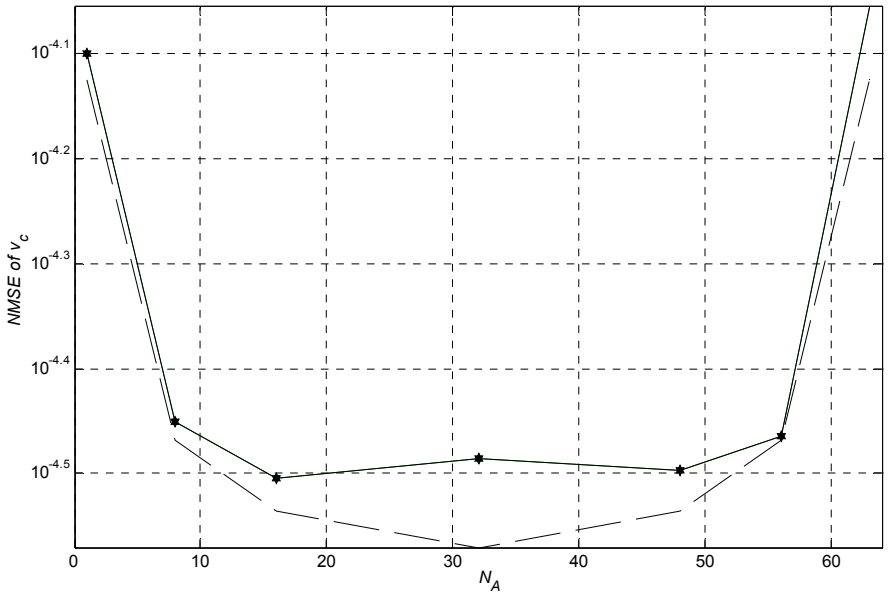

Figure 4.2 - Plot of the *MSE* of v_c against N_A for a AWGN channel

As shown in the figure, the plot is symmetrical about $N_A = N/2 = 32$. Hence applying the estimator in 2 systems with N_A and N-N_A activated sub-carriers respectively would yield the same *MSE*. Furthermore, we observe that *MSE* decreases as N_A increases and is minimised when the system is half loaded. The *MSE* then increases as N_A increases to N-1. We note that the estimator cannot be applied in an unloaded or fully loaded system. This is because the energy of the null sub-carriers or the activated sub-carriers is constant for both systems at all frequency offsets.

4.2.3 *MSE* of modified cost function against *P*

As given by (3.17), the use of a modified cost function which sums the total energy of all null sub-carriers placed at circular distance of less than or equal to P was discussed. A simulation was carried out to verify the theoretical *MSE* result for a system with N=64, N_b=64, N_A=32. The placement of the activated sub-carriers is consecutive. Figure 4.3 shows the experimental and theoretical results indicated by solid and dashed lines respectively.

The figure shows that as P increases, the *MSE* decreases and is minimum when all null sub-carriers are used for the cost function. This meant that the use of the modified cost function causes a loss in performance in terms of *MSE*. Hence, depending on the required accuracy of the estimator, the modified cost function can be used instead of the original cost function to reduce the number of computations required.

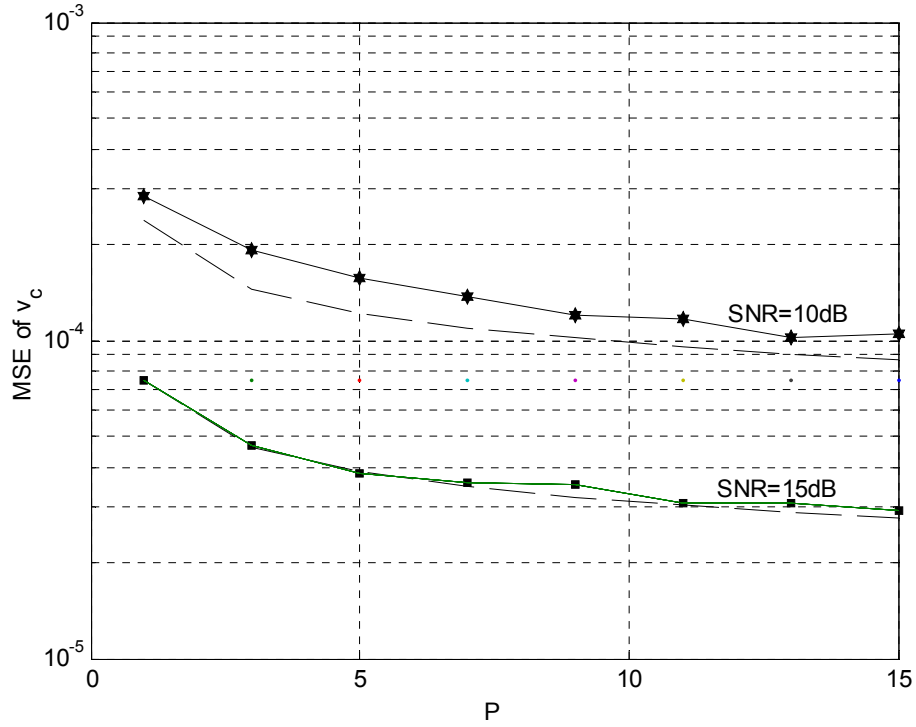

Figure 4.3 - Plot of the MSE of v_c against P using modified cost function for a AWGN channel

4.2.4 *MSE* against N_X

In Section 2.2 (Figure 2.5) a simulation was conducted for a system with parameters N=64, N_b=64, N_A=32 where the subcarriers were placed in a manner such that there were alternating clusters of N_X activated and N_X null sub-carriers (depicted in Figure 2.4). The average ICI power was found to be minimum when N_X =1, i.e. when the activated sub-carriers were equally spaced apart.

We note a similar trend was in the *MSE* of the estimator. As shown in Figure 4.4, the *MSE* is also minimum when N_X=1, where the activated sub-carriers are placed maximally apart and is maximum when N_X=32, where the activated sub-carriers are placed consecutively.

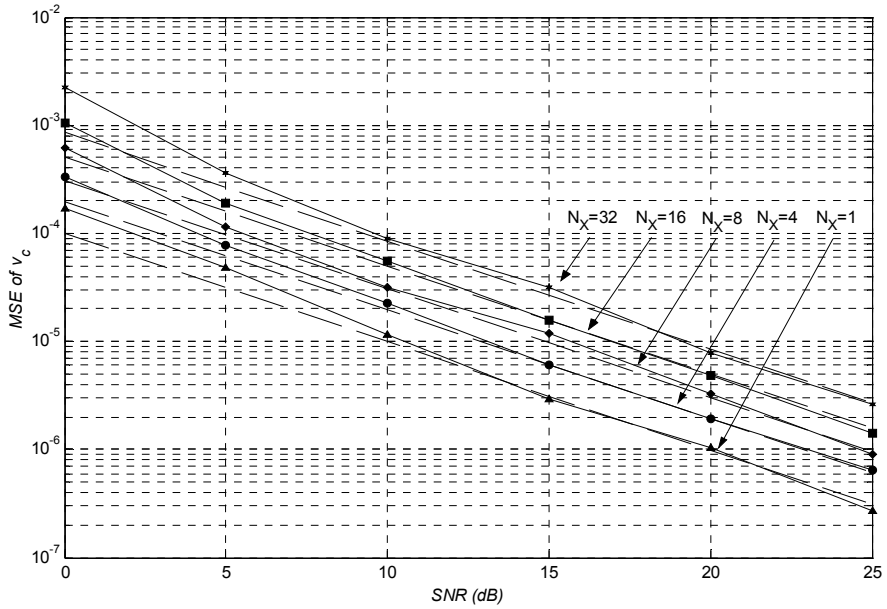

Figure 4.4 - Plot of the MSE of v_c against SNR with various N_X for a AWGN channel

4.3 Performance of estimator in a Rayleigh Channel

Simulations were carried out to test the performance of estimator in a Rayleigh channel with a normalised exponential power profile, i.e. $E[c[n]]^2 = \left(e^{-n/L+1}\right) \Big/ \left(\sum_{l=0}^{L} e^{-l/L+1}\right)$, n= 0, 1,…8 and L =8. Using the same SNR definition as in the AWGN only case, experimental and theoretical results obtained were compared. The issue of the cost function ambiguity is highlighted and a random carrier placement strategy, coupled with deterministic frequency hopping is proposed and compared with the performance of the deterministic hopping strategy in [13].

4.3.1 MSE against N_X

A simulation over 1600 trials was carried out with the parameters N=64, N_b=64 N_A=32 and the carrier placement is such that clusters of N_X=4, 8, 16, 32 activated sub-carriers alternates with the clusters of the same number of null sub-carriers (Figure 2.4). Figure 4.5 depicts the experimental results for both the AWGN and the Rayleigh channel with channel order L=8. We note that due to the periodicity in the arrangement of the sub-carriers, the maximum acquisition range is only $\pm N_X/2$

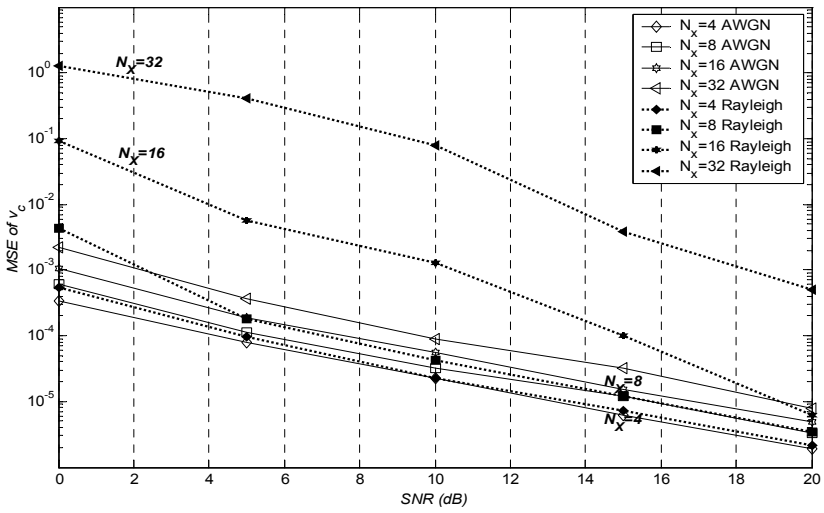

Figure 4.5 – *MSE* of estimator in Rayleigh Channel with N_X=4, 8, 16, 32

From the figure, there is degradation in *MSE* when the estimator is used in a Rayleigh channel. This degradation is most severe when the maximum number of activated sub-carriers are clustered together, i.e. N_X=32 and becomes less significant with the reduction of N_X. At N_X =1, where the activated sub-carriers are equally spaced, there is little difference in the *MSE* between the AWGN and Rayleigh channel. Hence it is observed that spacing the activated sub-carriers apart provide robustness against the channel nulls. However, periodicity in the arrangement of the sub-carriers means that the acquisition range is reduced.

Figure 4.6 shows an example where the estimate error, v, exceeds the sub-carrier spacing for the case of N_X=32 at SNR=15dB. In this case, the presence of channel nulls in the region corresponding to DFT bin indices k=0 to 5 causes a 'false' local minimum to have a lower cost than the 'true' global minimum.

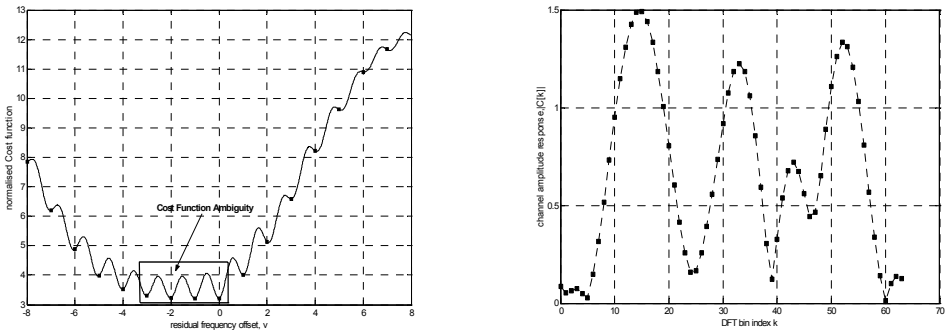

a) Cost Function **b) Channel Amplitude Response**

Figure 4.6 - Simulation example showing the problem of 'channel nulls'

In [23], the problem of cost function ambiguity is highlighted, but little experimental evidence has been provided to substantiate the claim. In a practical situation, it is unlikely that the channel null, if it does occur, will coincide exactly with the centre of

a DFT bin. Hence, the presence of AWGN, which perturbs the cost function, determines if the problem of cost function ambiguity does become significant.

Simulations were done to support the claim that 'channel nulls' does pose a problem, especially at low *SNR* and is a major cause for the degradation in MSE of the estimator for a Rayleigh channel.

Specifically, we consider a system with N=64, N_b=64, N_A=32, 62. The activated sub-carriers are placed consecutively from sub-carrier index k=6 onwards. The number of occurrences where the absolute estimate error, $|v_e| > 1$ were recorded. Figure 4.7 shows the plot of the probability of such an event against *SNR*.

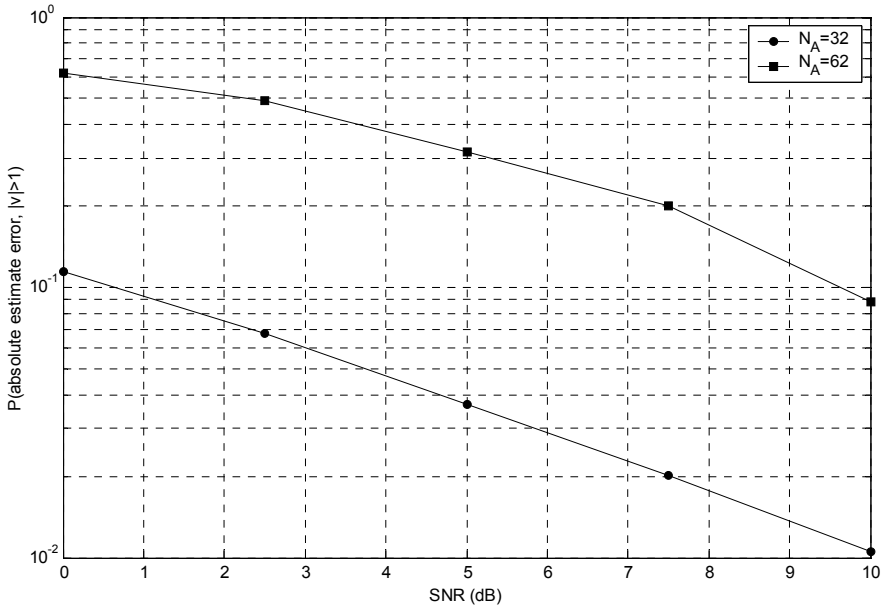

Figure 4.7 – Plot showing the probability of occurrence of absolute normalised estimate error exceeds 1, against SNR/dB

From the figure, it is observed that the frequency of occurrence is much higher for N_A=62 (near full load) than for N_A=32 (half load).

In addition, the frequency response for each occurrence of such an event was recorded for the case of N_A=32. The amplitude responses collected were then divided into 2 categories, $|C[6]|>|C[37]|$ and $|C[6]|\leq |C[37]|$ respectively and the mean was computed for the various *SNR*. Figure 4.8 shows the plot of the mean amplitude response.

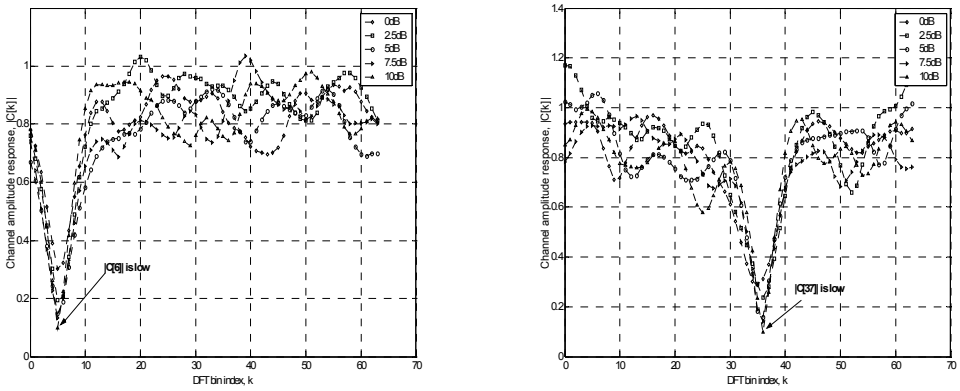

a) Category A - $|C[6]|> |C[37]|$ b) Category B - $|C[6]|\leq |C[37]|$

Figure 4.8 – Plot of mean amplitude response for occurrences where the absolute normalised estimate error exceeds 1

As shown in the figure, sharp notches in the amplitude responses were observed for the DFT bins, k=6 or k=37. This gives supporting experimental evidence to the discussion in Section 3.2.2 (ii), where the presence of "channel nulls" at the starting or ending index of the activated sub-carriers results in cost function ambiguity.

4.3.2 Random placement of sub-carriers coupled with deterministic hopping over blocks

In [13], deterministic hopping is used to combat the effects of the channel nulls. Specifically the activated sub-carriers are placed in a periodic manner as described by Figure 2.4. The sub-carrier placement of each OFDM symbol is the placement for the previous symbol rotated by 1. This provides robustness against the channel nulls but reduces the maximum possible estimation range, except in the case where N_X=32 as discussed previously. Hence we propose a random placement of the sub-carriers on a OFDM symbol and this placement is deterministically hopped over the N_b OFDM symbols as in [13]. For a system with a total of N sub-carriers and N_A sub-carriers activated, the indices of the activated sub-carriers in the first OFDM symbol are chosen in the following manner:

1. Choose N numbers from a uniform distribution on the interval [0, 1].
2. The N numbers are sorted in ascending order with their indices.
3. Select the first N_A indices from the sorted array as the activated carriers.

The random placement of the sub-carriers tends to spread the activated sub-carriers among the sub-carriers. This is desirable as it provides robustness against the channel nulls and *MSE* is minimised when the activated sub-carriers/null sub-carriers are spaced equally apart. Moreover, the probability of a random carrier placement being periodic is also very small. This allows full estimation range. We note that the proposed random placement alone does not provide much robustness against the channel nulls when the system becomes heavily loaded. For example, in the case where N=64, N_A=63, random placement of the sub-carriers would still result in consecutive placement of the activated carriers. Hence coupling random placement with deterministic hopping over the N_b OFDM symbols will handle such scenarios.

Simulations were carried out to evaluate the performance of the proposed strategy. Figures 4.9-4.12 show the *MSE* against SNR curves for:

i) Random placement of sub-carriers in an AWGN channel (dashed line);

ii) Deterministic hopping [13] with consecutive activated sub-carrier placement in a Rayleigh channel (solid line);

iii) Random placement without deterministic hopping in a Rayleigh channel (solid line with square markers); and

iv) Random placement coupled with deterministic hopping in a Rayleigh channel (solid line with diamond markers).

The system parameters are N=64, N_b=64. N_A=10 (Figure 4.9), N_A=32 (Figure 4.10), N_{Act}= 60 (Figure 4.11) and N_A= 63 (Figure 4.12)

It is observed that random placement alone can cope with the channel nulls in a Rayleigh channel and shows a general better performance than deterministic hopping with consecutive activated sub-carrier placement. Exceptions occur when the system becomes nearly fully loaded, i.e. N_A =60, 63. In such cases, random placement fails unless coupled with deterministic hopping.

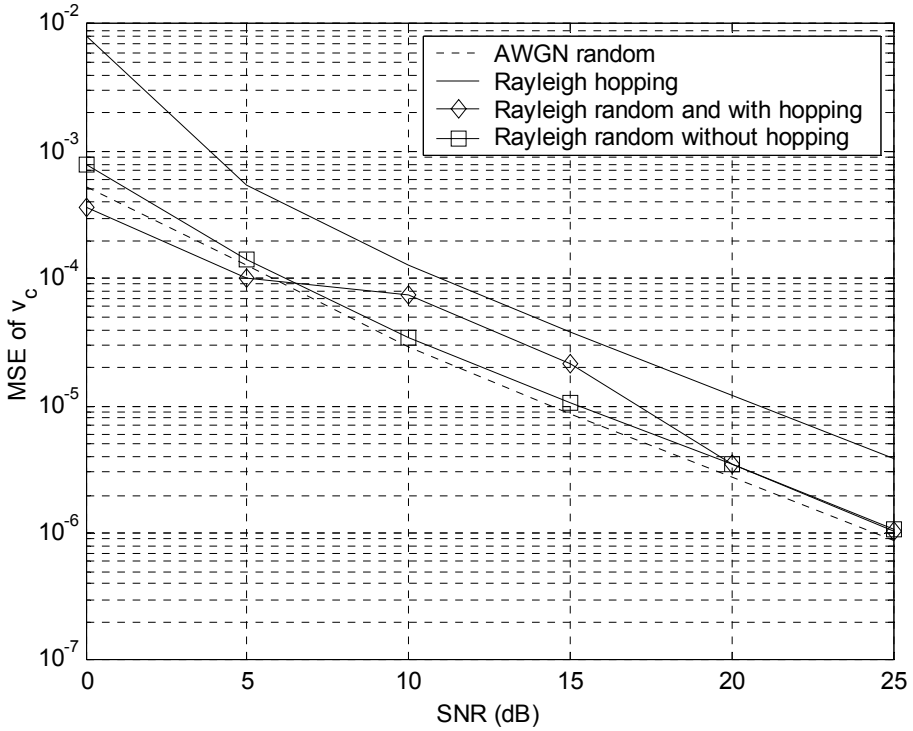

Figure 4.9 - Plot of MSE against SNR for N_A=10

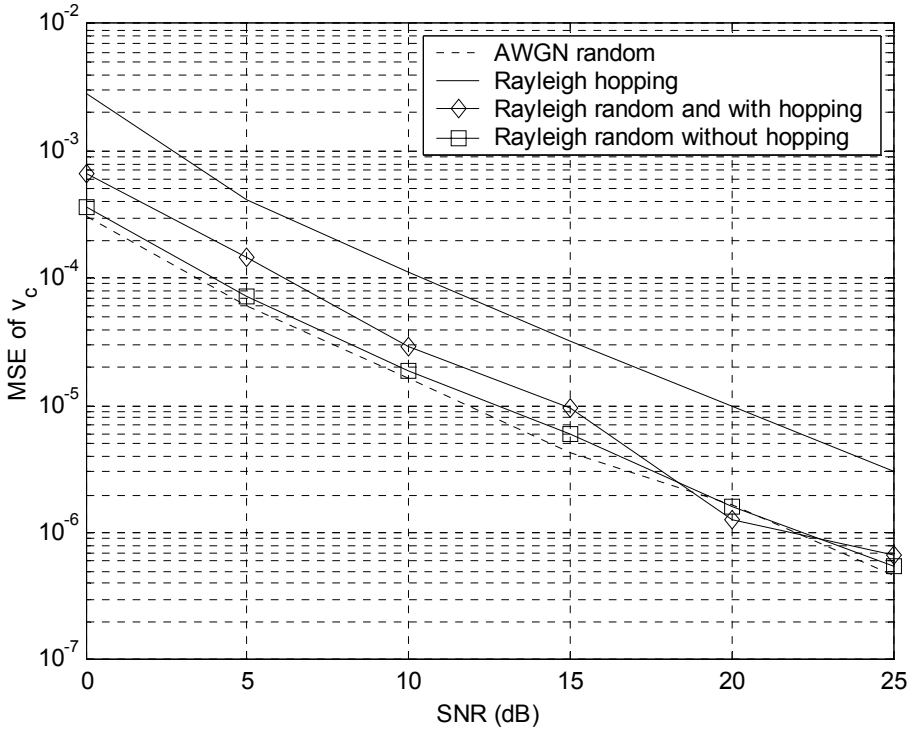

Figure 4.10 - Plot of MSE against SNR for N_A=32

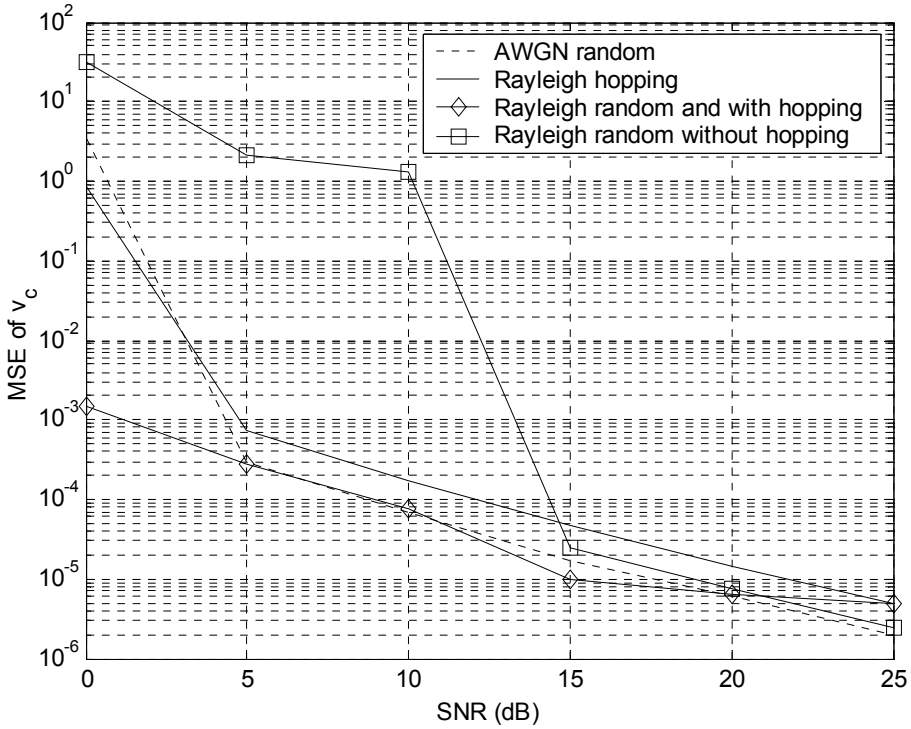

Figure 4.11 - Plot of MSE against SNR for N_A=60

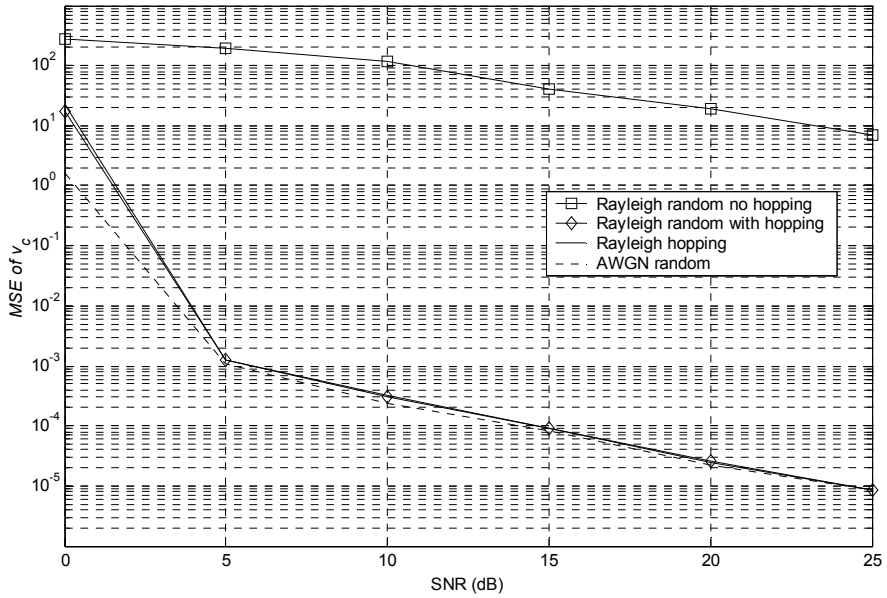

Figure 4.12 - Plot of MSE against SNR for N_A=63

CHAPTER 5

Search schemes for finding global cost function minimum

As discussed in Chapter 3, the shape of the cost function varies with the placement of the activated sub-carriers. It typically contains multiple local maxima and minima, among which the global minimum (for $J_{N,Z}(v_c)$, the cost function involving the total energy of the null sub-carriers) or global maximum (for $J_{A,Z}(v_c)$, the cost function involving the total energy of the activated sub-carriers) has to be found to yield the MLE of the carrier frequency offset.

In this section, we suggest and compare a number of techniques for finding the global minimum/maximum point of the cost function without having to resort to exhaustive search. The techniques proposed do not require setting of a weight parameter as in Gradient Descent that directly affects its convergence rate. Convergence is guaranteed. We restrict our discussion to search schemes to find the global minimum of the cost function, $J_{N,Z}(v_c)$. Nonetheless, the same schemes could be applied to finding the global maximum of the cost function, $J_{A,Z}(v_c)$.

In many scenarios, offset estimation is required over a range greater than sub-carrier spacing. Intuitively, this suggests sampling the cost function at integer values of v_c. A fine search could then be conducted at the sub-carrier interval about the integer, $v_{c,n}$ that yielded the least cost function. However, we have found empirically that this does result in the selection of the wrong interval, even in an ideal channel, as depicted in Figure 5.1. In this case, sampling $J_{N,Z}(v_c)$ at integer intervals yields the lowest cost at $v_c = -2$, inferring a fine search over the interval [-2.5, -1.5] for the global minimum. However, the correct interval to be searched should have been [-0.5, 0.5]. Further complications arise as the shape of the cost function varies for different sub-carrier placement.

Hence, we adopt the more conventional approach of determining the local minima before finding the global minimum, which is the local minimum with the lowest cost function

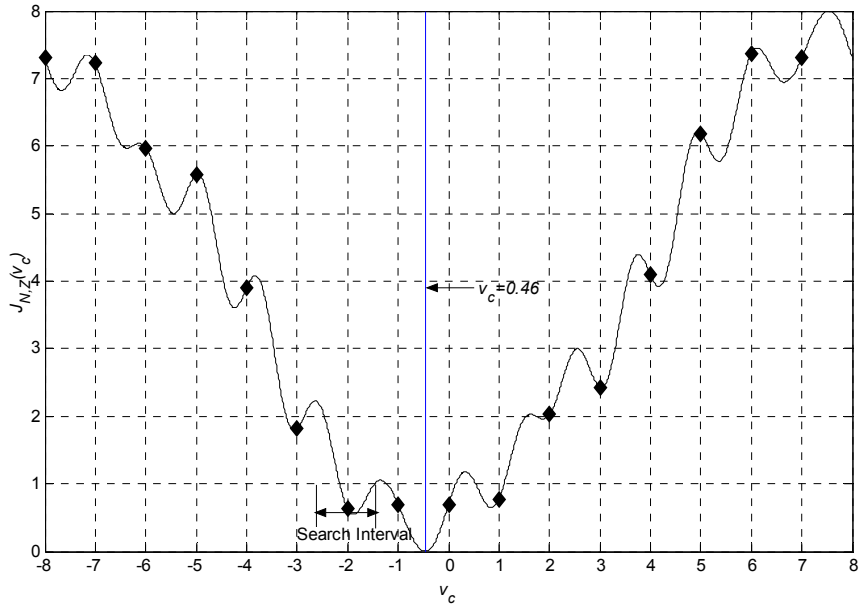

Figure 5.1 – Incorrect search interval when $J_{N,Z}(v_c)$ is sampled at integer intervals and fine search is conducted over integer interval that yielded the lowest cost

5.1 Direct Search of global minimum using cost function

In this sub-section, we discuss the direct search of global minima using the cost function $J_{N,Z}(v_c)$.

5.1.1 Initial Bracketing of Local Minima Using Cost Function

The approach is simple. The global minimum must be a turning point as the cost function is non-negative, continuous and wraps around *N*. The cost function typically consists of a series of local minima and maxima, and exhibits some regularity. Hence, general global minimisation algorithms such as Simulated Annealing or Genetic Algorithms, usually intended for more complicated cost functions, are not required.

The first task is to locate or bracket the local minima. This can be accomplished by searching for turning points within the desired acquisition range. The separation between 2 neighbouring minima is approximately around 1 carrier spacing. Hence, the cost function is first coarsely sampled at intervals of α and using this sequence of samples, detection of turning points is then conducted to determine the bracketing intervals of the local minima.

This may seem to be computationally prohibitive since the cost function needs to be evaluated at intervals of α and the number computations increases linearly with the acquisition range. For the full acquisition range, this would mean N/α cost function evaluations. However, upon inspection of the cost function, we note that frequency offset correction and *N*-pt DFT need not be performed for N/α values of v_c, by considering the following property:

Denote the integer and fractional components of v_c as $v_{c,i}$ and $v_{c,f}$ respectively, i.e. $v_c = v_{c,i} + v_{c,f}$

$$\begin{aligned}
\left|Z_m[k]^2\right|_{v_c = v_{c,i} + v_{c,f}} &= \left|\sum_{n=0}^{N-1}\left(r_m[n] e^{-j\frac{2\pi}{N}nk} e^{-j\frac{2\pi}{N}(v_{c,i}+v_{c,f})t} \right)\right|^2 \\
&= \left|\sum_{n=0}^{N-1}\left(r_m[n] e^{-j\frac{2\pi}{N}nk} \right) e^{-j\frac{2\pi}{N}(v_{c,i}+v_{c,f})t} \right|^2 \\
&= \left|\sum_{n=0}^{N-1}\left(r_m[n] e^{-j\frac{2\pi}{N}(l+v_{c,i})n} e^{-j\frac{2\pi}{N}v_{c,f}t} \right) e^{-j\frac{2\pi}{N}v_{c,i}m(N+L)} \right|^2 \\
&= \left| Z_m[(k+v_{c,i}) \bmod N] \right|^2 \Big|_{v_c = v_{c,f}}
\end{aligned} \tag{5.1}$$

Using this property, only $1/\alpha$ N-pt DFTs have to be carried out and the cost function can be evaluated using the following expression

$$J_{N,Z}(v_c = v_{c,i} + v_{c,f}) = \frac{1}{N_b}\sum_{m=0}^{N_b-1}\left(\sum_{k \in \Omega_{N,m}} \left| Z_m[(k+v_{c,i}) \bmod N] \right|^2 \Big|_{v_c = v_{c,f}} \right) \tag{5.2}$$

This drastically reduces the number of the DFTs and the 'trial' offset corrections that are required, especially when the offset range is over the maximum possible range of $\pm 0.5N$, which is usually large.

The next step involves detecting the presence of local minima. We use the fact that a local minima is bracketed by the interval $[a, c]$ if there exists an offset b such that $a<b<c$ such that $J_{N,Z}(a) > J_{N,Z}(b)$ and $J_{N,Z}(b) < J_{N,Z}(c)$.

Hence, the set of coarse sample points are arranged in ascending order of v_c, as denoted by $\{v_{c,1}, v_{c,2}, \ldots, v_{c,n}, \ldots v_{c,N/\alpha}\}$. A local minimum is present in the interval $[v_{c,n-1}, v_{c,n+1}]$ if

$$J_{N,Z}\left(v_{c,n-1}\right) > J_{N,Z}\left(v_{c,n}\right) \tag{5.3a}$$

$$J_{N,Z}\left(v_{c,n}\right) < J_{N,Z}\left(v_{c,n+1}\right), \tag{5.3b}$$

The triplet of co-ordinates $\left(v_{c,n-1}, J_{N,Z}\left(v_{c,n-1}\right)\right)$, $\left(v_{c,n}, J_{N,Z}\left(v_{c,n}\right)\right)$ and $\left(v_{c,n+1}, J_{N,Z}\left(v_{c,n+1}\right)\right)$ are retained for fine estimation of the local minimum. Figure 5.2 shows a typical result of the local minima extracted. In this figure, each triplet of squares indicates the bracketing interval containing a local minimum. Following this, many search algorithms [25] can be applied and are discussed as follows

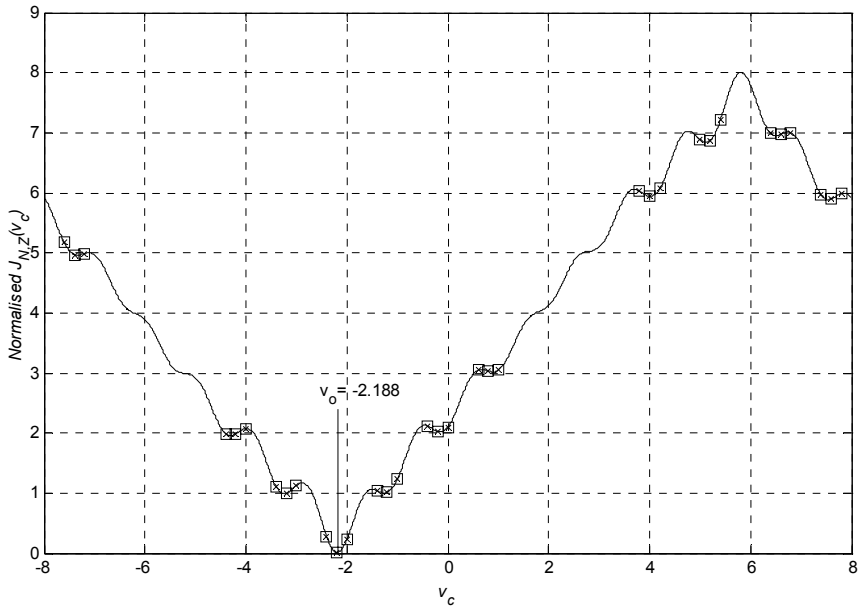

Figure 5.2 – The bracketing intervals containing the local minima extracted from $J_{N,Z}\left(v_c\right)$

5.1.2 Finding a Local Minimum from a Bracketing Interval

Upon the extraction of the bracketing intervals for the local minima, the next step is to conduct a fine search for the local minimum within each bracketing interval. The methods adopted are as discussed below:

5.1.2.1 Golden Search

Golden Search uses the successive bracketing of a minimum of a cost function to provide an improving estimate of the true minimum value of the function. Convergence is guaranteed provided that the initial bracketing interval is correct. Given a bracketing triplet of co-ordinates $\left(v_{c,n-1}, J_{N,Z}\left(v_{c,n-1}\right)\right)$, $\left(v_{c,n}, J_{N,Z}\left(v_{c,n}\right)\right)$ and $\left(v_{c,n+1}, J_{N,Z}\left(v_{c,n+1}\right)\right)$ respectively, the cost function is evaluated at a new point, $v_{c,new}$ within the larger of the two intervals, $[v_{c,n-1}, v_{c,n}]$ and $[v_{c,n}, v_{c,n+1}]$. If $J_{N,Z}\left(v_{c,new}\right) < J_{N,Z}\left(v_{c,n}\right)$, then $v_{c,n}$ is set the value of $v_{c,new}$. $v_{c,n-1}$ and $v_{c,n+1}$ are replaced, if necessary, with closest points to the left and right of $v_{c,n}$ respectively. Otherwise, $v_{c,n-1}$ or $v_{c,n+1}$, (the one which is closer to $v_{c,new}$) is set the value of $v_{c,new}$. The process repeats until $|v_{c,new}-v_{c,n}|<\varepsilon$, where ε is the required precision. Figure 5.3 shows an iteration example.

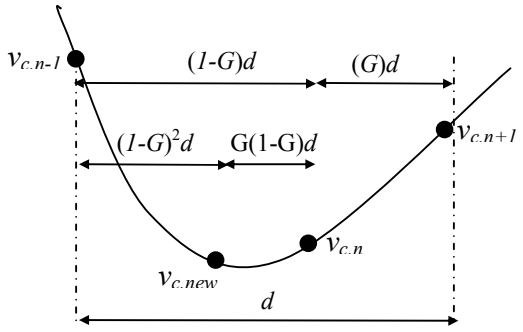

Figure 5.3 - An iteration of Golden Search

Note: In the Golden Section method, given a triplet $[v_{c,n-1}, v_{c,n}, v_{c,n+1}]$, a new point is chosen in the bigger of the 2 intervals as shown. The new triplet after the iteration is $[v_{c,n-1}, v_{c,new}, v_{c,n}]$.

It can be easily shown that the point $v_{c,new}$ should be chosen at distance $0.5\left(3-\sqrt{5}\right)$, known as the Golden Ratio, denoted by G, that of the larger interval, from $v_{c,n}$, so that the width of new bracketing interval is the same, regardless of whether $v_{c,n}$ is being replaced by $v_{c,new}$. This is indicated in Figure 5.3.

Convergence is guaranteed since the cost function given by is well behaved and the bracketing intervals have been determined from Section 5.1. The required number of iterations to reach a precision of ε is given by

$$n \approx \log_{(1-G)^{-1}}\left(\frac{\varepsilon_0}{\varepsilon}\right) \tag{5.4}$$

where ε_0 is the initial bracketing interval and is equal to 2α based on Section 5.1.

5.1.2.2 Parabolic Interpolation

Although golden search guarantees convergence, it is slow since it does not take into account the properties of the cost function. Since the cost function near each local minimum is convex and can be approximated to be parabolic, it may be more efficient to fit the triplet of co-ordinates to a parabola and determine the minimum using the fitted curve, Using the bracketing triplet of points found in Section 5.1.1, a curve fit is done using

$$J_{N,Z}\left(v_c\right) \approx w_2 v_c{}^2 + w_1 v_c + w_0 \tag{5.5}$$

A linear system of equations is formed using the triplet of co-ordinates obtained from Section 5.1 as given by

$$\begin{bmatrix} J_{N,Z}(v_{c,n-1}) \\ J_{N,Z}(v_{c,n}) \\ J_{N,Z}(v_{c,n+1}) \end{bmatrix} = \begin{bmatrix} v_{c,n-1}{}^2 & v_{c,n-1} & 1 \\ v_{c,n}{}^2 & v_{c,n} & 1 \\ v_{c,n+1}{}^2 & v_{c,n+1} & 1 \end{bmatrix} \begin{bmatrix} w_2 \\ w_1 \\ w_0 \end{bmatrix} \tag{5.6}$$

Solving for the coefficients w_1, w_2 and w_0, the interpolated minimum point is given by $-w_1/w_2$ and can be evaluated using (5.7)

$$v_{c,new} \approx -\frac{w_1}{w_2} = -\frac{\left(v_{c,n+1}{}^2 - v_{c,n}{}^2\right)J_{N,Z}(v_{c,n-1}) + \left(v_{c,n-1}{}^2 - v_{c,n+1}{}^2\right)J_{N,Z}(v_{c,n}) + \left(v_{c,n}{}^2 - v_{c,n-1}{}^2\right)J_{N,Z}(v_{c,n+1})}{2\left[\left(v_{c,n} - v_{c,n+1}\right)J_{N,Z}(v_{c,n-1}) + \left(v_{c,n+1} - v_{c,n-1}\right)J_{N,Z}(v_{c,n}) + \left(v_{c,n-1} - v_{c,n}\right)J_{N,Z}(v_{c,n+1})\right]} \quad (5.7)$$

Evaluating the cost function at the interpolated minimum, $v_{c,new}$, and comparing the costs at original 3 points used for interpolation, the 3 co-ordinates that yield the least cost are used for parabolic interpolation at the next iteration. This is as shown in Figure 5.4.

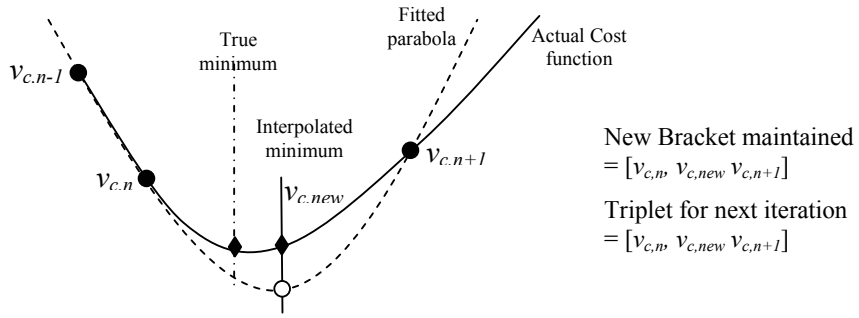

Figure 5.4 – Iteration of Parabolic Interpolation

Parabolic interpolation, however, does not guarantee convergence, and this could occur due to misfit. To ensure convergence, we maintain and update the bracketing triplet [*a, b, c*], $a<b<c$, such that $J_{N,Z}(a) > J_{N,Z}(b)$ and $J_{N,Z}(b) > J_{N,Z}(c)$ whenever possible, after each iteration.

If the interpolated minimum, $v_{c,new}$, lies outside of this bracketing interval [a, c] or the evaluated cost at $v_{c,new}$ is higher than each of the 3 points used for parabolic fitting, an iteration of golden search is applied, which ensures progressive convergence. In the worst-case scenario, the number of iterations would be twice that of golden search.

5.2 Transforming problem of minima search to root search

The previous methods discussed adopt the approach of direct cost function minimisation. The problem of finding the global minima however, can be transformed to one of searching for roots of the derivative of the cost function as depicted in Figure 5.5.

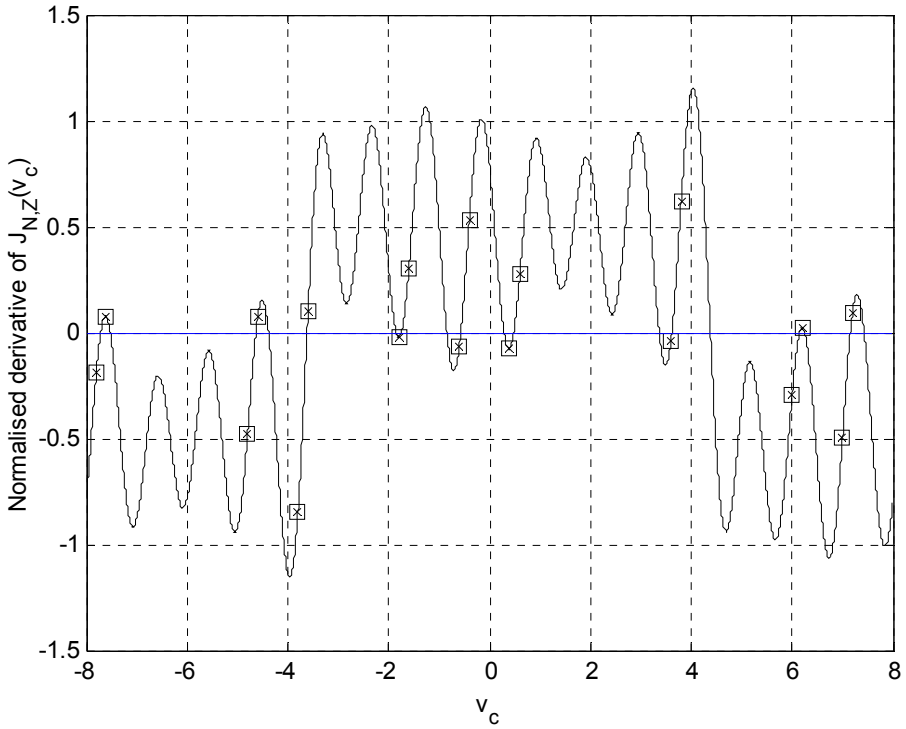

Figure 5.5 – Derivative of $J_{N,Z}(v_c)$

The attractiveness of this method is due to the fact that partial derivative of the cost function w.r.t. $v_{c,new}$ can be evaluated directly without the need for numerical differences approximation methods and is given by:

$$\frac{\partial J_{N,Z}(v_c)}{\partial v_c} = \frac{1}{N_b}\sum_{m=0}^{N_b-1}\sum_{k\in\Omega_{N,m}} \mathrm{Re}\left[\frac{\partial Z_m[k]}{\partial v_c} Z_m^*[k]\right] \tag{5.8a}$$

where

$$\frac{\partial Z_m[k]}{\partial v_c} = -j2\pi\sum_{n=0}^{N-1}\left([n+m(N+L)]r_m[n]e^{-j\frac{2\pi}{N}v_c[n+m(N+L)]}\right)e^{-j\frac{2\pi}{N}nk} \tag{5.8b}$$

The property described by (5.8a), also holds for its derivative (5.8b). Upon obtaining the roots, the cost function has to be evaluated at the roots to determine which of the roots coincides with the global minima. It is easily seen that (5.8b) can also be implemented in a efficient FFT-like manner.

5.2.1 Bracketing of Local Minima using Derivative

The bracketing of the local minima can also be accomplished using the derivative of the cost function instead of Section 5.1. A local minima is determined to be bracketed within an interval $\left[v_{c,n}, v_{c,n+1}\right]$ if

$$\left.\frac{\partial J_{N,Z}(v_c)}{\partial v_c}\right|_{v_c=v_{c,n}} < 0 \quad \text{and} \tag{5.9a}$$

$$\left.\frac{\partial J_{N,Z}(v_c)}{\partial v_c}\right|_{v_c=v_{c,n+1}} > 0\,. \tag{5.9b}$$

Similar to Section 5.1, the derivatives are first evaluated at coarse intervals of α and any pair of consecutive samples is deemed to bracket a local minimum based on the

above criterion. As compared to the method for detection of local minima using the cost function, the initial bracketing interval is α, which is half that using the cost function as in Section 5.1.

5.2.2 Locating roots of cost function derivative

As in the case of root search, the next step is to conduct a fine search to locate the root within each bracketing interval.

5.2.2.1 Bisection

Bisection is a sure but slow method of refining the estimate of the root. For a bracketing interval, $[v_{c,n} \quad v_{c,n+1}]$ and the derivatives at $\left[\left.\frac{\partial J_{N,Z}(v_c)}{\partial v_c}\right|_{v_c=v_{c,n}}, \left.\frac{\partial J_{N,Z}(v_c)}{\partial v_c}\right|_{v_c=v_{c,n+1}}\right]$ respectively, the derivative at the midpoint, $v_{c,new}=0.5(v_{c,n}+v_{c,n+1})$ is evaluated. If $\left.\frac{\partial J_{N,Z}(v_c)}{\partial v_c}\right|_{v_c=v_{c,new}} > 0$, then $v_{c,n+1}= v_{c,new}$, else $v_{c,n}= v_{c,new}$. The process is repeated until $|v_{c,new}-v_{c,n}|<\varepsilon$, where ε is the desired precision.

Linear interpolation could also be utilized and this may speed up the process. Instead of evaluating the midpoint as in Bisection, the derivative is evaluated at $v_{c,new} = v_{c,n} - \left(v_{c,n+1} - v_{c,n}\right)\left(\frac{\partial J_{N,Z}(v_{c,n})}{\partial v_c} \Big/ \left(\frac{\partial J_{N,Z}(v_{c,n+1})}{\partial v_c} - \frac{\partial J_{N,Z}(v_{c,n})}{\partial v_c}\right)\right)$. The criterion for updating the bracketing interval is the same as normal bisection.

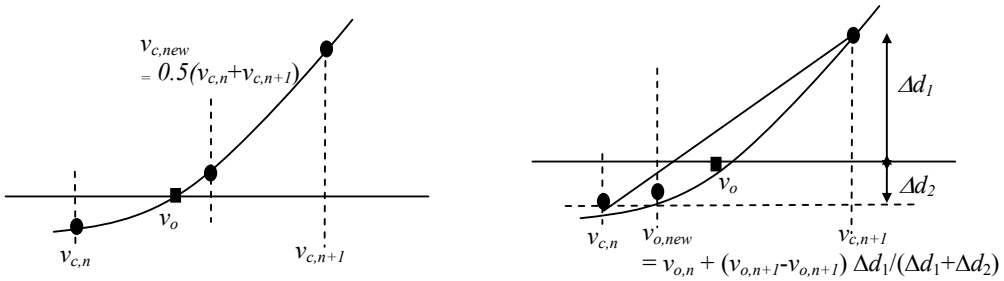

a. Bisection

b. Bisection with linear Interpolation

Figure 5.6 – One iteration of Bisection

5.2.2.2 Newton Raphson Method

Using Taylor's expansion, the derivative of the cost function can be further approximated using (5.10), ignoring terms containing 3rd derivative and above,

$$\frac{\partial J_{N,Z}\left(v_{c,n+1}\right)}{\partial v_c} = \frac{\partial J_{N,Z}\left(v_{c,n}\right)}{\partial v_c} + \frac{\partial J^2_{N,Z}\left(v_{c,n}\right)}{\partial v_c^2}\left(v_{c,n+1} - v_{c,n}\right) \tag{5.10a}$$

where $\left(v_{c,n+1} - v_{c,n}\right)$ is assumed to be small. Hence, if $v_{c,n}$ is the previous estimate close to the root, the next estimate where the root lies, denoted by $v_{c,n+1}$ is obtained by setting L.H.S of (14) to zero and rearranging the terms to give

$$v_{c,n+1} = v_{c,n} - \frac{\partial J_{N,Z}\left(v_{c,n}\right)}{\partial v_c} \Bigg/ \frac{\partial J^2_{N,Z}\left(v_{c,n}\right)}{\partial v_c^2} \tag{5.10b}$$

The 2nd partial derivative of the cost function, can be evaluated directly like 1st partial derivative, as given by

$$\frac{\partial^2 J_{N,Z}\left(v_c\right)}{\partial v_c^2} = \sum_{m=0}^{N_b-1} \sum_{k\in\Omega_{N,m}} \mathrm{Re}\left\{ \frac{\partial^2 Z_m[k]}{\partial v_c^2} Z_m^*[k] + \left| \frac{\partial Z_m[k]}{\partial v_c} \right|^2 \right\} \tag{5.11a}$$

where,

$$\frac{\partial^2 Z_m[k]}{\partial v_c^2} = -4\pi^2 \sum_{n=0}^{N-1} [n + m(N+L)]^2 r_m[n] e^{-j\frac{2\pi}{N} v_c [n+m(N+L)]} e^{-j\frac{2\pi}{N} nl}$$

(5.11b)

A reasonable starting point could be obtained using the bisection method. This method of approximation, popularly known as the Newton Raphson method is powerful as its rate of convergence is quadratic. To ensure convergence, the bracketing interval is updated at each iteration and bisection is used if iteration causes the estimate to fall outside of the bracketing interval.

5.3 Further Reduction of Computational Load

If carrier offset estimation is required over the maximum range, $\nu \in (-N/2, N/2]$, searching for all local minima before determining which is the global minima can still require many computations when the number of sub-carriers in the system is large. The computational workload could be alleviated by searching for the local minima only within bracketing intervals that are likely to contain the global minimum. From Section 5.1, the set of bracketing triplets has been found. If $[v_{m-1}, v_m, v_{m+1}]$ is the bracketing triplet such that $J_{N,Z}(v_m)$ is the minimum among the coarse sample points, A fine search is only performed using the bracketing triplet $[v_{n-1}, v_n, v_{n+1}]$, if

$$J_{N,Z}(v_m) + \beta((0.5(J_{N,Z}(v_{m-1}) + J_{N,Z}(v_{m+1})) - J_{N,Z}(v_m)) > J_{N,Z}(v_n) \qquad (5.12)$$

5.4 Simulation results

Simulations were conducted to test the performance of the techniques mentioned above. The total number of subcarriers, *N,* is 64, and the number of activated carriers is 32. Activated sub-carriers are arranged in a consecutive manner. The Rayleigh fading channel with an exponential power delay profile is modelled using a FIR filter with 5 taps, i.e. L=4.

For the initial bracketing, a suitable value for the coarse sampling interval, α, to detect all local minima is required. The values of 0.1, 0.2, 0.25, 0.3 and 0.5 were tested. For each α setting, the bracketing intervals were verified against those obtained when α is set to a very small value of 0.01. Over 1000 trials, we found that α=0.2 to be able to extract all the bracketing intervals.

Table 1 shows the number of iterations to estimate each local minimum to the prescribed precision, $\varepsilon_0=10^{-5}$. The initial bracketing interval is set to 0.2. Simulations with SNR from 0 to 30dB in steps of 5dB over 100 trials each indicated that the number required does not vary with SNR. Newton Raphson method requires the least number of iterations, followed by parabolic fitting, bisection with linear interpolation, bisection and golden search being the slowest.

Table 1 – Average number of iterations required to estimate local minimum

Method	Golden Search	Parabolic Interpolation	Bisection	Bisection with interpolation	Newton Raphson
No. of Iterations	22.51	5.69	15	7.68	3.78

Simulations were also carried out to determine the number of errors that arose from using the approach in Section 5.3. An error is deemed to have occurred when the global minimum obtained by searching all the local minima is different from that using the approach in Section 5.3. Figure 5.7 shows the error rate over 10000 trials with different values of β at a poor SNR of 0dB and a single block for estimation while Figure 5.8 shows the average number of bracketing intervals that has to be evaluated. The average total number of local minima for this experiment setting is 52 per trial. When β is set to 1, no errors occurred over 10000 trials with the average number of bracketing intervals evaluated being 2.02.

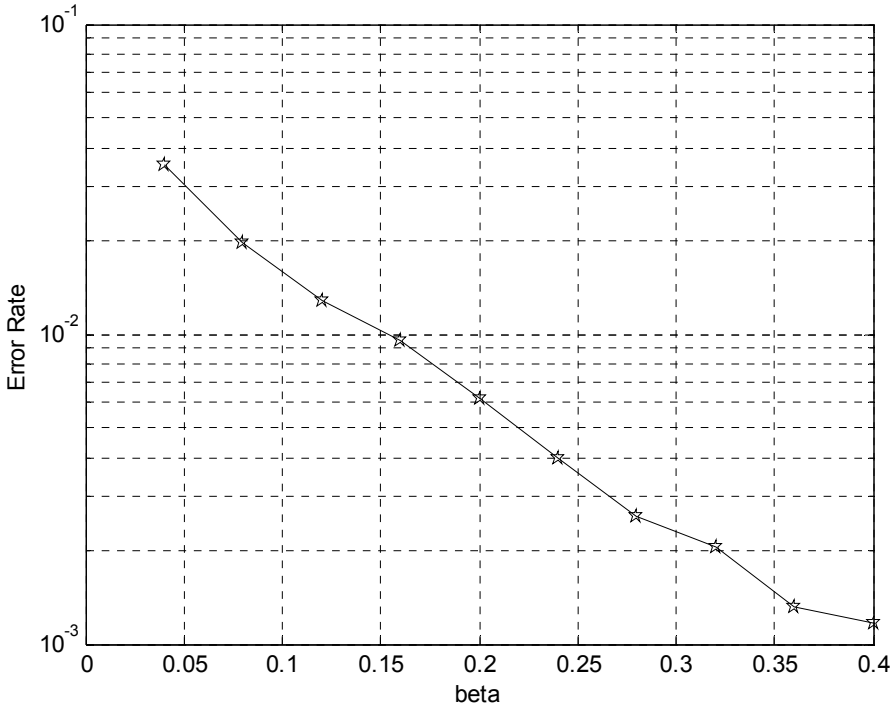

Figure 5.7 - Plot of error rate against β

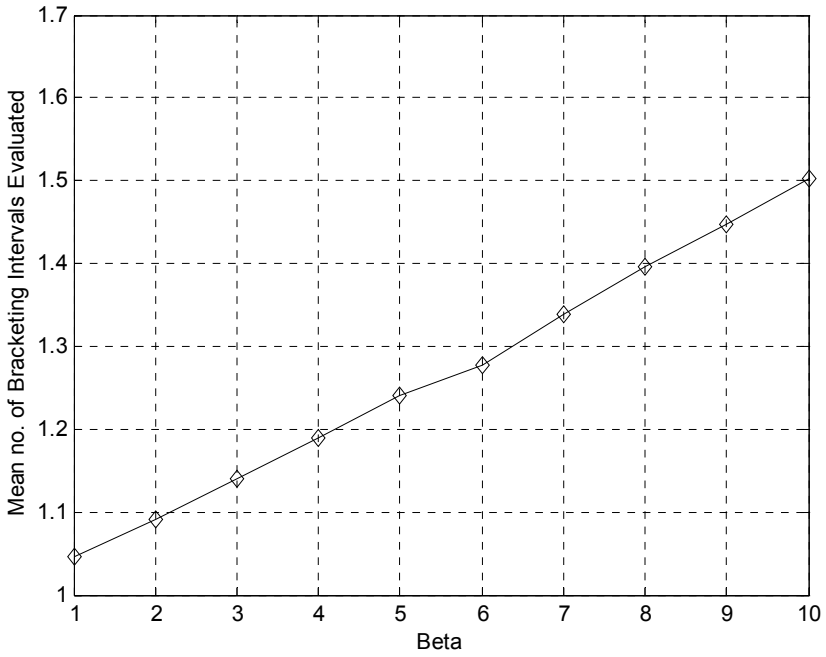

Fig 5.8 - Plot of mean number of bracketing intervals evaluated against β

Chapter 6

Conclusions and future topics

6.1 Conclusions

In this thesis, we have established a more general and flexible OFDM system (in comparison to [13,23]) that allows the activated sub-carriers to be arbitrarily placed over each of the N_b OFDM symbols used in the estimation of the carrier frequency offset. The signal model for such a system is formulated in Chapter 2 and the effects of intercarrier interference due to a carrier frequency offset was also examined. We suggested and provided an explanation that spacing the activated sub-carriers equally apart when the system is at less than half load and spacing the null sub-carriers equally apart when the system is at more than half load yields the least average inter-carrier interference among all sub-carrier placement strategies. We have validated this claim via computer simulations for systems with less than or equal to 20 sub-carriers. Correspondingly the SIR ratio would also be highest using such a carrier placement strategy.

In Chapter 3, we formulated the maximum likelihood estimator (MLE) of the carrier frequency offset based on our flexible OFDM system. The MLE is the frequency offset correction that yields the least total energy in the DFT bins assigned to the null sub-carriers. We provided a detailed proof, using the Parseval's relation, to explain why this is equivalent to finding the frequency offset that maximizes the total energy in the DFT bins assigned to the activated sub-carriers.

More significantly, applying the approach in [23], we have derived a more general criterion to avoid cost function ambiguity due to the channel nulls through judicious placement of the sub-carriers over the N_b OFDM symbols used in estimation.. Providing a physical interpretation of the criterion, we have also shown that deterministic hopping of the sub-carriers, which was first introduced in [13], can avoid cost function ambiguity.

Chapter 4 presented a derivation of the *NMSE* of the estimator using the small perturbation analysis adopted in [13] for our flexible system. We note an error in the expression given in [13] and that this derivation is not applicable when channel nulls causes ambiguity in the cost function. Subsequently, we showed that the experimental results match well with the theoretical predictions in an AWGN channel.

Simulations were also carried out for a Rayleigh channel with an exponential power delay profile. Experimental evidence showed that occurrences of large estimate errors corresponded to instances where the channel nulls occurred at locations predicted by the criterion derived earlier. We suggested a random carrier placement scheme that tends to space the activated sub-carriers among the entire set of sub-carriers and gives

a low probability of occurrence of a periodic carrier placement. This allows maximum carrier estimation range and provides resilience to the channel null problem. The performance of this scheme was compared against [13]

In Chapter 5, we explored minima search techniques which are more efficient than uniform exhaustive search, and ensures convergence without the need to set a appropriate weight parameter as required by gradient descent methods, In addition, by taking the 1st and 2nd derivatives of the cost function, which can be evaluated directly in a FFT like manner, we propose transforming the problem of minima search to one of root search. The fast Newton Raphson approach can then be used to accelerate the search. Finally, we proposed a criterion to narrow the scope of search and reduce computations. The performance of the search schemes were compared and the Newton Raphson technique is the most efficient (in terms of the iterations required to reach convergence) while the proposed criterion is effective.

6.2 Suggestions for further works

The estimation of carrier frequency offset remains a challenging problem in the implementation of OFDM systems. This work examines the use of the MLE, which is semi-blind, requiring knowledge of the null sub-carrier placement but not the transmitted data symbols.

Further studies can be done on the incorporation of pilot symbols into the system. A cost function and the criteria for avoiding cost function ambiguity can be developed using an approach similar to this work. The introduction of pilot symbols is likely to improve the performance of the carrier frequency offset estimator. In this thesis, we analyzed the effect of the placement of the null sub-carriers on ICI and the estimate's MSE. Future work can include the analysis of how positioning of the pilot symbols in the system can affect the estimator's performance. Furthermore, since pilot symbols can be used in channel estimation, a joint estimate of the carrier frequency offset and the channel can be developed. In an OFDM system, some sub-carriers may be affected by the presence of channel nulls, rendering the sub-carrier unsuitable for data transmission. If information about the channel can be fed back to the transmitter, the placement of sub-carriers can be made adaptive so as to maximize the overall system performance, which includes minimizing both the channel and the frequency offset estimation error.

Last but not least, the estimation of carrier frequency offset in a multi-user system presents a difficult task as each user has a different carrier frequency offset w.r.t to the base station. However, the deployment of such a multi-user system is highly desirable and this presents a potential research topic.

References

[1] Proakis, J.G., "Digital Communications", *McGraw-Hill*, New York 1989

[2] R. Chang, "Synthesis of band limited orthogonal signals for multichannel data transmission," BSTJ, vol. 46 pp1775-1796, December 1966.

[3] M. Zimmermann and A. Kirsch, "The AN/GSC-10/KATHRYN/ variable rate modem for HF radio," *IEEE Trans. Commun. Techn*, vol CCM-15, pp. 197-205 April 1967.

[4] S. Weinstein and P. Ebert, "Data transmission by frequency division multiplexing using the discrete fourier transform," *IEEE Trans. Commn. Techn*., vol. COM-19 pp. 628-634, Oct 1971.

[5] L. Cimini. "Analysis and simulation of a digital mobile channel using orthogonal frequency division multiplexing," *IEEE Transactions on Communications* vol. 33 pp. 665-675, July 1985.

[6] M. Alard and R. Lassalle, "Principles of modulation and channel coding for digital broadcasting for mobile receivers," *EBU Review, Technical* No. 224, pp. 47-69 Aug 1987

[7] Horosaki B., "An orthogonal multiplexed QAM system using the discrete fourier transform," *IEEE Transactions on Communications*, Vol. COM-29, pp. 982-989, July 1981.

[8] Yiyan Wu and William Y. Zhou, "Orthogonal frequency division multiplexing: a multicarrier modulation schememe", *IEEE Transactions on Consumer Electronics*, Vol. 41. pp. 392-398, No. 3 August 1995.

[9] P. H. Moose, "A technique for orthogonal frequency division multiplexing frequency offset correction," *IEEE Transac. Commun*. Vol. 42, pp 2908-2914, Oct 1994.

[10] T. Pollet, M. Van Bladel and M. Moenaclaey, "BER sensitivity of OFDM systems to carrier frequency offset and Wiener phase noise," *IEEE Trans. Commun*, vol 43, pp. 191-192, Feb/Mar/Apr1995

[11] T. M. Schimdl and D.C. Cox, "Robust frequency and timing synchronisation for OFDM," *IEEE Trans. Commun*., vol. 45, no. 12, pp. 1613-1621, Dec 1997

[12] M. Morelli and U. Mengali, "An improved frequency offset estimator for OFDM applications," *IEEE Commun. Lett*, vol. 3, pp. 75-77, Mar. 1999.

[13] S. Barbarossa, M. Pompili and G. B. Giannakis, “timing and frequency synchronisation of orthogonal frequency multiple access systems,” *in Proc. Int Conf. Communications*, vol. 6, Helsinki, Finland, June 11-15, 2001, pp. 1674-1678

[14] J. van de Beek, M. Sandell and P.O Borjesson, “ML estimation of time and frequency offset in OFDM systems,” *IEEE Transac. Signal Processing*, vol 45, pp. 1800-1805, July 1997.

[15] H. Bolcskei, “Blind high-resolution uplink synchronisation of OFDM-based multple access schemes,” *in Proc. IEEEWorkshop Signal Processing Advances in Wireless Communications*, Annapolis, MD, 1999, pp. 166-169

[16] F. Classen and H. Meyr, “ Frequency synchronixation algorithms for OFDM systems suitable for communications over frequency-selective fading channels,” *in Proc. Vehicular tech. Conf.*, vol. 3, 1994, pp. 1655-1659.

[17] X. Ma G.B Giannakis and S. Barbarossa, ”Non-data-aided frequency-offset and channel estimation in OFDM and related block transmissions,” *in Proc. Int. Conf. Communications*, vol 6, Helsinki, Finland, June 11-15, 2001, pp 1866-1870.

[18] H. Liu and U. Tureli, “ A high efficiency carrier estimator for OFDM communications,” *IEEE Commun. Lett*, vol 2 pp. 104-106, April 1998

[19] U. tureli, H. Liu. And M. D. Zoltowski, “OFDM blind carrier offset estimation: ESPIRIT,” *IEEE Trans. Commun.*, vol 48, pp 1459-1461 Sept 2000.

[20] M. Luise and R. Reggiannini, “ Carrier frequency offset acquisition and tracking for OFDM systems, “ *IEEE Trans. Commun.*, vol 44. pp. 1590-1598, Nov 1996

[21] N. Lashkarian and S. Kiaei, “Class of cyclic-based estimator for OFDM communications,” *IEEE Commun. Lett*., vol 2, pp 104-106, Apr 1998.

[22] S. Kapoor, D. J. Marchok, and Y.-F Huang, “Pilot assisted synchronisation for wireless OFDM using pilot carriers,” *in Proc. Vehicular Technol. Conf*., vol, 3, 1998, pp 2077-2080

[23] M. Ghogho, A.Swami, and G. Giannakis, “Optimised null-subcarrier selection for CFO estimation in OFDM in OFDM over frequency-selective fading channels,” *in Proc. Globecom-2001*, San Antonio, TX, Nov. 2001, pp. 202-206.

[24] Steven M. Kay, “Fundamentals of Statistical Singal Processing: Estimation Theory, PTR Prentice Hall, Englewood Cliffs, New Jersey 07632

[25] W.H.Press B.P.Flannery S.A.Teukolsky W.T.Vetterling, Numerical Recipes in C, *Cambridge University Press* 1988.

Appendix A

List of Publications

[1] Kim Piau Ng, T. T. Tjhung, "Blind Frequency Offset Estimator for OFDM Systems - Efficient Minima Search," *in Proc. ICICS-PCM*, Dec 2003, 2C4.6-P0383.